12-2015

Synthesis and Characterization of Oleophobic Fluorinated Polyester Films

Tugba Demir
Clemson University, tdemir@g.clemson.edu

SYNTHESIS AND CHARACTERIZATION OF OLEOPHOBIC FLUORINATED POLYESTER FILMS

A Dissertation
Presented to
the Graduate School of
Clemson University

In Partial Fulfillment
of the Requirements for the Degree
Doctor of Philosophy
Material Science and Engineering

---

by
Tugba Demir
December 2015

Accepted by:
Dr. Igor Luzinov, Committee Chair
Dr. Phillip Brown
Dr. Thompson Mefford
Dr. Douglas Hirt

ABSTRACT

The study presented in this dissertation is dedicated to the synthesis and characterization of oleophobic fluorinated polyester films. Specifically, the blending of oleophilic polyethylene terephthalate (PET) with low surface energy materials such as fluorinated polyesters has been used in order to fabricate oleophobic PET films. First, fluorinated polyesters (P(PF-oate-R)) possessing different end-groups (-COOH, -OH and -CF_3) are synthesized via polycondensation reaction of isophthaloyl chloride with perfluoro ether alcohols. Then, they are solvent-blended with PET at various concentrations to obtain oleophobic polyester films of different compositions. In addition, the films are annealed to investigate the effect of annealing on surface properties of the films. The results show that the obtained PET/P(PF-oate-R) polyester films demonstrate low wettability that depended on the polyester end-groups, film compositions, and annealing. It is found that PET blended with fluorinated polyesters terminated with CF_3 groups exhibit higher contact angle (CA) with water and oils than other polyesters. In addition, CA increases with increasing P(PF-oate-R) polyester content in blends.

To facilitate the oleophobicity of PET films, the fluorinated polyesters terminated with -CF_3 groups with two different M_w were synthesized and blended with PET. The results reveal that at low concentrations, low molecular weight polyesters migrate to the surface easily, resulting in higher surface coverage. Thus, it leads to higher water and oil repellency. On the other hand, when they are used at high concentrations, higher molecular weight polyesters in blends reduce the wettability of the surface to the higher level. It is found that the wettability of the PET film surface depends on not only *the* M_w

of polyesters, but also on *annealing* protocol. To this end, the effects of the annealing temperature on surface wettability are also examined.

DEDICATION

I dedicate this dissertation to my parents Kadri and Umran Demir, my sisters Asuman, Busra and brother Erkan who always have been there for me, and believe in me. Their support, love and encouragement have sustained me throughout my life. I would also like to dedicate this to my aunts Sukran, Semran, Aynisah and Humeyra who were always supportive and never let me feel alone during this journey.

ACKNOWLEDGMENTS

First and foremost, my sincerest gratitude goes to my advisor, Dr. Igor Luzinov, who I have been lucky enough to work with these past six years. I would like to thank him for his guidance, his patience, and encouragements during my graduate study at Clemson University. It has been a privilege to grow as a scientist with his guidance, and if I had to repeat this process I would once more make the same decision. I must also extend my thanks to my committee members: Dr. Phillip J. Brown, Dr. O. Thompson Mefford and Dr. Douglas Hirt for their insightful comments, suggestions, and time.

I am thankful to Dr. Bogdan Zdyrko and Dr. Ruslan Burtovyy for their support and willingness to teach me throughout my time. I appreciate their time and helpful suggestions for my research.

I would also like to express my appreciation to my research group with whom I have studied and worked: Dr. Fehime Vatansever, Dr. Anna Paula, Dr. Yuriy Galabura, Dr.James Giammarco, Dr. Marius Chyasnavichyus, Dr. Michael Seeber, Mykhailo Savchak, Jake Townsend, Nikolay Borodinov and Liying Wei.

I would like to acknowledge Kimberly Ivey, who was always there for a great conversation, as well as to teach and educate me on all her instruments. She was always willing to discuss and help me no matter how busy she was. I am thankful to Dr. Alex Kitaygorodskiy for providing training to us in NMR spectrometer and Dr. Gleb Yushin and his student, Naoki Nitta from University of Georgia Institute of Technology for doing XPS measurements on our samples.

I also thank all my friends whom I consider as family: Fehime Vatansever, Sine Kontbay, Ayse Korucu, H. Levent Tekinalp, Sule & Mustafa Bekaroglu, Ayse & Mustafa Bahar, Ozgun &Ziya Ozdemir, M. Oguz Kesimci, Begum &Uzay Damali, Nuray Ates, Ayse Tascan, Gamze & Mahmut Ersan, Sevda & Mehmet Sari, Kezban & Ali Kuru, Nefise Karanfil, Serife Yucesan, Seda Uzun, Aslican Yilmaz, Elif Can, Melek Bayram and Ali Erdem.

Finally, I would like to express my deepest gratitude to my mother, Umran; my father, Kadri; my brother, Erkan; and my sisters, Asuman and Busra for their love and support throughout my life. I could not have come this far without them. Special thanks also go to my aunts, Humeyra, Semran, Sukran and Aynisah for their continuous encouragement.

Last, but not least, I would like to thank Allah for all the gifts He has bestowed on me.

TABLE OF CONTENTS

Page

Table of Contents (Continued) Page

Table of Contents (Continued) Page

LIST OF TABLES

Table Page

LIST OF FIGURES

Figure Page

List of Figures (Continued) Page

CHAPTER ONE

INTRODUCTION

There are numerous examples in nature of materials that are capable of removing water and oil from their surfaces. To understand this phenomenon, significant work has been accomplished in studying and mimicking the fabrication of these surfaces to achieve water/oil repellency [1, 2] and self-cleaning features [3-8]. Significant efforts have been directed toward nano- or micro-structure fluoro-coated surfaces that are promising for oil repellency. However, no extensive research has been conducted to obtain and optimize on oleophobic poly(ethylene terephthalate) (PET) surfaces. This work aims to fill this gap.

PET is a conventional polymer material used for the production of fabrics, membranes, and fibers. PET products prevail in the market over those made from novel polymers with better characteristics due to their potential for recycling, their relatively low production cost, and widely available equipment and technology for their production. PET has very good physical characteristics, such as high-impact resistance, a high melting point, good barrier properties, low water adsorption, and high chemical resistance. However, applications for this material are still limited in some fields because PET surfaces are completely wettable by hydrocarbons.

To this end, the ultimate goal of this dissertation was to fabricate oleophobic PET films using fluorinated polyester systems and characterize them. For this purpose, fluorinated polyesters with different end-groups were synthesized and characterized. These polymers were used as additives in a PET matrix to fabricate oleophobic polyester coatings. This dissertation is structured as follows:

Chapter 2 of this dissertation gives a literature review of methods for the synthesis of oleophobic surfaces and their properties. It also provides a description of the methods used for the synthesis of fluorinated polyesters, their characterizations, and their utilization for the fabrication of oleophobic surfaces.

Chapter 3 provides a description of the experimental techniques used in this work.

Chapter 4 focuses on the synthesis of fluorinated polyesters with different end-groups. Specifically, fluorinated isophthaloyl polyesters were synthesized via the condensation polymerization of isophthaloyl chloride with perfluoro ether alcohols. **Chapter 4** describes the results of the characterization of their chemical, physical, and thermal properties.

Chapter 5 describes the fabrication of oleophobic films, including the methodology for the preparation of oleophobic PET films. This method is based on the addition of fluorinated polyesters into a PET matrix. The blending of PET with fluorinated polyesters at different concentrations can significantly reduce the surface energy of the films to decrease their wettability with hydrocarbons. **Chapter 5** also discusses the effect of annealing of the blended films on the level of wettability of the surfaces.

Chapter 6 focuses on the effects of the molecular weight of fluorinated polyesters on the wettability of PET blended films. Specifically, fluorinated diester isophthaloyl polyesters with two different molecular weights were blended with PET at different concentrations. It was found that high molecular weight fluorinated polyester exhibits

lower oleophobicity than lower molecular weight blends at the lower concentration. At high concentrations, former blends exhibits higher water and oil repellency than latter blends.

Chapter 7 discusses the films prepared in **Chapter 6** being annealed at different temperatures in order to investigate the effect of annealing temperature on the wettability and morphology of the coatings. In addition, the thermal properties of annealed samples are also investigated.

Chapter 8 concludes and summarizes the findings of this dissertation.

References

1. Zheng, X.; Guo, Z.; Tian, D.; Zhang, X.; Li, W.; Jiang, L., Underwater Self-Cleaning Scaly Fabric Membrane for Oily Water Separation. *ACS Applied Materials & Interfaces* **2015,** *7* (7), 4336-4343.
2. Latthe, S.; Terashima, C.; Nakata, K.; Fujishima, A., Superhydrophobic Surfaces Developed by Mimicking Hierarchical Surface Morphology of Lotus Leaf. *Molecules* **2014,** *19* (4), 4256.
3. Koch, K.; Bhushan, B.; Jung, Y. C.; Barthlott, W., Fabrication of artificial Lotus leaves and significance of hierarchical structure for superhydrophobicity and low adhesion. *Soft Matter* **2009,** *5* (7), 1386-1393.
4. Damle, V. G.; Tummala, A.; Chandrashekar, S.; Kido, C.; Roopesh, A.; Sun, X.; Doudrick, K.; Chinn, J.; Lee, J. R.; Burgin, T. P.; Rykaczewski, K., "Insensitive" to Touch: Fabric-Supported Lubricant-Swollen Polymeric Films for Omniphobic Personal Protective Gear. *ACS Applied Materials & Interfaces* **2014,** *7* (7), 4224-4232.
5. Akhtar, N.; Holm, V. r. R. A.; Thomas, P. J.; Svardal, B.; Askeland, S. H.; Holst, B., Underwater Superoleophobic Sapphire (0001) Surfaces. *The Journal of Physical Chemistry C* **2015,** *119* (27), 15333-15338.
6. Wang, Y.; Bhushan, B., Wear-Resistant and Antismudge Superoleophobic Coating on Polyethylene Terephthalate Substrate Using SiO2 Nanoparticles. *ACS Applied Materials & Interfaces* **2015,** *7* (1), 743-755.
7. Rangel, T. C.; Michels, A. F.; Horowitz, F. v.; Weibel, D. E., Superomniphobic and Easily Repairable Coatings on Copper Substrates Based on Simple Immersion or Spray Processes. *Langmuir* **2015,** *31* (11), 3465-3472.
8. Howarter, J. A.; Genson, K. L.; Youngblood, J. P., Wetting Behavior of Oleophobic Polymer Coatings Synthesized from Fluorosurfactant-Macromers. *ACS Applied Materials & Interfaces* **2011,** *3* (6), 2022-2030.

CHAPTER TWO

LITERATURE REVIEW

In general, “wetting” is the ability of a liquid to spread uniformly over a solid , which is a result of the intermolecular interactions that occur when the liquid comes in contact with the surface. In this case, solid/liquid interactions are stronger than the liquid/liquid interactions. These wettable surfaces are hydrophilic/oleophilic. However, when the liquid/liquid interactions are stronger than the solid/liquid ones, liquid droplets will deposit on solid surfaces without spreading. Thus, hydrophobic/oleophobic, otherwise called low surface energy coatings, are formed. The high levels of water and oil repellency allows use of low surface energy coatings in the most demanding environments such as in textiles, automotive, and electronics.

The research described in this dissertation focuses on the synthesis of low surface energy films using fluorinated polyesters, with an emphasis on possible ways of improving liquid repellency properties. Thus, **Chapter 2** gives an overview of the current methods used for the fabrication of low surface energy films. In addition, synthesis and characterization methods for fluorinated polyesters are presented as the key steps in the successful preparation of the repellent surfaces. Techniques that can be used to improve the performance of the water/oil repellency and its evaluation are also described.

2.1. Low Surface Energy Films

Low surface energy films are of significant interest for wide applicability in various fields, including self-cleaning surfaces [1-5], fuel cells [6-11], and membranes [12-15]. Low surface energy coatings, especially hydrophobic ones (contact angle (CA)

of water ≥ 90°) are employed by nature. One of the most common examples of natural hydrophobic surfaces are “Lotus leaves: Nelumbo nucifera.” In 1997, Neinhuis and Barthlott presented an overview of more than 200 species with water contact angles >150° for the leaves [16]. Neinhuis and Barthlott discovered that the surface of lotus leaves possessed nano-sized epicuticular waxes (hydrophobic wax crystals) on the upper side of the epidermal cells, which act as microstructure that enhances roughness (Figure 2.1) [16-18]. Thus, the combination of hydrophobic waxes and the presence of micro/nanostructures results in the repulsion of water from the surface. Therefore, rain droplets on the leaf surface roll off, carrying dust and dirt particles and leaving behind a clean surface (self-cleaning surfaces). Since there is a wide range of applications for hydrophobic surfaces, numerous studies have focused on the mechanism of the hydrophobicity as well as methods of fabricating artificial surfaces by mimicking nature [19-21].

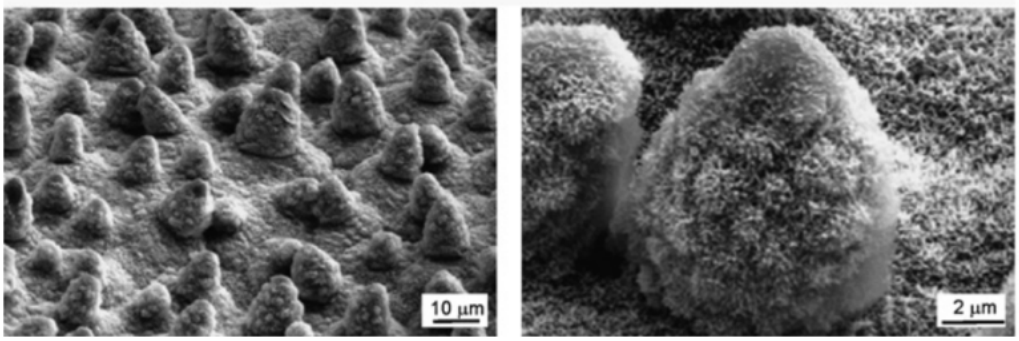

Figure 2.1. SEM micrographs of the Lotus (Nelumbo nucifera) leaf surface, which consists of a microstructure formed by papillose epidermal cells covered with epicuticular wax tubules on surface, which create a nanostructure. Reproduced from Ref [18] with permission from the Royal Society of Chemistry.

In addition to hydrophobic surfaces, oleophobic surfaces (CA of oil ≥ 90°) are interesting for a number of applications, such as anti-fouling and anti-bacterial coatings, stain-free materials, and spill-resistant protective coatings [5, 22-26]. However, it is more difficult to impede the wetting of oils than water due to their lower surface tension (25-40 mN/m) in comparison to water (72 mN/m). The general idea behind the ability of repelling a liquid from a surface is that the surface energy of the coating should be significantly lower than the surface tension of the liquid. Otherwise, the liquid will spread over the surface. Therefore, hydrocarbon based coatings are typically good at repelling water since hydrocarbons possess a relatively lower surface tension. Hydrocarbon based oils, however, do not work in the same way, because if the oils have lower surface energy than hydrocarbon based coatings, they wet the surface. Therefore, to develop an effective oleophobic surface, the surface energy of the solid surface should be significantly lower than that of the oils [19].

To date, oleophobic surfaces have been also obtained by a combination of chemical and geometric approaches (**Figure 2.2**). The chemical approach is to coat the surface with fluorinated compounds possessing low surface energy. Chemistry alone is not enough to achieve significant repellency of oils from surfaces and, consequently, geometric factors (formation of rough surface structures) are required.

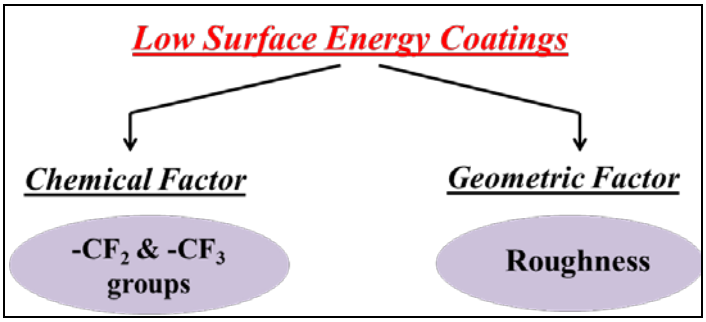

Figure 2.2. Parameters required for preparation of low surface energy coatings.

Numerous studies have been conducted to investigate oleophobic coatings on various substrates [27-34]. Effective oleophobic surfaces are typically characterized by high surface roughness, very low wettability hysteresis, and low surface free energy [35]. It is well established that the chemical structure of oleophobic coatings is based on fluorinated carbon groups, such as the $-CF_2$ and $-CF_3$ groups, due to their low surface energy. Therefore, perfluoro acids [36-38], perfluoro silanes [19, 30, 39-43], and fluorinated polymers [11, 44-52] have attracted significant interest for the development of oleophobic coatings. Furthermore, layer-by-layer [53, 54], micelle deposition [55], and the sol-gel method [56-59] are examples of techniques that were developed for preparing such surfaces.

2.2. Fluorocarbon-Containing Compounds

The unique characteristics of the fluorine atom result in the interesting properties of the compounds that contain them. It is well known that fluorine has very low polarizability and high electronegativity (3.98) compared to hydrogen (2.20) and carbon (2.55). In addition, carbon-fluorine (C-F) bonds are polarized due to the high electronegativity of fluorine [60]. However, there is no permanent dipole moment in

fluorinated compounds, such as perfluoro alkanes, due to their symmetric distribution of charge [61]. The lack of a permanent dipole moment in these compounds contributes to their oil- and water-repellency, as well as to their low surface energy, low refractive index, and reduced adhesion to surfaces. In addition, the bond energy of the C-F bond is higher than the carbon-hydrogen (C-H) bond, resulting in greater thermal stability.

The surface energy of fluor-containing surface is dependent on two main factors: i) the nature and packing of the surface atoms or chemical groups and ii) the C/F atom ratio. When the surface is covered with closed-packed non-polar groups, the C-F groups possess lower surface energy than hydrocarbons (CH_2>CH_3>CF_2>CF_3) due to their high electronegativity [36, 62]. In addition, Hiesh *et al.* demonstrated that the F/C atomic ratio plays a role in influencing the hydrophobicity and oleophobicity [63]. When more fluorine atoms were introduced, a lower surface energy and higher contact angles were achieved. Due to these unique features, fluoro-carbon-containing compounds such as fluorinated chemicals (perfluoro acids, perfluoro silanes) and fluorinated polymers have attracted much attention for the preparation of oleophobic coatings [36-52]. Hare *et al.* obtained the least wettable surface with the lowest surface energy (6mN/m) when the highly oriented closed-packed fluorocarbon tails with their $–CF_3$ groups extended outward [36]. In addition, they found that the surface tension of liquids should be 6mN/m or less in order to wet such surfaces. On the other hand, surfaces prepared by highly oriented closely packed hydrocarbons could become fully wettable with liquids which possessed surface tensions less than 15 mN/m since most of the oils possessed surface

tensions in the range of 30-17 mN/m (e.g., hexane 18.5 mN/m and hexadecane 27.5 mN/m)

2.2.1. Perfluoro Acids

Since the 1950s, perfluoro acids have received scientific and industrial interest for surface coatings, fire-fighting foams, and in the production of non-stick coatings on cookware and textile materials to repel water and oils. Perfluoro acids can be either physically adsorbed on metal surfaces or they can be chemically deposited on various substrates. For instance, Zisman *et al.* prepared oleophobic platinum surfaces modified by the adsorption of perfluorinated acids (perfluoro-butyric, caprylic, and lauric acids) from solution [36]. Today, the use of perfluoro acids is not as common due to bio-persistence and the toxicity of long-chain perfluorinated acids (C>8). This is true especially for perfluorooctanoic acids (PFOA) and perfluorooctane sulfonic acid (PFOS) or higher homologue perfluoro acids, which have raised worldwide environmental concerns [64] Therefore, much research has focused on either using shorter acids or developing alternatives to them.

2.2.2. Perfluoro Silanes

Perfluoro silanes (R-Si-X; X: Cl, OAlkyl) have been widely used to prepare hydrophobic and oleophobic coatings through different deposition methods. The chemical structure of perfluoro silanes consists of two parts (**Figure 2.3**). The first is the hydrolytically sensitive part, which can react with inorganic substrates, especially glasses, with the formation of stable Si-O-Si bonds [65]. Thus, the chemically stable monolayer of silane films can be synthesized. The second is the fluorocarbon substitution

part, which can bring the hydrophobicity and oleophobicity to the substrate surface [39, 65].

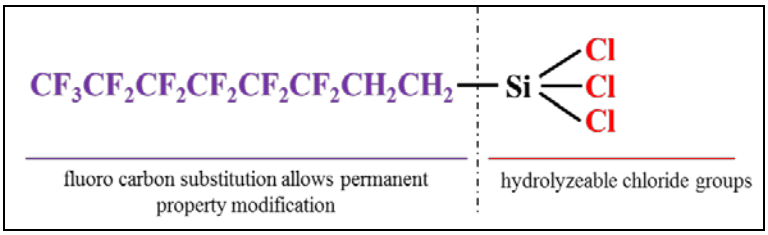

Figure 2.3. Structure of 1H,1H, 2H, 2H-Perfluorooctyltrichlorosilane [65].

It is well known that the number of hydroxyl groups on the substrate surface and their accessibility for bonding play a key role in rendering a surface hydrophobic/oleophobic. For instance, if the perfluoro silane groups react with all hydroxyl groups on the substrate, the surface becomes "shielded"; thus, hydrophobic/oleophobic surfaces are obtained [66]. Generally, not every hydroxyl group will react, but as long as the majority of the groups do, the substrate will be effectively shielded. Therefore, the reactivity of the perfluoro silane groups is important in the treatment.

To date, numerous types of perfluoro silanes have been synthesized and characterized to be used in the fabrication of repellent coatings. Sol-gel [67, 68] and chemical vapor deposition [65] are employed to obtain coatings. Although perfluoro silanes are the main chemical used for different applications, sometimes the monolayer of perfluoro silane is not sufficient to obtain a low surface energy surface. To this end,

instead of perfluoro silane, fluorinated polymers have been used for low surface energy coatings [69-72].

2.2.3. Fluorinated Polymers

Since polytetrafluoroethylene (PTFE) was discovered in 1938, attention has been focused on the preparation of fluorinated polymers due to their outstanding features such as high thermal and photochemical stability, excellent resistance to chemicals, low reflective index, and low-friction [73]. In addition, polymers with fluorocarbon chains have lower surface energy than those with hydrocarbon or silicone chains, and, therefore, fluorinated polymers are used as bulk or an additive to give water and oil repellency to material surfaces [74, 75]. Furthermore, they can be used in specialized applications such as spacecraft coatings to resist to atomic oxygen and fire-resistant coatings for cables due to their high chemical and thermal stability.

To date, more than 30 different fluorinated polymers are commercially available. In addition, number of studies have focused on the synthesis and characterization of new fluorinated polymers in order to improve their unique properties. According to the literature, fluorinated polymers can be categorized in two groups **(Figure 2.4)**: i) fully fluorinated polymers [73, 76] and *ii) semi-fluorinated polymers* [77]. The fully fluorinated polymers possess fluorinated backbones and may have fluorinated side-chains. They offer the advantages of chemical inertness in aggressive environments, superior non-stick properties, and thermal and chemical resistance enhancement.

Fully fluorinated polymers were synthesized using fluoro-olefins [78]. These can be either homopolymers or copolymers. The most well-known fluorinated homopolymer

is PTFE, which was synthesized from a tetrafluoroethylene monomer through radical polymerization. Furthermore, perfluoro polyether polymers (PFPE) are a unique class of fluorinated polymers with the chemical repeat unit $–(CF_2CF_2O)_x-(CF_2O)_n-$ [78]. They exhibit low surface energy, high toughness, durability, and low toxicity [64]. In addition to homopolymers, copolymers such as tetrafluoroethylene with hexafluoropropylene (FEP) have also been used in a broad range of industrial applications [71, 79, 80].

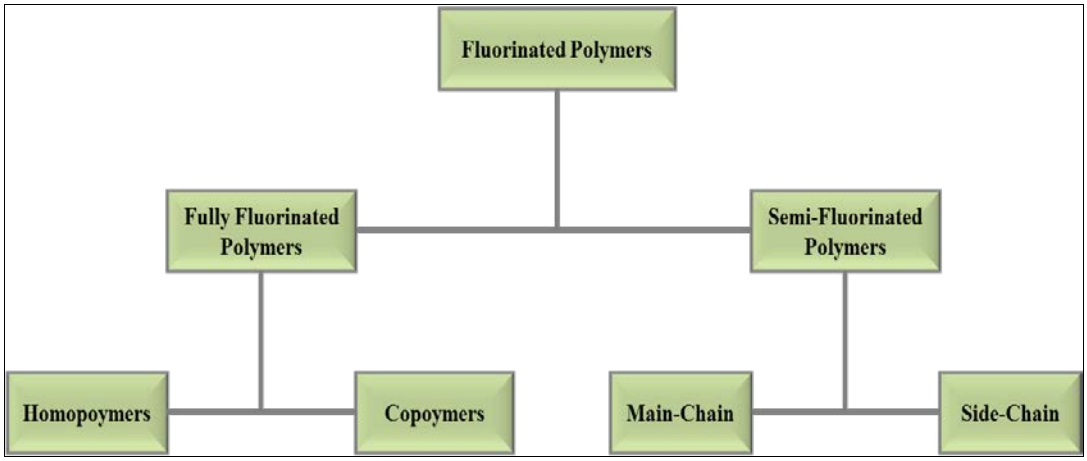

Figure 2.4. Categorizations of fluorinated polymers

The different types of fully fluorinated polymers are limited by the availability of unique, suitably reactive fluorine-containing monomers. To this end, numerous researchers have investigated the synthesis and characterization of semi-fluorinated polymers that consist of fluorinated and non-fluorinated segments [81-90]. Depending on the position of fluorinated segments in the polymer chain, semi-fluorinated polymers are also categorized in two groups: *ii-a) main-chain* [81, 82] and *ii-b) side-chain* [83-85]. The main-chain semi-fluorinated polymers contain partially fluorinated backbones, which

may also have fluorinated side chains. In this category, the polymers can be homopolymers, such as polyvinylidene difluoride (PVDF) [86], or copolymers [87-90].

The difference between the main-chain semi-fluorinated polymers and fully fluorinated polymers is that the former possesses non-fluorinated segments in its backbone. This difference changes both the physical and chemical properties. There are instances in which having one property hinders another property. Consequently, it is important to select polymers based on the ultimate application. For example, most of the fully fluorinated polymers, such as PTFE, exhibit chemical inertness to a wider range of chemicals than do partially fluorinated polymers. However, PFTE has lower mechanical properties at normal ambient temperatures.

2.2.3.1. Semi-Fluorinated Polymers

Semi-fluorinated polymers containing fluorinated and non-fluorinated segments lead to novel functional materials which exhibit properties such as hydrophobicity/oleophobicity, high thermal and chemical stability and excellent mechanical properties at extreme temperatures, low flammability, good electric properties, and low surface energy [91-93]. Depending on the position of fluorinated segments in polymer, main-chain semi-fluorinated polymers (in backbone) or side-chain semi-fluorinated polymers (as pendant group or tails) can be synthesized. Sometimes, main-chain polymers also have side chain fluorinated segments. To date, a significant number of polymers with fluorinated groups in the main chain and side chain have been reported in the literature, including fluorinated polyamines [52, 93]; vinyl polymers, such as polyacrylates/methacrylates [14, 45, 51, 94]; polyethers [69, 95-98]; polystyrenes [99-

103]; polyurethanes [52, 93, 104-107]; and polyester [84, 108, 109]. These polymers have been synthesized by the polymerization of the corresponding fluorinated monomers with non-fluorinated counterparts in a suitable polymerization process such as; free radical polymerization; living cationic, living anionic, and living radical polymerizations; and emulsion and polycondensation polymerizations. Research on the fluorinated condensation polymers is limited, however, it is compared to that on fluorinated addition polymers due to the difficulty of polymer synthesis [84, 109].

2.3. Condensation Polymers

Condensation polymers are synthesized by the condensation reaction of two or more bi/multifunctional monomers with the elimination of small molecules such as water, hydrogen chloride, and methanol [110-113]. Compared to addition polymerization, condensation polymerizations proceed by a stepwise reaction between any of the various sized species in the reaction system. For instance, one proceeds from monomer to dimer, trimer, and tetramer, etc. (**Figure 2.5**) [114].

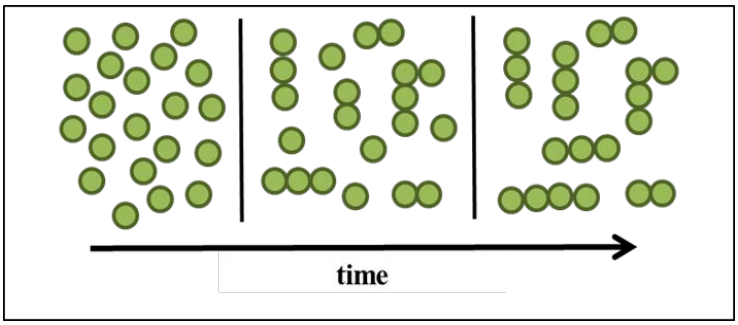

Figure 2.5. Schematic of condensation polymerization.

Condensation polymers form more slowly than addition polymers. Therefore, high molecular weight of the polymer is obtained at the end of the condensation

polymerization (>99% conversion)[114]. Consequently, polymer chain size significantly depends on the conversion of polymerization. The molecular weight of condensation polymers also depends on the stoichiometric ratio between functional groups. Therefore, high degree monomer purity is also required. For instance, if the the bifunctional monomers are not pure enough, even a small amount of monofunctional monomers can cause the polymerization to end early, resulting in a lower molecular weight polymer. In addition, the polymerization reaction must be a very high yield reaction with the absence of side reaction [114].

To date, numerous condensation polymers such as polyesters, polyamides, polyethers, and polyanhydrides have been synthesized (**Figure 2.6**) [70, 115-123].

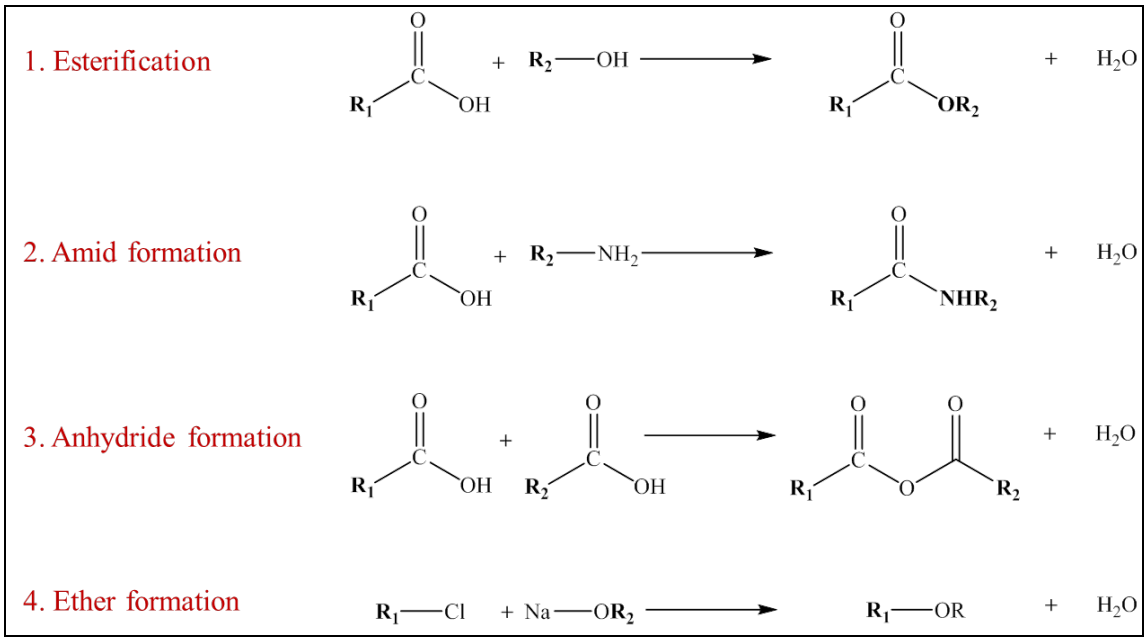

Figure 2.6. Basic condensation reactions of functionalities.

Among condensation polymers, polyesters are formed from the reaction of diols or hydroxyl-terminated polyether with diacids (derivatives) and with the elimination of

water or hydrochloric acid, for example [57, 115, 117, 121]. It is well known that poly(ethylene terephthalate) (PET) is one of the most common polyesters and was invented in 1941 by J. Rex Whinfield and J. T. Dickson in England [124]. It was synthesized via either trans-esterification or via direct esterification of acid (derivatives) with alcohols or hydroxyl-terminated polyether [125-129]. Among these esterification techniques, the former is normally used to synthesized polymers with a higher molecular weight, whereas the latter is used to produce lower molecular weight polymers due to the difficulty of obtaining stoichiometric equilibrium [110, 130-132]

PET is generally synthesized in two steps. First, terepthalic acid is reacted with methanol to form dimethyl terephthalate ester, which can easily be purified through a distillation process. Then, dimethyl terephthalate is reacted with ethylene glycol at a low temperature, resulting in the formation of oligoester with the hydroxyl end group [132-134]. Finally, polyester with high molecular weight is produced via the ester interchange between oligoester that occurs at 250°C. Polyester is a semi-crystalline polymer with a melt temperature of about 250°C- 275°C. Due to these properties, polyester is used in various applications such as plastics for the beverage industry as well as fibers for tires, cords, belts, filter cloth, brushes, clothing, and carpets due to its barrier property, high strength, and enhanced chemical and thermal stability [135-138].

2.3.1. Fluorinated Polyesters

Polyesters exhibit good thermal stability, low water absorption, and excellent mechanical properties and are, therefore, applied widely in various industries [139-143]. However, despite their outstanding properties, they are not soluble in organic solvents

and are completely wettable to most hydrocarbons. This usually limits their utility in numerous applications. For instance, low surface energy along with high chemical and thermal stability and good mechanical properties are required for application in coatings. Therefore, the inclusion of fluorocarbon groups into polyesters has received scientific and industrial attention in numerous applications including protective coatings, electronics, and textiles [144-147].

To date, numerous studies have focused on the synthesis of fluorinated or semi-fluorinated polyesters. It was reported that E. Burgoyne *et al.* synthesized the first fluorinated polyester, Subsequently, 1,1-dihydroperfluorobutyl perfluorobutyrate was produced by [148] . They found that 1,1-dihydroperfluorobutanol reacted slowly with perfluorobutyl chloride while it did not react with perfluoro butyric acid, even when excess of acid was used. In the similar manner, totally fluorinated polyesters were produced via the reaction of perfluoro di-alcohols with perfluoro diacid chlorides [111, 149, 150]. Most of the studies investigated the synthesis and characterization of semi-fluorinated polyesters. Robitscher *et al*. investigated three general synthesis methods of fluorinated polyester from fluorinated diols: i) direct esterification with dicarboxylic acids, ii) trans-esterification of diethyl esters using various catalysts, and iii) reaction with dicarboxylic acid chlorides (Schotten-Baumann reaction) [149, 151]. They found that the best method of preparing fluorinated polyesters was the reaction of fluorine-containing diols with acid chlorides; thus, they were in agreement with the conclusions drawn initially by E. Burgoyne *et al.* [148]. Esters formed rapidly when they were reacted with

each other. Although a direct esterification technique could be used for the preparation of high molecular weight polyesters, longer reaction times are typically required.

Currently, extensive literature reports on the synthesis and characterization of aliphatic and aromatic fluorinated polyesters [112, 152-156]. It was found that aliphatic fluorinated polyesters possess low thermal stability due to their flexible chains and the absence of a rigid crystalline structure. On the other hand, since aromatic fluorinated polyesters were synthesized by the incorporation of a rigid benzene ring in the polymer backbone, these aromatic polyesters were used widely in the automotive and electronic industries given their excellent thermal stability, good solvent resistance, and mechanical properties [155, 157, 158]. However, most aromatic fluorinated polyesters are non-soluble in organic solvents and have high glass transition temperatures due to their rigid structures, thus resulting in difficult processing. Therefore, most research has focused on improving the processing features of such aromatic fluorinated polyesters. For example, their solubility was improved without the loss of enhanced thermal stability by the incorporation of flexible aliphatic elastic units into the polymer backbone. The flexibility of the elastic units helps polymer chains to dissolve easily into solvents [152, 159, 160].

Generally, most fluorinated polyesters are synthesized via a condensation reaction of fluorinated di-alcohols with acids (derivatives) [112, 150-153, 156]. However, certain studies report that the reactivity of di-alcohols was reduced by the inductive effect of fluorine. In order to increase di-alcohol reactivity, fluorinated di-alcohols which possessed additional methylene spacers between the hydroxyl functionality and fluorine atoms were synthesized [72, 161, 162].

In addition, a few studies have focused on fluorinated polyesters formed from fluorinated acid derivatives with hydrocarbon diols [152]. Zhu et al. synthesized fluorinated polyesters from the polycondensation reaction of tetrafluorophthalic anhydride with ethylene glycol [152]. Another study reported that the synthesis of poly(neopentyl glycol hexafluoroglutarate) proceeded by the condensation of neopentyl glycol and glutaric acid in solution [162].

2.4. Polymer Blends

Polymer blends have received considerable attention both in academia and in practical fields due to their improved properties such as adhesion, wettability, mechanical strength, and chemical stability relative to homo-polymer counterparts [163-166]. Polymer blends are obtained by mixing two or more polymers that can be one-phase material or form a two-phase structure (immiscible blends). The main advantages of the blending techniques are the simplicity in preparation as well as the adjustable properties of blend coatings, which can be easily altered by changing the blend compositions, the molecular weights of polymers, solution concentrations, the evaporation rate of solvents, and the parameters of the annealing processes [163-165, 167-172].

Fluorinated polymers possess excellent properties. However, their production cost is extremely high. Therefore, blending fluorinated polymers with non-fluorinated counterparts [99, 163, 164, 169] has gained interest to generate novel materials with enhanced physical and chemical properties that are more economically viable and practical. To date, fluorinated polymer blends are used for repellent coatings, membranes and electronics materials [77, 173, 174]. In general, the surface properties of polymer

blends can be tuned by their composition, which can differ greatly than in the bulk. In fact, surface composition depends on the surface segregation of polymer blends, which is caused by the difference of the surface energy of each of the blended polymers. The surface is generally enriched by the lower surface energy components to minimize the free energy of the system [100, 169]. Therefore, numerous works have focused on the quantitative study of the surface segregation of fluorinated polymers in blends in order to alter their surface energy [175-177]. For example, S. Affrossman *et al.* determined the surface composition of blends of perfluoro end-capped styrene (PF-PS) with hydrogen-terminated styrene [169, 178]. Both X-ray photoelectron spectroscopy (XPS) and secondary ion mass spectroscopy (SIMS) confirmed the expectation that this blend surface should be enriched with PF-PS. Furthermore, Won-Ki Lee *et al.* made a similar observation for blends of fluorinated polyesters with non-fluorinated ones [179]. They demonstrated that fluorinated polyester migrated to the surface and lowered surface energy significantly.

The molecular weight of polymers in blends also has a significant effect on surface segregations [180-184]. One of the schools of thought believes that the polymer chains at the air-polymer interface can be compressed along the direction perpendicular to the films surface, resulting in limited polymer chain conformations on the surface [185]. Thus, this decreases the conformational entropy of polymer chains at the surface as compared with that of a polymer chain in the bulk. The conformational entropy loss, which is a difference in the conformational entropy of polymers between at the surface and in the bulk, depends on the molecular weight of the polymers in the blends [177].

The component with the higher molecular weight experiences a much larger reduction of its conformation entropy as compared to lower ones at the surface. Thus, they are depleted from the surface, and lower molecular weight components migrate to the surface to minimize the surface energy [177]. Because of this, the high concentration of polymer chain-ends enrich the surface. Besides molecular weights, heat treatment of the surface also enhances surface segregation. Annealing above the thermal glass transition temperature (T_g) or melting temperature (T_m) of polymer results in an increase in the mobility of polymer chains, especially rigid chains, and permits the reorientation of hard domains. Consequently, as fluorinated polymer blends are annealed, the fluorinated polymer migrates to the surface during reorientation, resulting in surface enrichment with fluorinated groups to minimize the surface energy [172, 186, 187].

2.5. Wetting Phenomena

Wetting phenomena are important in numerous fields of technology such as adhesion, medicine, biomaterials, environments, and coatings/thin films[188]. In the early 1800s, Pierre Simon de Laplace and Thomas Young investigated the physicochemical properties of water and its wetting behavior on various materials [189]. In general, as two immiscible liquids contact each other, they change the shape of contact line in order to minimize their surface energy. In the bulk of liquids, there is cohesion energy that results from Van der Waals, hydrogen, and dipole bonding between the constituent molecules. There is a net force of interaction between the molecules in the bulk. However, the molecules at the interface between the two fluids possess higher energy compared the molecules in the bulk due to the net attractive force pointing toward the liquid interior

(**Figure 2.7**). In other words, the interfacial tension stems from the lack of cohesion energy at the interface. The interfacial tension is called either surface tension for liquids or surface energy for solids. The surface tension/energy is denoted by the symbol γ (sometimes also σ). It expresses how much energy is required to increase the liquid surface area by one unit, which can be defined in terms of Gibbs free energy (G)

$$dG = -SdT + VdP + \gamma dA \qquad (2.1)$$

$$\gamma \equiv \left(\frac{\partial G}{\partial A} \right)_{T,P} \qquad (2.2)$$

where S and T represent the entropy and temperature of the system. V, P, and A are the volume, pressure, and area of the droplet, respectively.

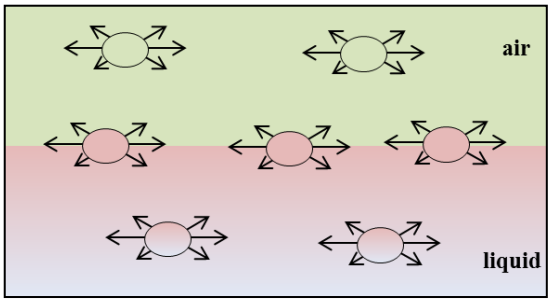

Figure 2.7. Scheme of liquid molecules at the surface which possess fraction of the attractive interactions as compared in the bulk.

2.5.1. Wettability of Solid Surfaces

Contact angle measurement analysis has been conducted to assess the surface wettability of coatings. As a liquid drop is placed on a solid surface, it either spreads over the surface or forms a drop with a definite angle of contact between the liquid and the solid phase (**Figure 2.8**). Based on this contact angle, the small displacement of the liquid

causes a change in the area of solid covered, resulting in a change in the surface free energy of the system, which can be determined as follows [190]:

$$\gamma \equiv \left(\frac{\partial G}{\partial A} \right)_{T,P} \qquad (2.2)$$

$$\Delta G = \Delta A(\gamma_{sl} - \gamma_{sv}) + \Delta A \gamma_{lv} \cos(\theta - \Delta\theta) \qquad (2.3)$$

where γ_{lv}, γ_{sv} and γ_{sl} represent to liquid–vapor, solid–vapor, and liquid–solid interfacial surface energies, respectively, and θ is the contact angle.

At equilibrium

$$\lim_{\Delta A \to 0} \frac{\Delta G^s}{\Delta A} = 0$$

and

$$(\gamma_{sl} - \gamma_{sv}) + \gamma_{lv} \cos\theta = 0 \qquad (2.4)$$

or

$$\gamma_{lv} \cos\theta = \gamma_{sv} - \gamma_{sl} \qquad (2.5)$$

In 1805, the Young Equation, which is a rearrangement of **Equation 2.5**, was derived by Thomas Young. He proposed the contact angle of liquid as a result of the mechanical equilibrium of a drop on an ideal smooth surface under the action of three interfacial surface energies [189],

$$\gamma_{lv} \cos\theta = \gamma_{sv} - \gamma_{sl} \qquad (2.5)$$

where θ_Y is the Young contact angle.

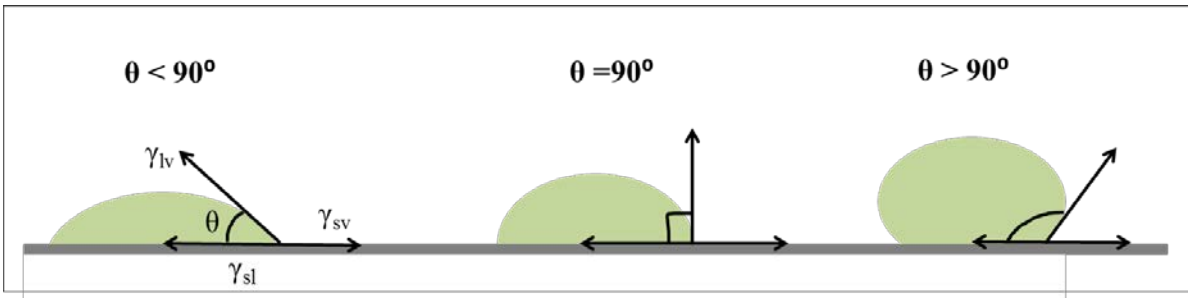

Figure 2.8. Images of contact angles of liquid drops on a smooth homogeneous solid surface.

The concept of the contact angle and its equilibrium state is important in order to determine the wettability of surfaces. **Figure 2.8** shows that a low contact angle is found when the liquid spreads on the surface, whereas a high contact angle is obtained when the liquid beads on the surface. Specifically, contact angles less than 90° correspond to hydrophilic/oleophilic surfaces, while hydrophobic/oleophobic surfaces are defined by contact angles that are greater than 90°. However, when the solid substrates are non-ideal—that is, both rough and chemically heterogeneous—the wettability behavior becomes more complex than in the Young Equation.

2.5.2. Wettability of Rough Surfaces

A proper surface texture can significantly increase oil repellency by allowing an air layer to be maintained in the space between the asperities during water/oil contact[18, 20, 55]. In comparison, a flat solid surface can have a CA of oil no more than 90°, even if its surface energy has been lowered by introducing -CF_3 groups. Hence, numerous methods such as electrochemical deposition, chemical/plasma etching, and micro-lithography have been utilized to fabricate rough surfaces and study their effects on the wetting behavior of water and oil. In addition to these methods, the deposition of treated

nanoparticles on the surface is another versatile method to generate surface roughness [1, 56, 191-194]. However, these methods are usually limited to special substrates, and, sometimes, hydrophobic and oleophobic surfaces still cannot be achieved. As a result, more than one method may need to be used to obtain necessary roughness.

To describe theoretically the effects of roughness on hydrophobicity and/or oleophobicity, the first attempt was made by Wenzel (**Figure 2.9**) [195].

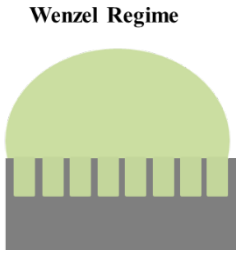

Figure 2.9. A schematic illustration of the Wenzel wetting regimes.

Wenzel proposed the following equation for the apparent contact angle θ_W formed when a liquid wets a rough surface completely (**Figure 2.9**):

$$\cos\theta_w = r\cos\theta_Y \qquad (2.6)$$

where r is the surface roughness defined as the ratio of the actual area of the rough surface to the projected area, and θ_Y is the Young's equilibrium contact angle on an ideally flat surface of the same material.

According to Wenzel's equation, hydrophobic/oleophobic flat surfaces have a θ_Y >90°, which only leads to a high apparent angle ($\theta_W > \theta_Y$); otherwise, the apparent angle becomes low ($\theta_W < \theta_Y$) on the hydrophilic/oleophilic surface, θ_Y <90°. To date, numerous studies are in qualitative agreement with this relationship. Uelzen and Muller investigated the effect of surface roughness on the apparent contact angle using different substrates, as

shown in **Figure 2.10** [196]. They concluded that the hydrophilicity and hydrophobicity can be definitely enhanced by roughness [196].

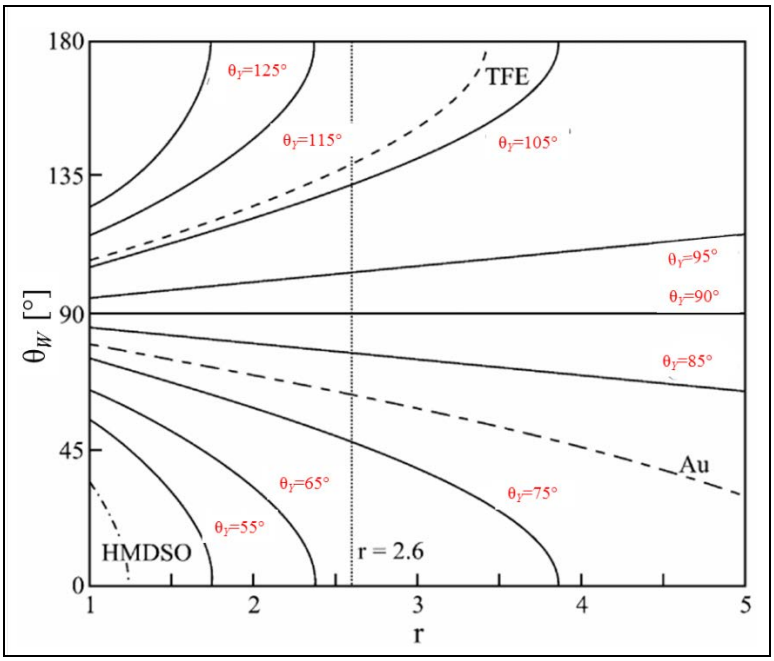

Figure 2.10. The apparent contact angle θ_W as a function of solid surface roughness as described by Wenzel's law. Adapted with permission from Elsevier [196].

In contrast to the Wenzel model [195], the Cassie and Baxter model [197], shown in **Equation 2.7**, describes the apparent contact angle of liquid θ_{CB} on a composite surface when a liquid droplet does not entirely wet the rough surface and leaves pockets of air between the droplet and solid surface (**Figure 2.11**).

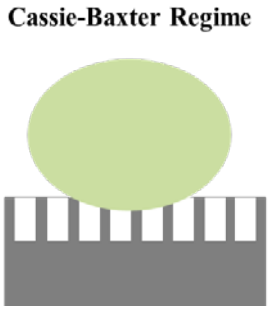

Figure 2.11. A schematic illustration of the Cassie-Baxter wetting regimes

Based on this model, θ_{CB} is always higher θ_Y, even when θ_Y is lower than 90°:

$$\cos\theta_{CB} = f_1 \cos\theta_{Y1} + f_2 \cos\theta_{Y2} \qquad (2.7)$$

where Young's contact angles θ_{Y1}, θ_{Y2} and area fraction f_1, f_2 of the component surfaces. When one of the components is air which is trapped in between the asperities (where θ_{Y2}=180°), the Cassie-Baxter equation can be reduced to

$$\cos\theta_{CB} = f_1(1+\cos\theta_{Y1}) - 1 \qquad (2.8)$$

where f_1 is a fraction of the liquid-solid interface (f_2=*1-*f_1, is the fraction of the liquid-air interface).

It is clearly seen that the presence of air in the film influences the contact angle measurements. When the air fraction, f_2, is increased, a higher contact angle is obtained even though composite wetting exhibits intrinsic contact angles less than 90°. However, when f_2 = 0, the Cassie-Baxter equation (**2.6**) reduces to the Wenzel equation (**2.5**) with f_1 = r. Therefore, it is known that the Cassie-Baxter state cannot be stable as the f_2 is reduced.

2.6. Methods for Determining the Surface Energy of a Coating

The knowledge of the surface free energy of a coating is important for optimizing various coating processes. However, the surface energy of coatings cannot be directly measured. It is calculated using the contact angle measurements for a set of homolog liquids on the coating surface. Then, these contact angle data fit a particular surface energy theory [198-203]. Several widely used methods to determine the surface energy of solids have been reported in the literature. The first is the Zisman method [203- 205]. Zisman proposed the surface energy of a solid to be equal to the surface tension of liquid which completely wet the solid surface. This surface tension is called critical surface tension, γ_c. In order to find γ_c of the film surface, the contact angle of a series of homolog liquids on film was measured. Then, the cosine value of the corresponding contact angles against the surface tension of liquids was plotted and extrapolated to $\cos\theta=1$ ($\theta=0°$) (**Figure 2.12**). At that point, the value of γc can be obtained. Such plots are also called "Zisman plots." According to the Zisman plot, it was found that the surface energy of LDPE had 22.8 mJ/m^2.

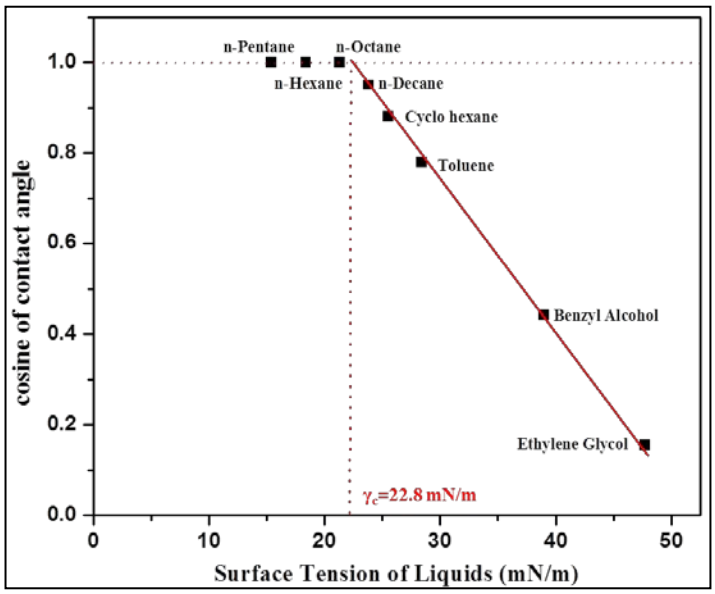

Figure 2.12. Zisman plot for low density of polyethylene. Replotted from Ref [206].

It is well known that the Zisman method is a one-parameter method. This means that surface energy of surfaces is only characterized corresponding to the surface tension of liquids by only one overall value. On other words, it does not take into account specific liquid/solid surface interactions. Because of this, the Zisman method is inadequate for polar surfaces and only valid for non-polar surfaces [205].

Another method was proposed by Owens and Wendt, which assumed that the surface energy of a solid (and of a liquid) is a sum of independent components and associated with specific interactions [202]. The polar components contain dipole-dipole, dipole-induced dipole, and hydrogen bonding interactions. On the other hand, dispersive components have van der Waals interactions between the solid surface and applied liquid. Therefore, the Owens-Wendth method exhibits a two parameter model, as shown in the following equation:

$$\gamma_l(1+\cos\theta) = 2\sqrt{\gamma_s^d \gamma_l^d} + 2\sqrt{\gamma_s^p \gamma_l^p} \qquad (2.9)$$

$$\gamma_s = \gamma_s^d + \gamma_s^p \qquad (2.10)$$

where γ_s and γ_l is the surface tension of the solid and liquid, respectively. The subscripts *d* and *p* correspond to the dispersion and polar components of the surface tension, respectively.

In order to determine the surface energy of a solid surface, at least two liquids with known surface tensions (overall, dispersive, and polar) are needed. When one of the hydrocarbon solvents—such as hexadecane and cyclohexane, which have only dispersive components—is used, it is easy to solve **Equation 2.10.** First, the dispersive component of a solid is found and then its polar component. Finally, the summation of the polar and dispersive components gives the surface energy of the solid. The Owens-Wendth method is valid for polymeric surfaces, which are moderately polar in nature [207-210].

2.6. Conclusions

In conclusion, numerous studies have focused on understanding the mechanism of oleophobicity as well as the methods of fabricating oleophobic surfaces. It is well known that fluorinated compounds play a vital role in the fabrication of oleophobic coatings due to their low surface energy as compared hydrocarbons. Thus, various fluorinated materials (acids/silanes/polymers) have been synthesized and used in both scientific and industrial applications. In the next chapters of this dissertation, we focus on the synthesis of fluorinated polyesters with different end-groups and which are then used for fabrication of oleophobic coatings.

2.7. References

1. Wang, Y.; Bhushan, B., Wear-Resistant and Antismudge Superoleophobic Coating on Polyethylene Terephthalate Substrate Using SiO2 Nanoparticles. *ACS Applied Materials & Interfaces* **2015,** *7* (1), 743-755.
2. Rangel, T. C.; Michels, A. F.; Horowitz, F. v.; Weibel, D. E., Superomniphobic and Easily Repairable Coatings on Copper Substrates Based on Simple Immersion or Spray Processes. *Langmuir* **2015,** *31* (11), 3465-3472.
3. Howarter, J. A.; Genson, K. L.; Youngblood, J. P., Wetting Behavior of Oleophobic Polymer Coatings Synthesized from Fluorosurfactant-Macromers. *ACS Applied Materials & Interfaces* **2011,** *3* (6), 2022-2030.
4. Akhtar, N.; Holm, V. r. R. A.; Thomas, P. J.; Svardal, B.; Askeland, S. H.; Holst, B., Underwater Superoleophobic Sapphire (0001) Surfaces. *The Journal of Physical Chemistry C* **2015,** *119* (27), 15333-15338.
5. Damle, V. G.; Tummala, A.; Chandrashekar, S.; Kido, C.; Roopesh, A.; Sun, X.; Doudrick, K.; Chinn, J.; Lee, J. R.; Burgin, T. P.; Rykaczewski, K., "Insensitive" to Touch: Fabric-Supported Lubricant-Swollen Polymeric Films for Omniphobic Personal Protective Gear. *ACS Applied Materials & Interfaces* **2014,** *7* (7), 4224-4232.
6. Mohanty, A. K.; Mistri, E. A.; Banerjee, S.; Komber, H.; Voit, B., Highly Fluorinated Sulfonated Poly(arylene ether sulfone) Copolymers: Synthesis and Evaluation of Proton Exchange Membrane Properties. *Industrial & Engineering Chemistry Research* **2013,** *52* (8), 2772-2783.
7. Zhu, X.; Zhang, H.; Zhang, Y.; Liang, Y.; Wang, X.; Yi, B., An Ultrathin Self-Humidifying Membrane for PEM Fuel Cell Application:Fabrication, Characterization, and Experimental Analysis. *The Journal of Physical Chemistry B* **2006,** *110* (29), 14240-14248.
8. Gauthier, E.; Hellstern, T.; Kevrekidis, I. G.; Benziger, J., Drop Detachment and Motion on Fuel Cell Electrode Materials. *ACS Applied Materials & Interfaces* **2012,** *4* (2), 761-771.
9. Subianto, S.; Mistry, M. K.; Choudhury, N. R.; Dutta, N. K.; Knott, R., Composite Polymer Electrolyte Containing Ionic Liquid and Functionalized Polyhedral Oligomeric Silsesquioxanes for Anhydrous PEM Applications. *ACS Applied Materials & Interfaces* **2009,** *1* (6), 1173-1182.
10. Valade, D.; Boschet, F.; Ameduri, B., Synthesis and Modification of Alternating Copolymers Based on Vinyl Ethers, Chlorotrifluoroethylene, and Hexafluoropropylene *Macromolecules* **2009,** *42* (20), 7689-7700.
11. Ghosh, S.; Mukherjee, R.; Ghosh, A.; Mohanty, A. K.; Banerjee, S., 2 - Fluorinated Poly(Arylene Ether)s: Synthesis, Properties, and Applications. In *Handbook of Specialty Fluorinated Polymers*, William Andrew Publishing: 2015; pp 11-96.
12. Zheng, X.; Guo, Z.; Tian, D.; Zhang, X.; Li, W.; Jiang, L., Underwater Self-Cleaning Scaly Fabric Membrane for Oily Water Separation. *ACS Applied Materials & Interfaces* **2015,** *7* (7), 4336-4343.

13. Oikawa, Y.; Saito, T.; Yamada, S.; Sugiya, M.; Sawada, H., Preparation and Surface Property of Fluoroalkyl End-Capped Vinyltrimethoxysilane Oligomer/Talc Composite-Encapsulated Organic Compounds: Application for the Separation of Oil and Water. *ACS Applied Materials & Interfaces* **2015,** *7* (25), 13782-13793.
14. Hsu, S.-H.; Chang, Y.-L.; Tu, Y.-C.; Tsai, C.-M.; Su, W.-F., Omniphobic Low Moisture Permeation Transparent Polyacrylate/Silica Nanocomposite. *ACS Applied Materials & Interfaces* **2013,** *5* (8), 2991-2998.
15. Velleman, L.; Losic, D.; Shapter, J. G., The effects of surface functionality positioning on the transport properties of membranes. *Journal of Membrane Science* **2012,** *411-412*, 211-218.
16. Neinhuis, C.; Barthlott, W., Characterization and Distribution of Water-repellent, Self-cleaning Plant Surfaces. *Annals of Botany* **1997,** *79* (6), 667-677.
17. Barthlott, W.; Neinhuis, C., Purity of the sacred lotus, or escape from contamination in biological surfaces. *Planta* **1997,** *202* (1), 1-8.
18. Koch, K.; Bhushan, B.; Jung, Y. C.; Barthlott, W., Fabrication of artificial Lotus leaves and significance of hierarchical structure for superhydrophobicity and low adhesion. *Soft Matter* **2009,** *5* (7), 1386-1393.
19. Zimmermann, J.; Rabe, M.; Artus, G. R. J.; Seeger, S., Patterned superfunctional surfaces based on a silicone nanofilament coating. *Soft Matter* **2008,** *4* (3), 450-452.
20. Latthe, S.; Terashima, C.; Nakata, K.; Fujishima, A., Superhydrophobic Surfaces Developed by Mimicking Hierarchical Surface Morphology of Lotus Leaf. *Molecules* **2014,** *19* (4), 4256.
21. Guo, Z.; Zhou, F.; Hao, J.; Liu, W., Stable Biomimetic Super-Hydrophobic Engineering Materials. *Journal of the American Chemical Society* **2005,** *127* (45), 15670-15671.
22. Fukada, K.; Nishizawa, S.; Shiratori, S., Antifouling property of highly oleophobic substrates for solar cell surfaces. *Journal of Applied Physics* **2014,** *115* (10), 103516.
23. Vilcnik, A.; Jerman, I.; Surca Vuk, A.; Kozelj, M.; Orel, B.; Tomsic, B.; Simoncic , B.; Kovac, J., Structural Properties and Antibacterial Effects of Hydrophobic and Oleophobic Sol-Gel Coatings for Cotton Fabrics. *Langmuir* **2009,** *25* (10), 5869-5880.
24. Lejars, M.; Margaillan, A.; Bressy, C., Fouling Release Coatings: A Nontoxic Alternative to Biocidal Antifouling Coatings. *Chemical Reviews* **2012,** *112* (8), 4347-4390.
25. Duong, T. H.; Briand, J.-F.; Margaillan, A.; Bressy, C., Polysiloxane-Based Block Copolymers with Marine Bacterial Anti-Adhesion Properties. *ACS Applied Materials & Interfaces* **2015,** *7* (28), 15578-15586.
26. Gugliuzza, A.; Drioli, E., A review on membrane engineering for innovation in wearable fabrics and protective textiles. *Journal of Membrane Science* **2013,** *446*, 350-375.
27. Luo, B. H. e. a., *Surface geometrical model modification and contact angle prediction for the laser patterned steel surface*. *Surface and Coatings Technology* **2010,** *205* (7), **2597-2604**.

28. Hsieh, C.-T., B.-S. Chang, and J.-Y. Lin, *I*mprovement of water and oil repellency on wood substrates by using fluorinated silica nanocoating. *Applied Surface Science* **2011,** *257* (18), 7997-8002.
29. Yan, L.; Ziyin, L.; Kyoung Sik, M.; Wong, C. P. In Novel ZnO nanowires/silicon hierarchical structures for superhydrophobic, low reflection, and high efficiency solar cells, *Electronic Components and Technology Conferenc*e (ECTC), 2011 IEEE 61st, May 31 2011-June 3 2011; 2011; pp 2114-2118.
30. Aulin, C.; Yun, S. H.; Wagberg, L.; Lindstrom, T., Design of Highly Oleophobic Cellulose Surfaces from Structured Silicon Templates. *ACS Applied Materials & Interfaces* **2009,** *1* (11), 2443-2452.
31. Ou, J.; Hu, W.; Liu, S.; Xue, M.; Wang, F.; Li, W., Superoleophobic Textured Copper Surfaces Fabricated by Chemical Etching/Oxidation and Surface Fluorination. *ACS Applied Materials & Interfaces* **2013,** *5* (20), 10035-10041.
32. Barthwal, S.; Kim, Y.; Lim, S.-H., Superhydrophobic and superoleophobic copper plate fabrication using alkaline solution assisted surface oxidation methods. *International Journal of Precision Engineering and Manufacturing* **2012,** *13* (8), 1311-1315.
33. Meng, H.; Wang, S.; Xi, J.; Tang, Z.; Jiang, L., Facile Means of Preparing Superamphiphobic Surfaces on Common Engineering Metals. *The Journal of Physical Chemistry C* **2008,** *112* (30), 11454-11458.
34. Lecollinet, G.; Delorme, N.; Edely, M.; Gibaud, A.; Bardeau, J. F.; Hindra, F.; Boury, F.; Portet, D., Self-Assembled Monolayers of Bisphosphonates: Influence of Side Chain Steric Hindrance. *Langmuir* **2009,** *25* (14), 7828-7835.
35. Kota, A. K.; Li, Y.; Mabry, J. M.; Tuteja, A., Hierarchically Structured Superoleophobic Surfaces with Ultralow Contact Angle Hysteresis. *Advanced Materials* **2012,** *24* (43), 5838-5843.
36. Hare, E. F.; Shafrin, E. G.; Zisman, W. A., Properties of Films of Adsorbed Fluorinated Acids. *The Journal of Physical Chemistry* **1954,** *58* (3), 236-239.
37. Bernett, M. K.; Zisman, W. A., Wetting of Low-Energy Solids by Aqueous Solutions of Highly Fluorinated Acids and Salts. *The Journal of Physical Chemistry* **1959,** *63* (11), 1911-1916.
38. Miccio, L. A.; Fasce, D. P.; Schreiner, W. H.; Montemartini, P. E.; Oyanguren, P. A., Influence of fluorinated acids bonding on surface properties of crosslinked epoxy-based polymers. *European Polymer Journal* **2010,** *46* (4), 744-753.
39. Pellerite, M. J.; Wood, E. J.; Jones, V. W., Dynamic Contact Angle Studies of Self-Assembled Thin Films from Fluorinated Alkyltrichlorosilanes. *The Journal of Physical Chemistry B* **2002,** *106* (18), 4746-4754.
40. Cao, L.; Gao, D., Transparent superhydrophobic and highly oleophobic coatings. *Faraday Discussions* **2010,** *146* (0), 57-65.
41. Li, H.; Wang, X.; Song, Y.; Liu, Y.; Li, Q.; Jiang, L.; Zhu, D., Super-"Amphiphobic" Aligned Carbon Nanotube Films. *Angewandte Chemie International Edition* **2001,** *40* (9), 1743-1746.
42. Shang, H. M.; Wang, Y.; Limmer, S. J.; Chou, T. P.; Takahashi, K.; Cao, G. Z., Optically transparent superhydrophobic silica-based films. *Thin Solid Films* **2005,** *472* (1-2), 37-43.

43. Valipour Motlagh, N.; Sargolzaei, J.; Shahtahmassebi, N., Super-liquid-repellent coating on the carbon steel surface. *Surface and Coatings Technology* **2013,** *235*, 241-249.
44. Yague, J. L.; Gleason, K. K., Enhanced Cross-Linked Density by Annealing on Fluorinated Polymers Synthesized via Initiated Chemical Vapor Deposition To Prevent Surface Reconstruction. *Macromolecules* **2013,** *46* (16), 6548-6554.
45. Li, G.; Xu, A.; Geng, B.; Yang, S.; Wu, G.; Zhang, S., Synthesis and characterization of fluorinated diblock copolymer of 2,2,2-trifluoroethyl methacrylate and methyl methacrylate based on RAFT polymerzation. *Journal of Fluorine Chemistry* **2014,** *165*, 132-137.
46. Conte, P.; Darmanin, T.; Guittard, F., Spider-web-like fiber toward highly oleophobic fluorinated materials with low bioaccumulative potential. *Reactive and Functional Polymers* **2014,** *74*, 46-51.
47. Darmanin, T.; Guittard, F., Superoleophobic polymers with metal ion affinity toward materials with both oleophobic and hydrophilic properties. *Journal of Colloid and Interface Science* **2013,** *408*, 101-106.
48. Zhu, X.; Loo, H.-E.; Bai, R., A novel membrane showing both hydrophilic and oleophobic surface properties and its non-fouling performances for potential water treatment applications. *Journal of Membrane Science* **2013,** *436*, 47-56.
49. Crawford, R. J.; Ivanova, E. P.; Ivanova, R. J. C. P., Chapter Five - Superhydrophobic Polymers. In *Superhydrophobic Surfaces*, Elsevier: Amsterdam, 2015; pp 67-85.
50. Wankhede, R. G.; Morey, S.; Khanna, A. S.; Birbilis, N., Development of water-repellent organic-inorganic hybrid sol-gel coatings on aluminum using short chain perfluoro polymer emulsion. *Applied Surface Science* **2013,** *283*, 1051-1059.
51. Coclite, A. M.; Shi, Y.; Gleason, K. K., Grafted Crystalline Poly-Perfluoroacrylate Structures for Superhydrophobic and Oleophobic Functional Coatings. *Advanced Materials* **2012,** *24* (33), 4534-4539.
52. Licchelli, M.; Marzolla, S. J.; Poggi, A.; Zanchi, C., Crosslinked fluorinated polyurethanes for the protection of stone surfaces from graffiti. *Journal of Cultural Heritage* **2010,** *12* (1), 34-43.
53. Brown, P. S.; Bhushan, B., Mechanically durable, superomniphobic coatings prepared by layer-by-layer technique for self-cleaning and anti-smudge. *Journal of Colloid and Interface Science* **2015,** *456*, 210-218.
54. Li, Y.; Liu, F.; Sun, J., A facile layer-by-layer deposition process for the fabrication of highly transparent superhydrophobic coatings. *Chemical Communications* **2009,** (19), 2730-2732.
55. Zhao, N.; Weng, L.; Zhang, X.; Xie, Q.; Zhang, X.; Xu, J., A Lotus-Leaf-Like Superhydrophobic Surface Prepared by Solvent-Induced Crystallization. *ChemPhysChem* **2006,** *7* (4), 824-827.
56. Yang, J.; Pi, P.; Wen, X.; Zheng, D.; Xu, M.; Cheng, J.; Yang, Z., A novel method to fabricate superhydrophobic surfaces based on well-defined mulberry-like particles and self-assembly of polydimethylsiloxane. *Applied Surface Science* **2009,** *255* (6), 3507-3512.

57. Periolatto, M.; Ferrero, F., Cotton and polyester surface modification by methacrylic silane and fluorinated alkoxysilane via sol-gel and UV-curing coupled process. *Surface and Coatings Technology* **2014,** *271*, 165-173.
58. Harton, S. E.; Templeman, C. G.; Vyletel, B., Percolation-Driven Multiscale Roughening for Superhydrophobic Polymer Nanocomposite Coatings. *Macromolecules* **2010,** *43* (7), 3173-3176.
59. Cao, L.; Jones, A. K.; Sikka, V. K.; Wu, J.; Gao, D., Anti-Icing Superhydrophobic Coatings. *Langmuir* **2009,** *25* (21), 12444-12448.
60. Hird, M., Fluorinated liquid crystals - properties and applications. *Chemical Society Reviews* **2007,** *36* (12), 2070-2095.
61. Krafft, M. P.; Riess, J. G., Chemistry, Physical Chemistry, and Uses of Molecular Fluorocarbon-Hydrocarbon Diblocks, Triblocks, and Related Compounds-Unique Apolar Components for Self-Assembled Colloid and Interface Engineering. *Chemical Reviews* **2009,** *109* (5), 1714-1792.
62. Giannetti, E., Thermal stability and bond dissociation energy of fluorinated polymers: A critical evaluation. *Journal of Fluorine Chemistry* **2005,** *126* (4), 623-630.
63. Hsieh, C.-T.; Chang, B.-S.; Lin, J.-Y., Improvement of water and oil repellency on wood substrates by using fluorinated silica nanocoating. *Applied Surface Science* **2011,** *257* (18), 7997-8002.
64. Guo, J.; Resnick, P.; Efimenko, K.; Genzer, J.; DeSimone, J. M., Alternative Fluoropolymers to Avoid the Challenges Associated with Perfluorooctanoic Acid. *Industrial & Engineering Chemistry Research* **2008,** *47* (3), 502-508.
65. Saini, G.; Sautter, K.; Hild, F. E.; Pauley, J.; Linford, M. R., Two-silane chemical vapor deposition treatment of polymer (nylon) and oxide surfaces that yields hydrophobic (and superhydrophobic), abrasion-resistant thin films. *Journal of Vacuum Science ; Technology A* **2008,** *26* (5), 1224-1234.
66. Jeong, H.-J.; Kim, D.-K.; Lee, S.-B.; Kwon, S.-H.; Kadono, K., Preparation of Water-Repellent Glass by Sol-Gel Process Using Perfluoroalkylsilane and Tetraethoxysilane. *Journal of Colloid and Interface Science* **2001,** *235* (1), 130-134.
67. Gelest.com Hydrophobicity Hydrophilicity and Silanes.
68. Meiners, F.; Ross, J. H.; Brand, I.; Buling, A.; Neumann, M.; Koster, P. J.; Christoffers, J.; Wittstock, G., Modification of silicon oxide surfaces by monolayers of an oligoethylene glycol-terminated perfluoroalkyl silane. *Colloids and Surfaces A: Physicochemical and Engineering Aspects* **2014,** *449*, 31-41.
69. De Marco, C.; Gaidukeviciute, A.; Kiyan, R.; Eaton, S. M.; Levi, M.; Osellame, R.; Chichkov, B. N.; Turri, S., A New Perfluoropolyether-Based Hydrophobic and Chemically Resistant Photoresist Structured by Two-Photon Polymerization. *Langmuir* **2013,** *29* (1), 426-431.
70. Bandyopadhyay, P.; Bera, D.; Banerjee, S., 4 - Fluorinated Polyamides: Synthesis, Properties, and Applications. In *Handbook of Specialty Fluorinated Polymers*, William Andrew Publishing: 2015; pp 187-226.
71. Chu, E. F.; Reddy, V.; Saltman, R. P., Fluoropolymer compositions. Google Patents: 1994.

72. Linear fluoroaliphatic polyesters from long-chain fluorinated diols. *ACS , Division of Polymer Chemistry* **1990,** *31* (1), 318-219.
73. Plunkett, R. J., Tetrafluoroethylene polymers. Google Patents: 1941.
74. Rixens, B. r. r.; Severac, R.; Boutevin, B.; Lacroix-Desmazes, P., Migration of additives in polymer coatings: fluorinated additives and poly(vinylidene chloride)-based matrix. *Polymer* **2005,** *46* (11), 3579-3587.
75. Berneit, M. K., Oligomeric fluorinated additives as surface modifiers for solid polymers. *Polymer Engineering & Science* **1977,** *17* (7), 450-455.
76. Knight, G. J.; Wright, W. W., The thermal degradation of perfluoro polymers. *Journal of Applied Polymer Science* **1972,** *16* (3), 739-748.
77. Decato, S.; Bemis, T.; Madsen, E.; Mecozzi, S., Synthesis and characterization of perfluoro-tert-butyl semifluorinated amphiphilic polymers and their potential application in hydrophobic drug delivery. *Polymer Chemistry* **2014,** *5* (22), 6461-6471.
78. Ebnesajjad, S., Introduction to fluoropolymers. In *Applied Plastics Engineering Handbook*, Elsvier Inc: 2011.
79. Durand, N.; Mariot, D.; Ameduri, B.; Boutevin, B.; Ganachaud, F., Tailored Covalent Grafting of Hexafluoropropylene Oxide Oligomers onto Silica Nanoparticles: Toward Thermally Stable, Hydrophobic, and Oleophobic Nanocomposites. *Langmuir* **2011,** *27* (7), 4057-4067.
80. Zhang, L.; Zha, D.-a.; Du, T.; Mei, S.; Shi, Z.; Jin, Z., Formation of Superhydrophobic Microspheres of Poly(vinylidene fluoride hexafluoropropylene)/Graphene Composite via Gelation. *Langmuir* **2011,** *27* (14), 8943-8949.
81. Yang, Y.; Mike, F. E.; Yang, L.; Liu, W.; Koike, Y.; Okamoto, Y., Investigation of homopolymerization rate of perfluoro-4,5-substituted-2-methylene-1,3-dioxolane derivatives and properties of the polymers. *Journal of Fluorine Chemistry* **2006,** *127* (2), 277-281.
82. Kadayakkara, D. K.; Damodaran, K.; Hitchens, T. K.; Bulte, J. W. M.; Ahrens, E. T., 19F spin lattice relaxation of perfluoropolyethers: Dependence on temperature and magnetic field strength (7.0 14.1 T). *Journal of Magnetic Resonance* **2014,** *242*, 18-22.
83. Hunt, M. O.; Belu, A. M.; Linton, R. W.; DeSimone, J. M., End-functionalized polymers. 1. Synthesis and characterization of perfluoroalkyl-terminated polymers via chlorosilane derivatives. *Macromolecules* **1993,** *26* (18), 4854-4859.
84. Ming, W.; Lou, X.; van de Grampel, R. D.; van Dongen, J. L. J.; van der Linde, R., Partial Fluorination of Hydroxyl End-Capped Oligoesters Revealed by MALDI-TOF Mass Spectrometry. *Macromolecules* **2001,** *34* (7), 2389-2393.
85. Valsecchi, R.; Mutta, F.; De Patto, U.; Tonelli, C., Countercurrent fractionation of methylol-terminated perfluoropolyoxyalkylene oligomers by supercritical carbon dioxide. *The Journal of Supercritical Fluids* **2014,** *88*, 85-91.
86. Zhang, H.; Zheng, J.; Zhao, Z.; Han, C. C., Role of wettability in interfacial polymerization based on PVDF electrospun nanofibrous scaffolds. *Journal of Membrane Science* **2013,** *442*, 124-130.

87. van de Grampel, R. D.; Ming, W.; van Gennip, W. J. H.; van der Velden, F.; Laven, J.; Niemantsverdriet, J. W.; van der Linde, R., Thermally cured low surface-tension epoxy films. *Polymer* **2005,** *46* (23), 10531-10537.
88. Liu, A.; Goktekin, E.; Gleason, K. K., Cross-Linking and Ultrathin Grafted Gradation of Fluorinated Polymers Synthesized via Initiated Chemical Vapor Deposition To Prevent Surface Reconstruction. *Langmuir* **2014,** *30* (47), 14189-14194.
89. Iacono, S. T.; Budy, S. M.; Mabry, J. M.; Smith, D. W., Synthesis, Characterization, and Surface Morphology of Pendant Polyhedral Oligomeric Silsesquioxane Perfluorocyclobutyl Aryl Ether Copolymers. *Macromolecules* **2007,** *40* (26), 9517-9522.
90. Levi, M.; Turri, S., Equilibrium and non-equilibrium polycondensation process of segmented poly-perfluoro(oxymethylene-ran-oxyethylene)-carbonates. *Journal of Fluorine Chemistry* **2004,** *125* (2), 339-344.
91. Zhao, X.; Chen, W.; Su, Y.; Zhu, W.; Peng, J.; Jiang, Z.; Kong, L.; Li, Y.; Liu, J., Hierarchically engineered membrane surfaces with superior antifouling and self-cleaning properties. *Journal of Membrane Science* **2013,** *441*, 93-101.
92. Genzer, J.; Efimenko, K., Recent developments in superhydrophobic surfaces and their relevance to marine fouling: a review. *Biofouling* **2006,** *22* (5), 339-360.
93. Zheng, F.; Deng, H.; Zhao, X.; Li, X.; Yang, C.; Yang, Y.; Zhang, A., Fluorinated hyperbranched polyurethane electrospun nanofibrous membrane: Fluorine-enriching surface and superhydrophobic state with high adhesion to water. *Journal of Colloid and Interface Science* **2014,** *421*, 49-55.
94. Xu, W.; An, Q.; Hao, L.; Zhang, D.; Zhang, M., Synthesis and characterization of self-crosslinking fluorinated polyacrylate soap-free latices with core-shell structure. *Applied Surface Science* **2012,** *268*, 373-380.
95. Wong, D. H. C.; Thelen, J. L.; Fu, Y.; Devaux, D.; Pandya, A. A.; Battaglia, V. S.; Balsara, N. P.; DeSimone, J. M., Nonflammable perfluoropolyether-based electrolytes for lithium batteries. *Proceedings of the National Academy of Sciences* **2014,** *111* (9), 3327-3331.
96. Schulte, V. A.; Hu, Y.; Diez, M.; Bunger, D.; Moller, M.; Lensen, M. C., A hydrophobic perfluoropolyether elastomer as a patternable biomaterial for cell culture and tissue engineering. *Biomaterials* **2010,** *31* (33), 8583-8595.
97. Wu, J., Perfluoropolyether polymer grafted polyaniline containing intermediate transfer members. Google Patents: 2012.
98. Fabbri, P.; Messori, M.; Pilati, F.; Taurino, R.; Tonelli, C.; Toselli, M., Hydrophobic and oleophobic coatings based on perfluoropolyether/silica hybrids by the sol-gel method. *Advances in Polymer Technology* **2007,** *26* (3), 182-190.
99. O'Rourke Muisener, P. A. V.; Jalbert, C. A.; Yuan, C.; Baetzold, J.; Mason, R.; Wong, D.; Kim, Y. J.; Koberstein, J. T.; Gunesin, B., Measurement and Modeling of End Group Concentration Depth Profiles for Fluorosilane Polystyrene and Its Blends. *Macromolecules* **2003,** *36* (8), 2956-2966.
100. Borkar, S.; Jankova, K.; Siesler, H. W.; Hvilsted, S. r., New Highly Fluorinated Styrene-Based Materials with Low Surface Energy Prepared by ATRP. *Macromolecules* **2004,** *37* (3), 788-794.

101. Munoz Bonilla, A.; Bousquet, A.; Ibarboure, E.; Papon, E.; Labrugere, C.; Rodriguez-Hernandez, J., Fabrication and Superhydrophobic Behavior of Fluorinated Microspheres. *Langmuir* **2010,** *26* (22), 16775-16781.
102. Yokoyama, H.; Sugiyama, K., Surface Hydrophobicity of Fluorinated Block Copolymers Enhanced by Supercritical Carbon Dioxide Annealing. *Langmuir* **2004,** *20* (23), 10001-10006.
103. Agarwal, S.; Horst, S.; Bognitzki, M., Electrospinning of Fluorinated Polymers: Formation of Superhydrophobic Surfaces. *Macromolecular Materials and Engineering* **2006,** *291* (6), 592-601.
104. Ho, T.; Wynne, K. J., A new fluorinated polyurethane: polymerization, characterization, and mechanical properties. *Macromolecules* **1992,** *25* (13), 3521-3527.
105. Jiang, G.; Tuo, X.; Wang, D.; Li, Q., Preparation, characterization, and properties of fluorinated polyurethanes. *Journal of Polymer Science Part A: Polymer Chemistry* **2009,** *47* (13), 3248-3256.
106. Wu, D.; Ming, W.; van Benthem, R. A. T. M.; de With, G., Superhydrophobic Fluorinated Polyurethane Films. *Journal of Adhesion Science and Technology* **2008,** *22* (15), 1869-1881.
107. Manvi, G. N.; Singh, A. R.; Jagtap, R. N.; Kothari, D. C., Isocyanurate based fluorinated polyurethane dispersion for anti-graffiti coatings. *Progress in Organic Coatings* **2012,** *75* (3), 139-146.
108. Synytska, A.; Appelhans, D.; Wang, Z. G.; Simon, F.; Lehmann, F.; Stamm, M.; Grundke, K., Perfluoroalkyl End-Functionalized Oligoesters:Correlation between Wettability and End-Group Segregation. *Macromolecules* **2007,** *40* (2), 297-305.
109. Ming, W.; Laven, J.; van der Linde, R., Synthesis and Surface Properties of Films Based on Solventless Liquid Fluorinated Oligoester. *Macromolecules* **2000,** *33* (18), 6886-6891.
110. Gallardo, A.; San Romun, J.; Dijkstra, P. J.; Feijen, J., Random Polyester Transesterification: Prediction of Molecular Weight and MW Distribution. *Macromolecules* **1998,** *31* (21), 7187-7194.
111. Pavlik, F. J., Esters of perfluoro-tertiaryalkyl alcohols and hydrocarbyl or holo-hydrocarbyl carboxylic acids. Google Patents: 1972.
112. Mera, A. E.; Griffith, J. R., Melt condensation and solution polymerization of highly fluorinated aliphatic polyesters. *Journal of Fluorine Chemistry* **1994,** *69* (2), 151-155.
113. Deopura, B. L.; Padaki, N. V.; Sinclair, R., Chapter 5 - Synthetic Textile Fibres: Polyamide, Polyester and Aramid Fibres. In *Textiles and Fashion*, Woodhead Publishing: 2015; pp 97-114.
114. Odian, G., *Principles of Polymerization*. Wiley: 2004.
115. Voronov, A.; Vasylyev, S.; Kohut, A.; Peukert, W., Surface activity of new invertible amphiphilic polyesters based on poly(ethylene glycol) and aliphatic dicarboxylic acids. *Journal of Colloid and Interface Science* **2008,** *323* (2), 379-385.
116. Sathiskumar, P. S.; Madras, G., Synthesis, characterization, degradation of biodegradable castor oil based polyesters. *Polymer Degradation and Stability* **2011,** *96* (9), 1695-1704.

117. Sharma, V.; Kundu, P. P., Condensation polymers from natural oils. *Progress in Polymer Science* **2008,** *33* (12), 1199-1215.
118. Wang, C.; Shen, B.; Zhou, Y.; Xu, C.; Chen, W.; Zhao, X.; Li, J., Sulfonated aromatic polyamides containing nitrile groups as proton exchange fuel cell membranes. *International Journal of Hydrogen Energy* **2015,** *40* (19), 6422-6429.
119. van Velthoven, J. L. J.; Gootjes, L.; Noordover, B. A. J.; Meuldijk, J., Bio-based, amorphous polyamides with tunable thermal properties. *European Polymer Journal* **2015,** *66*, 57-66.
120. Javadi, A.; Shockravi, A.; Koohgard, M.; Malek, A.; Shourkaei, F. A.; Ando, S., Nitro-substituted polyamides: A new class of transparent and highly refractive materials. *European Polymer Journal* **2015,** *66*, 328-341.
121. Kolb, N.; Winkler, M.; Syldatk, C.; Meier, M. A. R., Long-chain polyesters and polyamides from biochemically derived fatty acids. *European Polymer Journal* **2014,** *51*, 159-166.
122. Bailosky, L. C.; Bender, L. M.; Bode, D.; Choudhery, R. A.; Craun, G. P.; Gardner, K. J.; Michalski, C. R.; Rademacher, J. T.; Stella, G. J.; Telford, D. J., Synthesis of polyether polyols with epoxidized soy bean oil. *Progress in Organic Coatings* **2012,** *76* (12), 1712-1719.
123. Guo, R.; McGrath, J. E., 5.17 - Aromatic Polyethers, Polyetherketones, Polysulfides, and Polysulfones. In *Polymer Science: A Comprehensive Reference*, Elsevier: Amsterdam, 2012; pp 377-430.
124. Rex, W. J.; Tennant, D. J., Polymeric linear terephthalic esters. Google Patents: 1949.
125. Wang, W.; Ding, J.; Xiao, C.; Tang, Z.; Li, D.; Chen, J.; Zhuang, X.; Chen, X., Synthesis of Amphiphilic Alternating Polyesters with Oligo(ethylene glycol) Side Chains and Potential Use for Sustained Release Drug Delivery. *Biomacromolecules* **2011,** *12* (7), 2466-2474.
126. Kadkin, O.; Osajda, K.; Kaszynski, P.; Barber, T. A., Polyester polyols: Synthesis and characterization of diethylene glycol terephthalate oligomers. *Journal of Polymer Science Part A: Polymer Chemistry* **2003,** *41* (8), 1114-1123.
127. Tsai, C.-J.; Chang, W.-C.; Chen, C.-H.; Lu, H.-Y.; Chen, M., Synthesis and characterization of polyesters derived from succinic acid, ethylene glycol and 1,3-propanediol. *European Polymer Journal* **2008,** *44* (7), 2339-2347.
128. Tang, J.; Zhang, Z.; Song, Z.; Chen, L.; Hou, X.; Yao, K., Synthesis and characterization of elastic aliphatic polyesters from sebacic acid, glycol and glycerol. *European Polymer Journal* **2006,** *42* (12), 3360-3366.
129. Shanmugam, T.; Sivakumar, C.; Nasar, A. S., Hydroxyl-terminated hyperbranched aromatic poly(ether-ester)s: Synthesis, characterization, end-group modification, and optical properties. *Journal of Polymer Science Part A: Polymer Chemistry* **2008,** *46* (16), 5414-5430.
130. W, L. L.; Dong, T., Process for preparing high molecular weight polyesters. Google Patents: 2008.

131. Xun, M.-M.; Liu, Y.-H.; Guo, Q.; Zhang, J.; Zhang, Q.-F.; Wu, W.-X.; Yu, X.-Q., Low molecular weight PEI-appended polyesters as non-viral gene delivery vectors. *European Journal of Medicinal Chemistry* **2014,** *78*, 118-125.
132. Fakirov, S.; Gogeva, T., Poly(ether/ester)s based on poly(butylene terephthalate) and poly(ethylene glycol), 1. Poly(ether/ester)s with various polyether: polyester ratios. *Die Makromolekulare Chemie* **1990,** *191* (3), 603-614.
133. Langer, M. E.; Kwoh, D.; Khorshahi, F.; Jensen, A., Synthesis of polyesters from dimethyl terephthalate, ethylene glycol, poly(ethylene glycol) and 4,4'-bis(carbomethoxy)stilbene, and characterization by 1H and 2-D NMR. *Polymer* **1992,** *33* (22), 4862-4865.
134. Tsanaktsis, V.; Vouvoudi, E.; Papageorgiou, G. Z.; Papageorgiou, D. G.; Chrissafis, K.; Bikiaris, D. N., Thermal degradation kinetics and decomposition mechanism of polyesters based on 2,5-furandicarboxylic acid and low molecular weight aliphatic diols. *Journal of Analytical and Applied Pyrolysis* **2015,** *112*, 369-378.
135. Kandola, B. K.; Krishnan, L.; Deli, D.; Ebdon, J. R., Blends of unsaturated polyester and phenolic resins for application as fire-resistant matrices in fibre-reinforced composites. Part 2: Effects of resin structure, compatibility and composition on fire performance. *Polymer Degradation and Stability* **2015,** *113*, 154-167.
136. Segal, E. M.; Rhode-Barbarigos, L.; Adriaenssens, S.; Filomeno Coelho, R. D., Multi-objective optimization of polyester-rope and steel-rope suspended footbridges. *Engineering Structures* **2015,** *99*, 559-567.
137. Majumdar, A.; Butola, B. S.; Thakur, S., Development and performance optimization of knitted antibacterial materials using polyester-silver nanocomposite fibres. *Materials Science and Engineering: C* **2015,** *54*, 26-31.
138. Naskar, A. K.; Mukherjee, A. K.; Mukhopadhyay, R., Studies on tyre cords: degradation of polyester due to fatigue. *Polymer Degradation and Stability* **2004,** *83* (1), 173-180.
139. Kikuchi, H.; Funayama, Y.; Hanawa, H.; Honda, Y.; Ushiwata, T.; Nabeshima, S., Polyester imide resin insulating coating material, insulated wire using same, and coil. Google Patents: 2015.
140. Pimpan, V.; Sirisook, R.; Chuayjuljit, S., Synthesis of unsaturated polyester resin from postconsumer PET bottles: Effect of type of glycol on characteristics of unsaturated polyester resin. *Journal of Applied Polymer Science* **2003,** *88* (3), 788-792.
141. Shenoy, M. A.; Pereira, E. A.; Parikh, P. F., Aromatic polyesters based on bisphenol-A for liquid insulating systems: A synthetic approach. *Journal of Applied Polymer Science* **2005,** *95* (3), 606-614.
142. Donahue, C. J.; Exline, J. A.; Warner, C., Chemical Recycling of Pop Bottles: The Synthesis of Dibenzyl Terephthalate from the Plastic Polyethylene Terephthalate. *Journal of Chemical Education* **2003,** *80* (1), 79.
143. Shukla, B.; Dixit, V.; Singhal, R.; Nagpal, A. K.; Singh, P. K., Synthesis and Characterization of Solventless Polyester Varnish Based on Di Cyclo Penta Diene (DCPD). *Polymer-Plastics Technology and Engineering* **2007,** *46* (3), 191-198.
144. Jariwala, C. P.; Klun, T. P.; Linert, J. G.; Stern, R. M., Water- and oil-repellent compositions. Google Patents: 2005.

145. Weider, R.; Negele, M., Aromatic polyesters and polyester-carbonates having specific fluorine-containing bisphenol components, their preparation and their use. Google Patents: 1992.
146. Hayward, J.; Orem, M. W.; Reafler, G. G., Adhesion promoting composition and coated film. Google Patents: 1990.
147. Swartz, F., *Bull. Acad Royl. Belg.* **1892,** *3* (24), 474.
148. Burgoyne, E. E. and C. F. E., 2-Methylpentyl Trifluoroacetate. *This Journal* **1950,** *78*, 3276.
149. Paul, R.; Schweiker, G. C., Condensation elastomers from fluorine containing dicarboxylic compounds. Google Patents: 1962.
150. Keller, T. M., Synthesis of linear polyesters from fluorine-containing tertiary diols. *Journal of Polymer Science: Polymer Chemistry Edition* **1984,** *22* (10), 2719-2720.
151. Schweiker, G. C.; Robitschek, P., Condensation polymers containing fluorine. I. Synthesis of linear polyesters from fluorine-containing diols. *Journal of Polymer Science* **1957,** *24* (105), 33-41.
152. Zhu, Q.; Han, C. C., Synthesis and crystallization behaviors of highly fluorinated aromatic polyesters. *Polymer* **2007,** *48* (13), 3624-3631.
153. Zhang, L.; Huang, W.-Y., Synthesis of polyfluorinated aromatic polyesters. *Journal of Fluorine Chemistry* **2000,** *102* (12), 55-59.
154. Palsule, A. S.; Poojari, Y., Enzymatic synthesis of silicone fluorinated aliphatic polyesteramides. *Polymer* **2010,** *51* (26), 6161-6167.
155. Huang, Z.-Z.; Pei, X.-L.; Wu, T.; Sheng, S.-R.; Lin, S.-Y.; Song, C.-S., Synthesis and characterization of new fluorinated aromatic polyesters containing trifluoromethylphenoxy pendant groups. *Journal of Applied Polymer Science* **2010,** *119* (2), 702-708.
156. R, P. J.; W, P. E., Fluorine-containing linear polyesters. Google Patents: 1971.
157. Braun, M. J., Electronic device having a barrier film, barrier film for electronic devices, and use of and process for manufacturing the same. Google Patents: 2013.
158. Fei, X.; Hu, J.; Zhang, H.; Sha, P.; Piao, J.; Cui, Z.; Zhang, D., Synthesis of crosslinkable fluorinated polyesters for optical waveguide devices. *Journal of Polymer Science Part A: Polymer Chemistry* **2007,** *45* (24), 5923-5931.
159. M, O., Use of soluble fluoroaliphatic oligomers in resin composite articles. Google Patents: 1974.
160. Choi, E. J.; Hill, D. J. T.; Kim, K. Y.; O'Donnell, J. H.; Pomery, P. J., Synthesis, thermal and radiation sensitivities of fluorine containing methylene-bridged aromatic polyesters. *Polymer* **1997,** *38* (14), 3669-3676.
161. Kim, O.; Gross, R. A.; Hammar, W. J.; Newmark, R. A., Microbial Synthesis of Poly(hydroxyalkanoates) Containing Fluorinated Side-Chain Substituents. *Macromolecules* **1996,** *29* (13), 4572-4581.
162. Reis-Nunes, R. C.; Riande, E.; Chavez, N. C.; Guzman, J., Comparative Study of the Conformational Characteristics of Partially Fluorinated Polyesters and Their Hydrogenated Counterparts. *Macromolecules* **1996,** *29* (24), 7989-7994.
163. Thomas, R. R.; Lloyd, K. G.; Stika, K. M.; Stephans, L. E.; Magallanes, G. S.; Dimonie, V. L.; Sudol, E. D.; El-Aasser, M. S., Low Free Energy Surfaces Using Blends

of Fluorinated Acrylic Copolymer and Hydrocarbon Acrylic Copolymer Latexes. *Macromolecules* **2000,** *33* (23), 8828-8841.
164. Linemann, R. F.; Malner, T. E.; Brandsch, R.; Bar, G.; Ritter, W.; Mulhaupt, R., Latex Blends of Fluorinated and Fluorine-Free Acrylates: Emulsion Polymerization and Tapping Mode Atomic Force Microscopy of Film Formation. *Macromolecules* **1999,** *32* (6), 1715-1721.
165. Walz, S. M.; Malner, T. E.; Mueller, U.; Muelhaupt, R., Depth profiling of latex blends of fluorinated and fluorine-free acrylates with laser-induced secondary mass spectrometry. *Journal of Polymer Science Part B: Polymer Physics* **2003,** *41* (4), 360-367.
166. Koh, K.; Sugiyama, S.; Morinaga, T.; Ohno, K.; Tsujii, Y.; Fukuda, T.; Yamahiro, M.; Iijima, T.; Oikawa, H.; Watanabe, K.; Miyashita, T., Precision Synthesis of a Fluorinated Polyhedral Oligomeric Silsesquioxane-Terminated Polymer and Surface Characterization of Its Blend Film with Poly(methyl methacrylate). *Macromolecules* **2005,** *38* (4), 1264-1270.
167. Bokerr, A.; Herweg, T.; Reihs, K., Selective Alteration of Polymer Surfaces by Thermal Cleavage of Fluorinated Side Chains. *Macromolecules* **2002,** *35* (13), 4929-4937.
168. Inan, T. Y.; Dogan, H.; Unveren, E. E.; Eker, E., Sulfonated PEEK and fluorinated polymer based blends for fuel cell applications: Investigation of the effect of type and molecular weight of the fluorinated polymers on the membrane's properties. *International Journal of Hydrogen Energy* **2010,** *35* (21), 12038-12053.
169. Affrossman, S.; Bertrand, P.; Hartshorne, M.; Kiff, T.; Leonard, D.; Pethrick, R. A.; Richards, R. W., Surface Segregation in Blends of Polystyrene and Perfluorohexane Double End Capped Polystyrene Studied by Static SIMS, ISS, and XPS. *Macromolecules* **1996,** *29* (16), 5432-5437.
170. Sohn, E.-H.; Kim, B. G.; Chung, J.-S.; Lee, J.C., Comb-like polymer blends of poly(oxyethylene)s with CH3-terminated and CF3-terminated alkylsulfonylmethyl side chains: Effect of terminal CF3 moiety on the surface properties of the blends. *Journal of Colloid and Interface Science* **2010,** *343* (1), 115-124.
171. Politakos, N.; Kortaberria, G.; Zalakain, I.; Mondragon, I.; Avgeropoulos, A., Enhancing the hydrophobic properties of various commercial polymers through mixtures and coatings with a fluorinated diblock copolymer in low concentrations. *European Polymer Journal* **2013,** *49* (7), 1841-1851.
172. Yoon, S. C.; Ratner, B. D., Surface and bulk structure of segmented poly(ether urethanes) with perfluoro chain extenders. 3. Effects of annealing, casting solvent, and casting conditions. *Macromolecules* **1988,** *21* (8), 2401-2404.
173. Iacono, S. T.; Budy, S. M.; Smith, D. W.; Mabry, J. M., Preparation of composite fluoropolymers with enhanced dewetting using fluorinated silsesquioxanes as drop-in modifiers. *Journal of Materials Chemistry 20* (15), 2979-2984.
174. Yang, C.; Castelvetro, V.; Bianchi, S.; Alderighi, M.; Zhang, Y., Hierarchical dual-sized film surface morphologies self-generated from fluorinated binary latex blends boost hydrophobicity and lipophobicity. *Journal of Colloid and Interface Science* **2012,** *378* (1), 210-221.

175. Mielczarski, J. A.; Mielczarski, E.; Galli, G.; Morelli, A.; Martinelli, E.; Chiellini, E., The Surface-Segregated Nanostructure of Fluorinated Copolymer-Poly(dimethylsiloxane) Blend Films. *Langmuir* **2010,** *26* (4), 2871-2876.
176. Sundaram, H. S.; Cho, Y.; Dimitriou, M. D.; Finlay, J. A.; Cone, G.; Williams, S.; Handlin, D.; Gatto, J.; Callow, M. E.; Callow, J. A.; Kramer, E. J.; Ober, C. K., Fluorinated Amphiphilic Polymers and Their Blends for Fouling-Release Applications: The Benefits of a Triblock Copolymer Surface. *ACS Applied Materials & Interfaces* **2011,** *3* (9), 3366-3374.
177. Tanaka, K.; Takahara, A.; Kajiyama, T., Surface Molecular Aggregation Structure and Surface Molecular Motions of High-Molecular-Weight Polystyrene/Low-Molecular-Weight Poly(methyl methacrylate) Blend Films. *Macromolecules* **1998,** *31* (3), 863-869.
178. Iyengar, D. R.; Perutz, S. M.; Dai, C.-A.; Ober, C. K.; Kramer, E. J., Surface Segregation Studies of Fluorine-Containing Diblock Copolymers. *Macromolecules* **1996,** *29* (4), 1229-1234.
179. Lee, W.-K.; Losito, I.; Gardella, J. A.; Hicks, W. L., Synthesis and Surface Properties of Fluorocarbon End-Capped Biodegradable Polyesters. *Macromolecules* **2001,** *34* (9), 3000-3006.
180. Mounir, E. L. S. A.; Takahara, A.; Kajiyama, T., Effect of Chain End Group-Substrate Interaction on Surface Molecular Motion of Polystyrene Ultrathin Films. *Polym J* **1999,** *31* (6), 550-556.
181. Dai, K. H.; Kramer, E. J.; Shull, K. R., Interfacial segregation in two-phase polymer blends with diblock copolymer additives: the effect of homopolymer molecular weight. *Macromolecules* **1992,** *25* (1), 220-225.
182. Bongiovanni, R.; Di Meo, A.; Pollicino, A.; Priola, A.; Tonelli, C., New perfluoropolyether urethane methacrylates as surface modifiers: Effect of molecular weight and end group structure. *Reactive and Functional Polymers* **2008,** *68* (1), 189-200.
183. Lee, H.; Archer, L. A., Functionalizing polymer surfaces by surface migration of copolymer additives: role of additive molecular weight. *Polymer* **2002,** *43* (9), 2721-2728.
184. Hariharan, A.; Kumar, S. K.; Russell, T. P., A lattice model for the surface segregation of polymer chains due to molecular weight effects. *Macromolecules* **1990,** *23* (15), 3584-3592.
185. Wool, R. P., *Polymer Interfaces*. Munchen, 1995.
186. Chhatre, S. S.; Tuteja, A.; Choi, W.; Revaux, A. l.; Smith, D.; Mabry, J. M.; McKinley, G. H.; Cohen, R. E., Thermal Annealing Treatment to Achieve Switchable and Reversible Oleophobicity on Fabrics. *Langmuir* **2009,** *25* (23), 13625-13632.
187. McLain, S. J.; Sauer, B. B.; Firment, L. E., Surface Properties and Metathesis Synthesis of Block Copolymers Including Perfluoroalkyl-Ended Polyethylenes. *Macromolecules* **1996,** *29* (25), 8211-8219.
188. Morra, M., *Water in Biomaterials Surface Science*. John Wiley and Sons: Chichester, 2001.
189. Young, T., An Essay on the Cohesion of Fluids. *Philosophical Transactions of the Royal Society of London* **1805,** *95*, 65-87.

190. Gibbs, J. W., *The collected works of*. London, 1957.
191. Hsiang, H.-I.; Liang, M.-T.; Huang, H.-C.; Yen, F.-S., Preparation of superhydrophobic boehmite and anatase nanocomposite coating films. *Materials Research Bulletin* **2007,** *42* (3), 420-427.
192. Sung, Y. H.; Kim, Y. D.; Choi, H.-J.; Shin, R.; Kang, S.; Lee, H., Fabrication of superhydrophobic surfaces with nano-in-micro structures using UV-nanoimprint lithography and thermal shrinkage films. *Applied Surface Science* **2015,** *349*, 169-173.
193. Huang, Y.-H.; Wu, J.-T.; Yang, S.-Y., Direct fabricating patterns using stamping transfer process with PDMS mold of hydrophobic nanostructures on surface of micro-cavity. *Microelectronic Engineering* **2010,** *88* (6), 849-854.
194. Prakash, R.; Papageorgiou, D. P.; Papathanasiou, A. G.; Kaler, K. V. I. S., Dielectrophoretic liquid actuation on nano-textured super hydrophobic surfaces. *Sensors and Actuators B: Chemical* **2013,** *182*, 351-361.
195. Wenzel, R. N., Resistance of solid surfaces to wetting by water. *Industrial & Engineering Chemistry* **1936,** *28* (8), 988-994.
196. Reprinted from "Reprinted from Thin Solid Films, 434 (1-2), Uelzen, T.; Muller, J., Wettability enhancement by rough surfaces generated by thin film technology. 311-315, Copyright (**2003)** with permission from Elsevier
197. Cassie, A. B. D.; Baxter, S., Wettability of porous surfaces. *Transactions of the Faraday Society* **1944,** *40* (0), 546-551.
198. Neumann, A. W.; Good, R. J.; Hope, C. J.; Sejpal, M., An equation-of-state approach to determine surface tensions of low-energy solids from contact angles. *Journal of Colloid and Interface Science* **1974,** *49* (2), 291-304.
199. Dupre, A., *Theorie Mecanique de La Chaleur*. Gauthier-Villars: Paris, 1869.
200. Girifalco, L. A.; Good, R. J., A Theory for the Estimation of Surface and Interfacial Energies. I. Derivation and Application to Interfacial Tension. *The Journal of Physical Chemistry* **1957,** *61* (7), 904-909.
201. Fowkes, F. M., Attractive forces at interfaces. *Industrial an Engineering Chemistry* **1964,** *56*, 40-52.
202. Owens, D. K.; Wendt, R. C., Estimation of the surface free energy of polymers. *Journal of Applied Polymer Science* **1969,** *13* (8), 1741-1747.
203. Fox, H. W.; Zisman, W. A., The spreading of liquids on low-energy surfaces. II. Modified tetrafluoroethylene polymers. *Journal of Colloid Science* **1952,** *7* (2), 109-121.
204. Fox, H. W.; Zisman, W. A., The spreading of liquids on low-energy surfaces. III. Hydrocarbon surfaces. *Journal of Colloid Science* **1952,** *7* (4), 428-442.
205. Zisman, W. A., Relation of the Equilibrium Contact Angle to Liquid and Solid Constitution. Contact Angle, Wettability, and Adhesion. *American Chemical Society*, Jan 1, 1964, 1-51. DOI:10.1021/ba-1964-0043.ch001.
206. a)http://www.kruss.de/fileadmin/user_upload/website/literature/kruss-tn306-en.pdf .b)https://en.wikipedia.org/wiki/Sessile_drop_technique
207. Mirabedini, S. M.; Pazoki, S.; Esfandeh, M.; Mohseni, M.; Akbari, Z., Comparison of drag characteristics of self-polishing co-polymers and silicone foul release coatings: A study of wettability and surface roughness. *Progress in Organic Coatings* **2006,** *57* (4), 421-429.

208. Stachewicz, U.; Li, S.; Bilotti, E.; Barber, A. H., Dependence of surface free energy on molecular orientation in polymer films. *Applied Physics Letters* **2012,** *100* (9), 094104.
209. Kowalonek, J.; Kaczmarek, H.; DÄ…browska, A., Air plasma or UV-irradiation applied to surface modification of pectin/poly(vinyl alcohol) blends. *Applied Surface Science* **2010,** *257* (1), 325-331.
210. Stachewicz, U.; Barber, A. H., Enhanced Wetting Behavior at Electrospun Polyamide Nanofiber Surfaces. *Langmuir* **2011,** *27* (6), 3024-3029.

CHAPTER THREE

EXPERIMENTAL

3.1. Chemical reagents used

Hydrogen peroxide:

Company Identification: Acros Organics.

MSDS Name: Hydrogen Peroxide (30% in Water) (Without Stabilizer), Reagent ACS.

CAS Number: 7722-84-1

Sulfuric acid 98%:

Company Identification: Acros Organics.

MSDS Name: Sulfuric acid, reagent ACS.

CAS Number: 7664-93-9

Chloroform:

Company Identification: VWR International LLC.

MSDS Name: Chloroform, ACS.

CAS Number: 67-66-3

Toluene:

Company Identification: Acros Organics.

MSDS Name: Toluene, reagent ACS.

CAS Number: 108-88-3

Methyl ethyl ketone:

Company Identification: Acros Organics.

MSDS Name: 2-Butanone, 99+%.

CAS Number: 78-93-3

Ethanol:

Company Identification: Mallinckrodt Baker Inc.

MSDS Name: Reagent alcohol, ACS.

CAS Number: 64-17-5

Methanol:

Company Identification: VWR International LLC.

MSDS Name: Methanol, ACS.

CAS Number: 67-56-1

Acetone:

Company Identification: VWR International LLC.

MSDS Name: Acetone, ACS.

CAS Number: 67-64-1

Tetrahydrofuran:

Company Identification: Alfa Aesar.

MSDS Name: Tetrahydrofuran, 99.8%

CAS Number: 109-99-9

1,1,1,3,3,3-Hexafluoro-2-propanol:

Company Identification: Oakwoodchemicals

MSDS Name: 1,1,1,3,3,3-Hexafluoro-2-propanol , 99%

CAS Number: 920-66-1

3.2. Chemicals Used for the Fabrication of Fluorinated Polyesters

Isophthaloyl chloride:

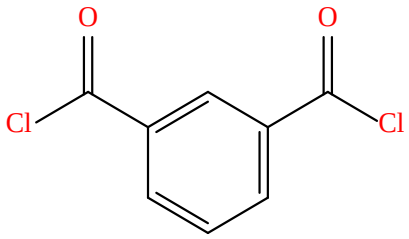

1H,1H,-Perfluoro-3,6,9-trioxatridecan-1-ol (PF-TriOxaTri-OH):

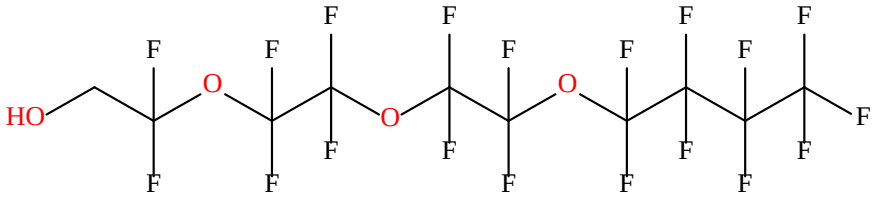

1H,1H,11H,11H-Perfluoro-3,6,9-trioxaundecane-1,11-diol:

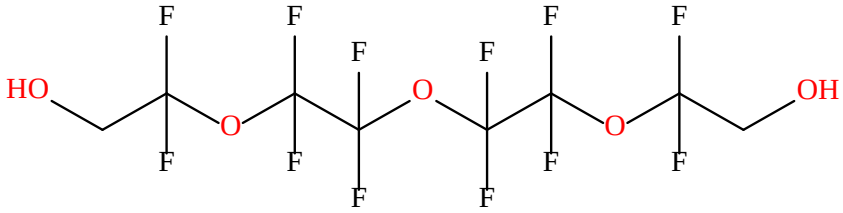

3.3. Structural Characterization Techniques of Polymers

3.3.1. Attenuated Total Reflectance Fourier Transform Infrared (FTIR)

The Fourier transform infrared (FT-IR) technique is used to analyze organic and inorganic chemicals [1]. FT-IR spectroscopy measures the absorption of infrared light by the samples in the wavenumber range of 4000 cm^{-1} to 400 cm^{-1} and yields infrared spectrums. Different functional groups absorb infrared light at different regions. Therefore, this technique is essential to identify and quantify chemicals.

One of the forms of FT-IR spectroscopy is attenuated total reflectance FTIR (ATR-FT-IR) spectroscopy, which is used to analyze solid and liquid chemicals without further preparation. The principle of ATR is that the beam is passed through the ATR crystals, and it reflects into the internal surface in contact with sample (**Figure 3.1**). It was reported in the literature that the penetration depth of the beam into the samples is between 0.5μ and 2μ. Furthermore, it was found that the penetration depth depends on the wavelength of the light, the angle of incidence, and the reflective index of both the ATR crystal and the medium [2]. When the beam exits the crystal, the detector collects the beam.

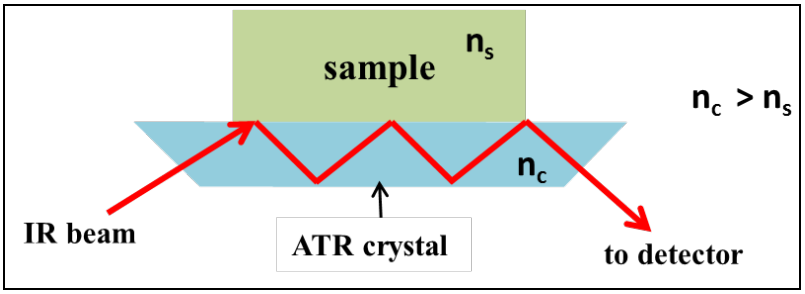

Figure 3.1. Schematic of ATR-FTIR**.**

3.3.2. Thermogravimetric Analysis (TGA)

Thermogravimetric analysis (TGA) is one of the thermal analysis techniques which measure the changes in the physical and chemical properties of a material by monitoring its weight loss or gain as a function of temperature (with constant heating rate) or time (at constant temperature). TGA is generally used to determine the thermal and oxidative stability of materials as well as their purity and humidity [3]. Therefore, it is essential to characterize polymeric materials such as thermoplastics, thermosets,

composites, films and fibers. Generally, the weight loss or gain of polymers due to the decomposition or oxidation is determined before use in different areas [5].

Figure 3.2 shows the TGA result of a poly(ethylene terephthalate) (PET) fiber. The percentage of weight loss of PET as a function of temperature under nitrogen was plotted. Approximately 3 mg of the sample were heated at a rate of 20°C/min. The decomposition temperature of the PET fiber was determined to be around 430°C.

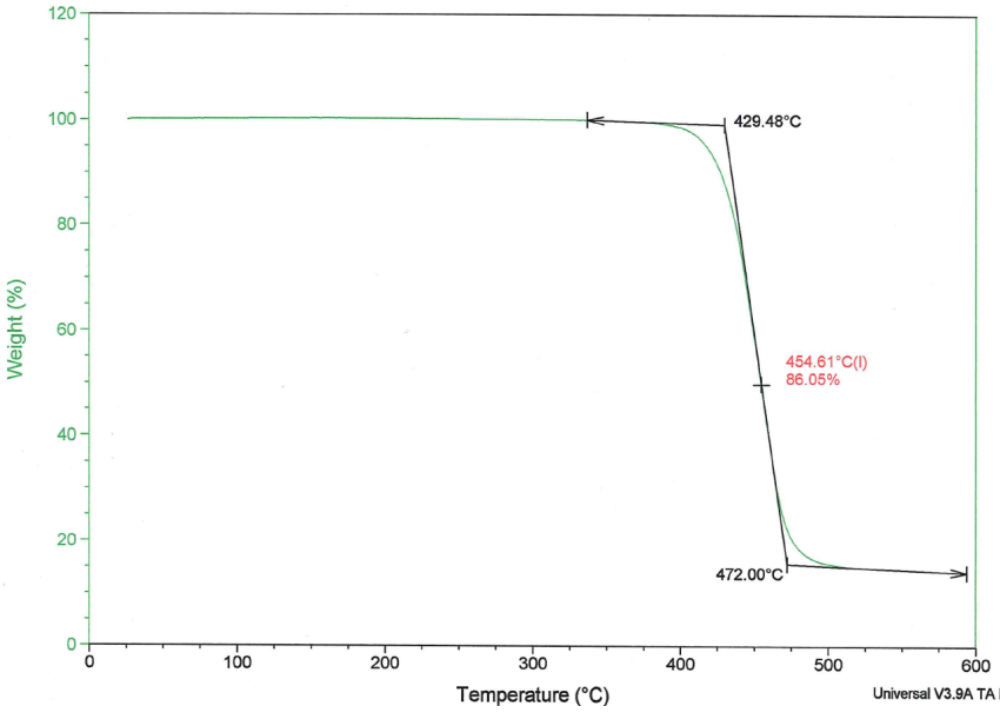

Figure 3.2. TGA of PET.

In this study, TGA analysis was employed to determine the decomposition temperature of fluorinated polyesters. A Perkin Elmer TGA was used, and the sample (-5 mg) was heated under a nitrogen atmosphere (gas flow = 20 mL/min) from 25 to 600°C at a heating rate of 20°C/min.

3.3.3. Differential Scanning Calorimetry (DSC)

Differential Scanning Calorimetry (DSC) measures how the physical properties of a sample change with temperature against time [3]. In other words, DSC measures the temperatures and heat flows associated with transitions in materials as a function of time and temperature in a controlled atmosphere [4, 5]. DCS measurements provide quantitative and qualitative information about physical and chemical changes that involve endothermic or exothermic processes or changes in heat capacity determined using following equation:

$$\Delta H = C_p \Delta T \qquad (3.1)$$

or in differential form

$$\frac{dH}{dt} = C_p \frac{dT}{dt} \qquad (3.2)$$

where ΔH is heat (J), C_p is specific heat (J/g °C), T is temperature (°C), dH/dt is the heat flow (J/min), and dT/dt is the heating rate (°C/min) the melting temperature (T_m), glass transition temperature (T_g) and also crystallization temperature (T_c) are determined by DCS. Furthermore, the percentage of the crystallinity is calculated using DSC data. The result yields the heat as a result of the primary crystallinity of the sample, and the percentage can be calculated by the following equation:

$$\%\ crystallinity = 100\left[\frac{\Delta H_f - \Delta H_c}{\Delta H^f_{crys}}\right] \qquad (3.3)$$

where ΔH_f is the fusion heat of the sample, ΔH_c is the heat of crystallization of the sample, and ΔH^f_{crys} is the enthalpy of fusion of the pure crystalline sample.

In this work, differential scanning calorimetry (DSC) (TA instrument, DSC 2920) is employed to determine the T_g and T_m of synthesized fluorinated polyesters and to calculate their % of crystallinity.

3.3.4. Nuclear Magnetic Resonance Spectroscopy (NMR)

Nuclear magnetic resonance (NMR) spectroscopy is one of the most powerful for determining the purity and concentration of samples as well as the chemical structure of molecules [6]. In this method, nuclei which have spin are used. When nuclei are exposed to an externally applied magnetic field in NMR (**Figure 3.3**), the energy transfer between the base energy level to a higher energy level is obtained. The energy differences between the levels correspond to the radio frequency energy, which is unique for each molecule [7]. Therefore, NMR gives information regarding the structure of the samples.

In this study, fluorine (^{19}F) NMR is used to determine the molecular structure of the fluorinated polyesters. Dried polymers were dissolved in deuterated acetone (with Tetramethylsilane TMS as reference) (30 mg/mL) for 24h. The ^{19}F NMR (300 MHz) of the samples were recorded on a Bruker Avance II spectrometer.

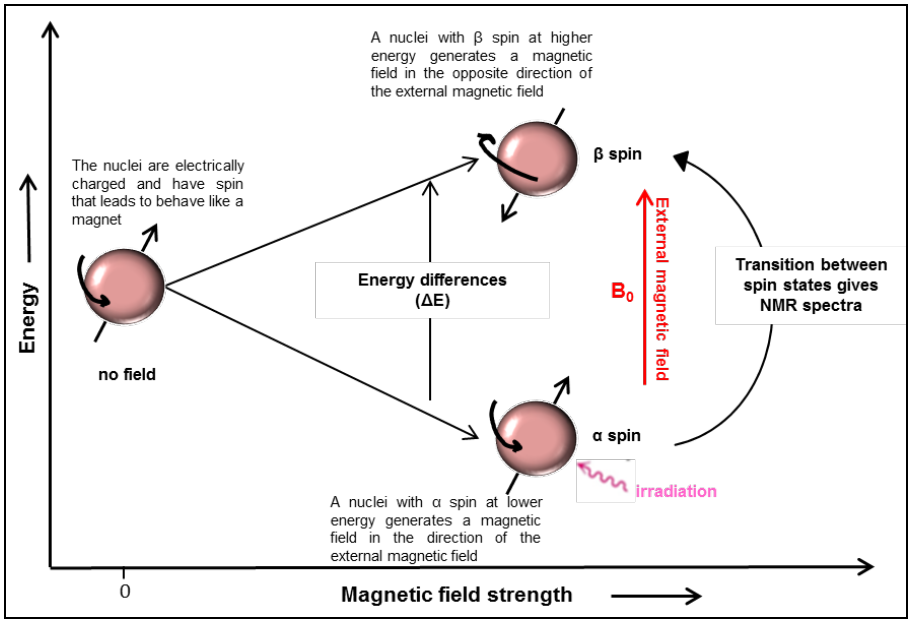

Figure 3.3. Principle of NMR. Redrawn from Ref [8].

3.4. General Experiment Procedures for Preparation of Films

3.4.1. Cleaning of Silicon Wafers

Before the deposition of the polymers onto silicon wafers (SEH America Inc.), they were initially cleaned with deionized water for 30min in a sonicator (75HT, VWR International LLC). During the sonication, the water was changed 3 times. After drying the samples with the steam of high purity nitrogen (National Specialty Gases), the samples were placed into the piranha solution consisting of concentrated sulfuric acid with hydrogen peroxide at a ratio of 3:1 at 80°C for 1h in sonication. The samples were then rinsed with deionized water 5 times and kept in water. They were dried with N_2 before use for polymer deposition.

3.4.2. Dip Coating

Dip coating is a process used for the preparation of thin polymer films on substrates. During coating, a substrate is immersed into a liquid polymer solution and is then withdrawn at a controlled speed **(Figure 3.4).** After solvent evaporation, the dry polymer film covers the substrate. The polymer film thickness is primarily affected by speed control, fluid viscosity, fluid density, and surface tension [9].

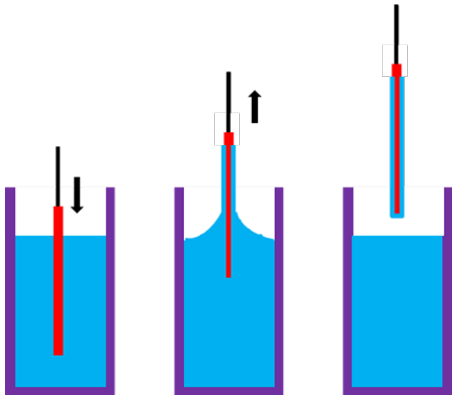

Figure 3.4. Scheme of film deposition by dip coating technique.

If the withdrawal speed is chosen such that the shear rates keep the system in the Newtonian regime, the film thickness can be estimated as [9]

$$h = 0.944\left(\frac{\eta v}{pg}\right)^{1/2}\left(\frac{\eta v}{\gamma}\right)^{1/6} \qquad (3.4)$$

where h is the film thickness, ν is the withdrawal speed, η is the liquid viscosity, ρ is the liquid density, g is the acceleration of gravity, and γ is the liquid surface tension. A Mayer Fientechnik D-3400 dip coater was placed in a clean room to avoid solution and dry film contaminations. Polymer films with different thicknesses were obtained via dip-coating the samples into solutions with different concentrations.

3.5. Polymer Film Characterization

3.5.1. Surface Morphology Characterization

Atomic force microscopy (AFM) is one of the scanning probe techniques used for the characterization of the surface morphology of polymer films and its physical properties on submicron scales (**Figure 3.5**) [10]. In this study, AFM studies were performed using a Dimension 3100 (Digital Instruments, Inc.) microscope. A tapping mode was used to study the surface morphology of the samples in ambient air. Silicon tips from MicroMasch with spring constants of 50 N/m were used. Imaging was done at scan rates in the range of 1-2 Hz.

In addition, the root mean square (RMS) of the film was evaluated by AFM using NanoScope version 5.3.0r3.sr3 software to characterize the roughness of the surfaces. The formula used for calculation RMS is as follows [11]:

$$RMS = \sqrt{\frac{1}{n\sum_{i=1}^{n}(h_1 - \bar{h})^2}} \qquad (3.5)$$

where h_i is the height of the i-th point of the total *n* points on the AFM image, and $\bar{h}$ is the arithmetic mean height of all points. The root mean square roughness calculated in this way statistically characterizes how the surface profile of the film deviates from the ideally flat state.

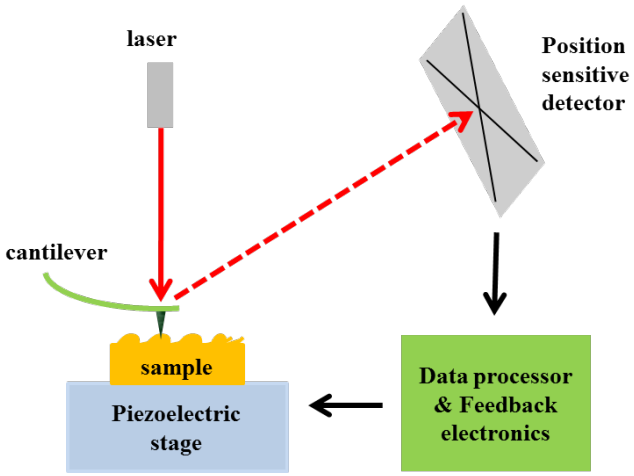

Figure 3.5. Scheme of AFM.

3.5.2. Surface Wettability Characterization

When a drop of liquid is placed on a solid surface, it either spreads to cover all the entire surface or it beads up. This behavior depends on the surface energy of both the liquid and solid. If the surface energy of the solid (γ_{sv}) is lower than that of the liquid (γ_{lv}), the liquid beads up, and thus a definite angle is formed between the solid/liquid interfaces. This angle is referred to as the contact angle (θ_c), as shown in **Figure 3.6.**

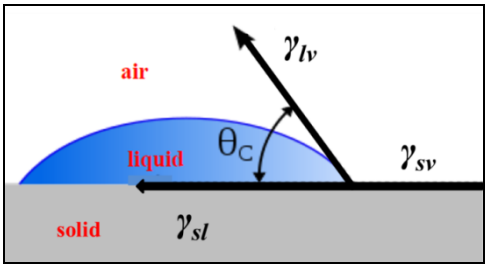

Figure 3.6. Scheme of contac angle of liquid on solid surface.

The determination of the measurements of the contact angle of liquids and their surface energies can be accomplished by the goniometer using an optical system to capture the profile of a pure liquid on a solid surface. The optical system consists of

device to drop accurately controlled volumes of liquid, a stage, a high resolution of camera, and a light source for imaging the shape of the liquid droplet on the solid surface. Then, the contact angle of liquids can be analyzed from images.

In this work, the contact angle measurements of water and hexadecane were conducted at room temperature, using the sessile drop method; equilibrating time was 60 sec. 1 μL droplets were used for all measurements. The results were recorded on a drop shape analysis instrument (DSA, Kruss, Germany) with DSA software, as shown in **Figure 3.7**.

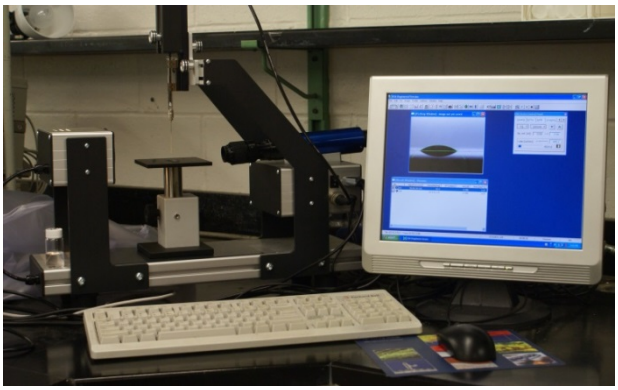

Figure 3.7. Contact angle measurement system (DSA Kruss)

In addition to the CA measurements, the surface free energies of the coatings and the spreading coefficients of hexadecane and water on films were calculated. The CAs on each were measured at least three times, and average values were reported and used for the surface energy calculations. To calculate the surface energies of the coatings, total free surface energy is assumed to be splittable. In other words, the surface free energy is the sum of the dispersive and polar components and can be calculated by the following equation:

$$\gamma_s = \gamma_s^d + \gamma_s^p \qquad (3.6)$$

where γ_s^d and γ_s^p are the dispersive and polar components, respectively, of the surface energy γ_s. These components can be derived from the system of two equations with two unknowns. If the CA with surface θ and the surface tension and polar and dispersive components of at least two liquids are known, we can write [12]

$$1+\cos\theta \approx 2\left[\frac{\sqrt{\gamma_s^d \gamma_1^d} + \sqrt{\gamma_s^p \gamma_1^p}}{\gamma_1}\right] \qquad (3.7a)$$

$$1+\cos\theta \approx 2\left[\frac{\sqrt{\gamma_s^d \gamma_2^d} + \sqrt{\gamma_s^p \gamma_2^p}}{\gamma_2}\right] \qquad (3.7b)$$

where γ_1^d, γ_2^d, γ_1^p, and γ_2^p are the dispersive and polar components of two different liquids (1) and (2), respectively.

3.5.3. Surface Elemental Composition Analysis

X-ray photoelectron spectroscopy (XPS) **(Figure 3.8)** is a surface chemical analysis technique which provides the elemental composition and chemical state information of a sample surface. In XPS, samples are irradiated with a beam of X-rays at specified energy, and then photoelectrons are emitted from the surface [13]. The kinetic energy of these emitted electrons is the experimental quantity measured by the spectrometer and the binding energy, which is a characteristic of the element that the electrons belong to, and can be determined using an equation that is based on the work of Ernest Rutherford (1914):

$$E_B = h\nu - E_K - W \qquad (3.8)$$

where *hv* is the photon (X-ray) energy, E_k is the kinetic energy of electron, and *W* is the work function of the spectrometer. From the binding energy, we can identify the elements on the surface and determine their quantities. It is well known that XPS is surface sensitive since photo-emitted electrons escape only from the top (~10 nm) surface of the sample. Thus, it provides true surface elemental composition information. Ultrahigh vacuum (UHV) is required to prevent interactions between the electrons and the environment.

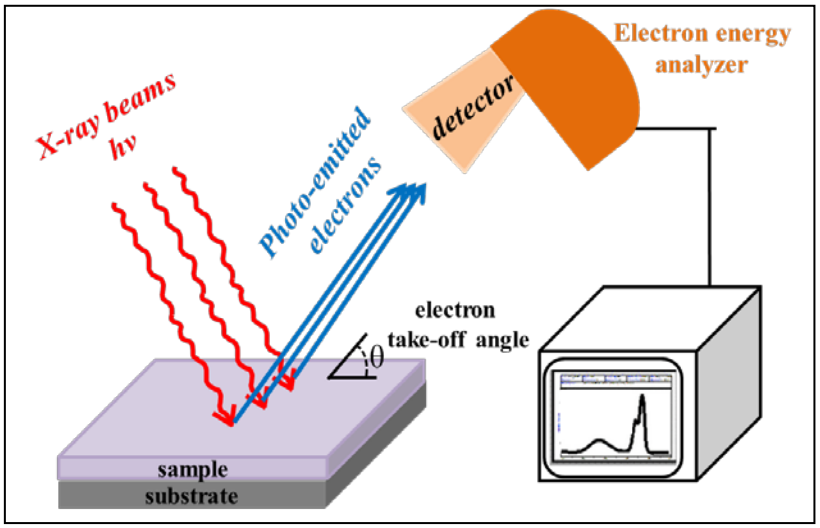

Figure 3.8. Basic components of XPS

In this study, the Kratos Ultra spectrometer of Georgia Institute of Technology was employed to perform XPS analysis. Samples were irradiated with monochromoated X-Rays (Al K_α at 15 kV) with takeoff angles of 0°, 30°, and 60°.

3.6. References

1. Smith, B.C., ed. Fundamentals of Fourier Transform Infrared Spectroscopy. 1996, *CRC Press*: London.
2. Maribella, F.M., Jr., Internal Reflection Spectroscopy:Theory and Applications. Principles, Theory, and Practice of Internal Reflection Spectroscopy, ed. Francis M. Maribella. 1993, New York: *Marcel Dekker,* Inc.
3. Haynie, D.T., Biological Thermodynamics. 2001, Cambridge: *Cambridge University Press.*
4. Haines, P.J. and F.W. Wilburn, Differential thermal analysis and differential scanning calorimetry, in Thermal Methods of Analysis. 1995, *Springer Netherlands.* p. 63-122.
5. Brown, M.E., Handbook of Thermal Analysis and Calorimetry. Vol. *1*. 1998, The Netherlands: *Elsevier Science* B. V.
6. Wrackmeyer, B., Book Review: J. W. Akitt, B. E. Mann. NMR and chemistry: An introduction to modern NMR spectroscopy. 4th edn, *Stanley Thornes (Publishers),* Cheltenham, UK, 2000. 400 pp., price £30. ISBN 0 7487 4344 8. Magnetic Resonance in Chemistry, 2002. **40**(4): p. 316-316.
7. Zheltikov, A., Understanding NMR Spectroscopy, James Keeler, John Wiley & Sons Ltd, Chichester, 2005, pp. 459, paperback, ISBN: 0470017872. J*ournal of Raman Spectroscopy,* 2006. *37*(12): p. 1456-1456.
8. http://chem.ch.huji.ac.il/nmr/whatisnmr/whatisnmr.html
9. Clegg, W., Crystal Structure Determination. *Oxford Chemistry Primers.* 1998: Oxford University Press.
10. Crawford, L.J. and N.R. Edmonds, Calculation of film thickness for dip coated antireflective films. *Thin Solid Film*s, 2006. *515* (3): p. 907-910.
11. Poggi, M.A.G., E.D.; Bottomley, L. A.; King W.P.; Oroudjev, E.; Hansma, H., , Scanning probe microscopy. *Analytical Chemistry,* 2004. ***12***(76): p. 3429-43.
12. Poon, C.Y. and B. Bhushan, Comparison of surface roughness measurements by stylus profiler, AFM and non-contact optical profiler. *Wear,* 1995. 190 (1): p. 76-88.
13. Owens, D.K. and R.C. Wendt, Estimation of the surface free energy of polymers. *Journal of Applied Polymer Science,* 1969. *13* (8): p. 1741-1747.
1. Venables, J.A., An introduction to surface analysis by electron spectroscopy *By John F. Watts Oxford University Press, New York (1990) 86 pages, illustrations $23.95 isbn 0-19-856425-2.* Scanning, 1992. 14 (4): p. 241-241.

CHAPTER FOUR

SYNTHESIS AND CHARACTERIZATION OF FLUORINATED POLYESTERS

4.1. Introduction

After the discovery of poly(tetrafluoro ethylene) (PTFE) [1], fully fluorinated polymers have received significant scientific and industrial attention. Semi-fluorinated polymers consisting of both fluorinated and non-fluorinated segments were also synthesized. To date, a significant number of polymers with fluorinated groups as a side moiety have been reported in the literature, as well. These include fluorinated polyamines [2], polyurethanes [3-6], polyesters [7-9], polysiloxanes [10, 11], polyethers [12], and vinyl polymers, such as polyacrylates/methacrylates [3, 13, 14], and styrenes [15-17]. Among them, fluorinated polymers, which possess either perfluoro side-chains or perfluoro end-groups, have drawn considerable attention due to their low surface energy, low friction coefficient, and ease of synthesis. In addition, most of them are soluble in organic solvents and can be melted unlike PTFE. For instance, Alla Synytska *et al.* synthesized perfluoroalkyl end-functionalized linear aromatic oligoesters [7]. It was found that the fluorinated segments tend to segregate in the surface region and bring the surface concentration of the CF_2 groups up to 2.4 times higher in comparison to their bulk concentration [7]. As a result, low surface energy was observed for the materials.

Numerous fluorinated polymers have been synthesized to employ their low-surface energy properties for industrial applications, such as antifouling [6, 18-20], self-cleaning coatings [18], fuel cells [21], and membranes [6, 22-24]. To the best of our

knowledge, most of the studies have been focused on the synthesis of fully fluorinated and side-chain semi-fluorinated polymers (typically acrylates [13]). There has been limited work reported on the synthesis of semi-fluorinated polymers, which possess fluoro segments in the backbone. In addition, only limited studies on fluorinated condensation polymers were reported in the literature [25-27]. The reason is the difficulty of employment the conventional methods of polymer synthesis, since the electronegativity of fluorine atoms may influence the behavior of fluorinated monomers in the polymerization process [26, 27]. According to literature, the fluorinated polyesters were synthesized by the condensation reaction of hydrocarbon acid (derivatives) with either perfluoro alcohols [26] or hydroxyl-terminated perfluoro ethers [28-31]. Apart from this, several research were done on the condensation polymerization of perfluorinated acid (derivatives) with hydroxyl-terminated polyethers or diols [25, 32-34].

Up to now, numerous patents were focused on the synthesis of aliphatic and aromatic fluorinated polymers. However, there is no significant research that studied fluorinated polyesters containing perfluoro ethers. To fill this gap, we conducted synthesis and characterization of the fluorinated polyesters. Specifically, the synthesis and characterization of fluorinated polyesters consisting of perfluoro ether segments in the backbone is presented in this chapter. In addition, we synthesized the fluorinated polyesters that were terminated with perfluoro ether groups to investigate how they influence the chemical and physical properties of the polyesters. Infrared spectroscopy and nuclear magnetic resonance spectroscopy were used to characterize the chemical

structures of polyesters. Furthermore, the thermal properties of polymers were determined using thermal gravimetric analysis (TGA) and differential scanning calorimetry (DSC).

4.2 Experimental Part

4.2.1 Materials

Fluorinated polyesters were synthesized by the condensation reaction of isophthaloyl chloride (IsoCl) purchased from Sigma-Aldrich, with perfluoro ether alcohols, such as 1H, 1H, 11H, 11H- perfluoro-3,6,9-trioxaundecane-1,11-diol (PF-TriOxaUD-diol) and 1H, 1H-perfluoro-3,6,9-trioxatridecan-1-ol (PF-TriOxaTri-OH), purchased from Synquest Laboratories. Triethylamine (Et_3N) (Sigma Aldrich) was used as an acid acceptor to trap the hydrochloric acid (HCl) formed during the reaction. Methyl ethyl ketone (MEK) (Sigma-Aldrich) was used as a solvent for the polymerization. Methyl ethyl ketone was dried using molecular sieves, as it contains a certain quantity of water, which, at the specific reaction temperature, causes hydrolysis of the chloride, resulting to a lower product yield.

4.2.2 Synthesis of Fluorinated Polyesters

A series of fluorinated polyesters possessing different end-groups were synthesized via polycondensation using the Schotten-Baumann (SB) reaction of IsoCl with perfluoro ether alcohol(s). A scheme of the reaction is given in **Figure 4.1**.

To regulate the end-groups of the fluorinated polyesters in the polycondensation reaction, the degree of polymerization ($\overline{DP}$), depending on the stoichiometric ratio (*r)* and

extent of the reaction/conversion fraction (p), can be quantified by a modified Carother's equation [35]:

$$\overline{DP} = \frac{1+r}{r+1-2rp} \tag{4.1}$$

$$r = N_{OH}^{0} / N_{Cl}^{0} \tag{4.1a}$$

$$p = N_{OH}^{reacted} / N_{OH}^{0} \tag{4.1b}$$

where N_{OH}^{o} and N_{Cl}^{o} are the number of –OH and –Cl groups present at the beginning of the reaction, and $N_{OH}^{reacted}$ is the number of –OH groups reacted with –Cl groups during the reaction.

If r=1, the relationship reduces to

$$\overline{DP} = \frac{1}{1-p} \tag{4.2}$$

When the –OH group is completely used up in the reaction, (that is, when p≈1), the equation becomes

$$\overline{DP} = \frac{1+r}{1-r} \tag{4.3}$$

According to **Equation 4.1**, $\overline{DP}$ is always higher at high conversion reactions, p, than at low conversions. Furthermore, it increases as r goes to unity. In our case, we regulated the end-groups of the fluorinated polyesters by changing r.

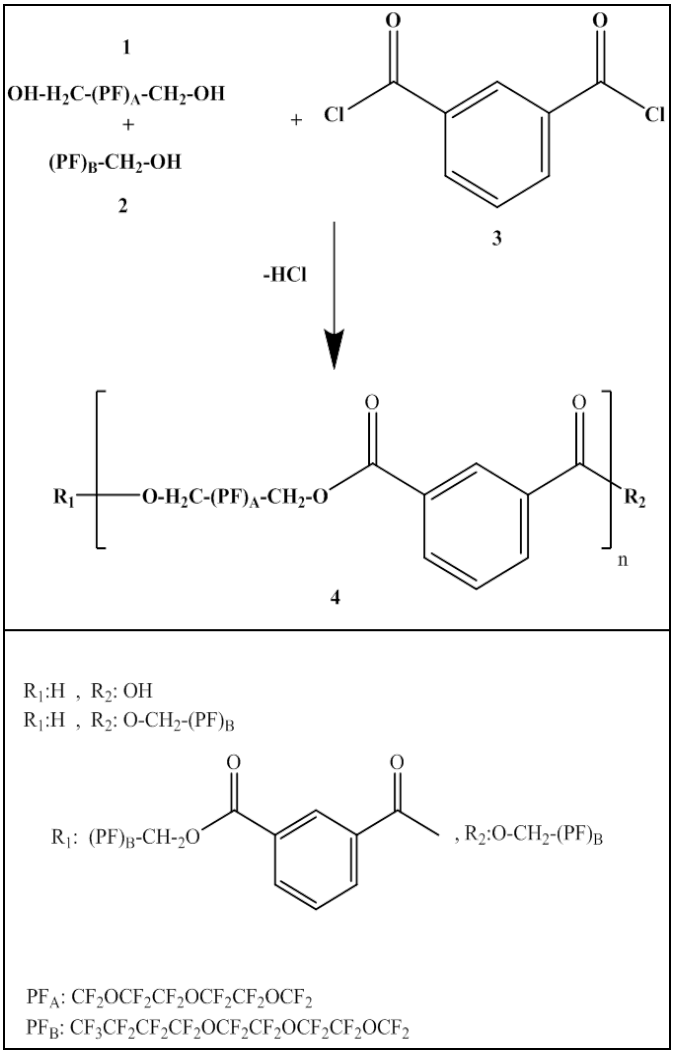

Figure 4.1. General procedure of synthesis of fluorinated polyester polymers.

In this study, three fluorinated polyesters with different end-groups were synthesized. **Table 4.1** shows the molar ratios of reactants used for the synthesis of the polyesters. When only the bi-functional monomers, IsoCl and PF-TriOxaUD-diol, were used, equimolar amounts of reactants (r =1), the first polymer (P1) such as fluorinated isophthaloic acid polyester P(OH-PF-oate-Iso-COOH) was synthesized. It possessed –

OH and-Cl end-groups. After rinsing with water, the -Cl groups were converted to –COOH groups.

For the second polymer (P2), fluorinated isophthaloyl polyester P(PF-oate-Iso–oate-PF-OH) with –OH and-CF_3 end- groups was synthesized. 10 mol% of PF-TriOxaUD-diol was replaced with perfluoro ether mono-alcohol (PF-TriOxaTri-OH) to terminate P2 polymer with CF_3 groups in one side. In addition, equimolar amount of –Cl and –OH groups were used (r =1) in this experiment.

When PF-TriOxaTri-OH was used in excess (Cl:OH 1:1.05; r <1), the third polymer (P3), fluorinated diester isophthaloyl polyester P(PF-oate-Iso-oate-PF) terminated with –CF_3 groups in both sides, was obtained.

Table 4.1. Molar ratios of both perfluoro di-alcohol (PF-diOH) and perfluoro mono-alcohol (PF-OH) to IsoCl and ratio of total OH:Cl in solution

	polymer	**PF-diOH: IsoCl**	**PF-OH: IsoCl**	**OH:Cl**	**$T_{melt\ polymerization}$/Time**
P1	P(OH-PF-oate-Iso-COOH)	1:1	-	1:1	150°C/7h
P2	P(PF-oate-Iso–oate-PF-OH)	0.9:1	0.2:1	1:1	150°C/7h 150°C/7h
P3	P(PF-oate-Iso–oate -PF)	0.9:1	0.3:1	1.05:1	200°C/5h

4.2.2.1 General Procedure of the Synthesis of Fluorinated Polyesters

In a typical synthesis of fluorinated polyesters, IsoCl in MEK solution was added drop-wise to the solution of perfluoro ether alcohols and Et_3N in dry MEK, which was pre-heated at 70°C for 30 min. The solution was stirred to allow the reaction to proceed at 70°C for 3h to form oligomers. The reaction media was cooled down to room temperature, and then it was kept overnight. Subsequently, $Et_3N.HCl$ salt was removed by centrifugation at 5000 rpm for 1h. The remaining solution was placed in 100 mL three-necked flask equipped with mechanical stirrer and was heated to 50°C for 4h, and then 70°C for an hour under nitrogen (N_2) stream to remove the MEK. After the solvent was removed, the reactive oligomers were heated at 150°C for 7h under N_2 to obtain higher molecular weight macromolecules.

4.2.2.2 Synthesis of P1 Polyester (Figure 4.2)

For the synthesis of P1, 4.96 g (24.4 mmol) of IsoCl in MEK (5ml) solution was added to the solution of 10g (24.4 mmol) of PF-TriOxaUD-diOH and 3.46 g (34.2 mmol) of triethylamine in MEK (15ml) and above-written procedure was followed. The final product was dissolved in acetone and then it was acidified by addition of water at 50°C to convert acid chloride end-groups of polyester into carboxylic acid groups. Subsequently, it was precipitated in water. After drying the product with N_2, a yellow P1 polyester was obtained (**Figure 4.2**) as ^{19}F NMR (300 MHz, CD_3COCD_3): δ-77.37-77.72(t, 2F), -80.68-80.84 (m, 4F) and -88.88-90.21 (m, 2F).

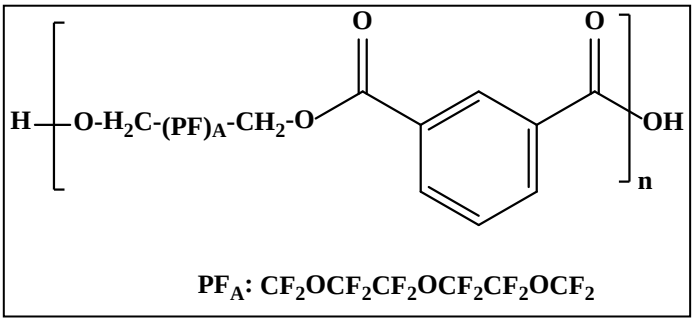

Figure 4.2. Chemical structure of P1: P(OH-PF-oate-Iso-COOH).

4.2.2.3 Synthesis of P2 Polyester (Figure 4.3)

A solution of 18g (43.9 mmol) of PF-TriOxaUD-diOH, 5.35 g (9.8 mmol) of PF-TriOxaTri-OH, and 9.88 g (97.6 mmol) of triethylamine in 20 ml MEK was prepared. Approximately 9.92 g (48.8 mmol) of IsoCl in MEK (10ml) was drop-wise added into the perfluoro ether alcohol solution to synthesize the P2 polymer using the procedure described above. The final product was dissolved in acetone and was then mixed with water at 50°C to convert unreacted acid chloride end-groups of polymer into carboxylic acid groups. After drying the product with N_2, a yellow P2 polymer was obtained (**Figure 4.3**). (^{19}F NMR (300 MHz, CD_3COCD_3): δ-77.36-77.73 (t, 2F), -80.72-80.80 (t, 2F), -81.92 (s, 3F), -84.17 (s, 2F), -89.08-89.69 (m, 4F), -127.22 (s, 4F).

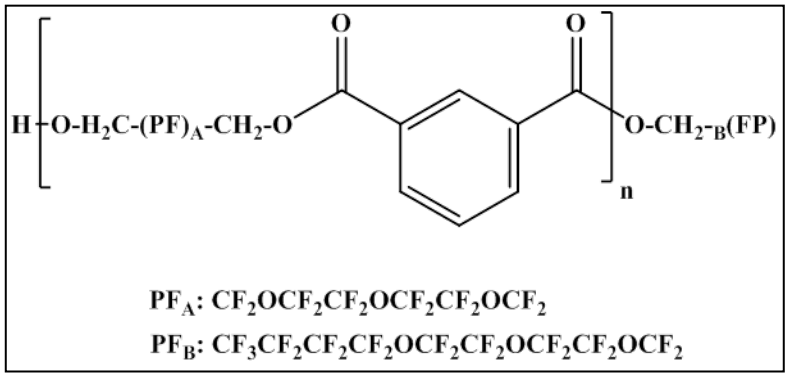

Figure 4.3. Chemical structure of P2: P(PF-oate-Iso–oate-PF-OH).

4.2.2.4 Synthesis of P3 Polyester (Figure 4.4)

PF-TriOxaTri-OH was used in excess to terminate both end-groups of the polyester chain with -CF_3 groups. To synthesize the P3 polymer, 9.92 g (48.8 mmol) of IsoCl in MEK (10ml) was added drop-wise to the solution 18g (43.9 mmol) of PF-TriOxaUD-diol, 8.3g (14.7 mmol) of PF-TriOxaTri-OH and 9.88 g (97.6 mmol) of triethylamine in MEK (20 ml), and above-written procedure was followed. The final product was heated further at 200°C for 5 h to remove low molecular moieties and prompt an additional polymerization. Yellow P3 polymer was obtained (**Figure 4.4**). (^{19}F NMR (300 MHz, CD_3COCD_3): δ-77.38-77.74 (t, 2F), -80.73-80.82 (m, 2F), -81.94 (s, 3F), -84.19 (s, 2F), -88.94-90.24 (m, 4F), -127.23 (s, 4F))

4.3. Results and Discussions

Polyesters are typically synthesized by polycondensation polymerizations at elevated temperature (> 150°C), which is needed for high conversion [34]. For instance, the most common polyester, the polyethylene terepthalate (PET) discovered by Whinfield and Dickson, is roduced by direct polycondensation of terephthalic acid with ethylene glycol (EG) at 220–270°C.

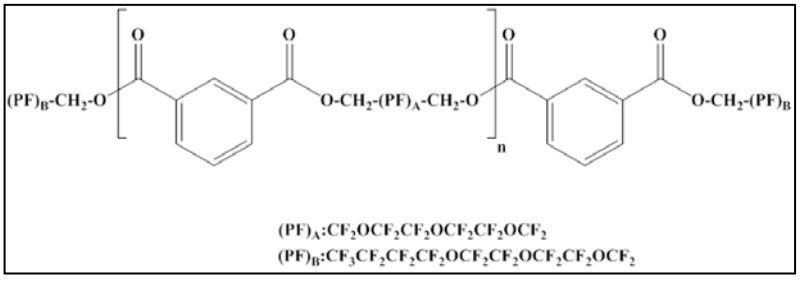

Figure 4.4 Chemical structure of P3:P(PF-oate-Iso–oate-PF)

The second most common method is transesterification of dimethyl terephthalate with EG employed at 270–280°C. However, for the synthesis of the fluorinated polyesters with different end groups, these conditions were too harsh due to the low boiling point of perfluoro ether alcohols. To overcome these limitations, an alternative method was employed in this work to synthesize fluorinated polyesters by taking advantage of the reactions between acid chlorides and diols (Schotten-Baumann (SB) reaction) in MEK. The drawback of the SB reaction in the solution was that low molecular weights fluorinated polyester were synthesized. Therefore, the reaction was continued in the melt at high temperatures under inert gas, N_2. This way, three fluorinated polyesters with different end groups, such as *P1, P2,* and *P3* polyesters were synthesized in two stages, *i) polycondensation in solution at low temperature* and *ii) polycondensation in melt at high temperatures*.

4.3.1 Selection of Monomer and Polymerization Conditions

The molar ratios IsoCl and perfluoro ether alcohols were calculated based on **Equation 4.1a** to synthesize fluorinated polyesters with different end groups. IsoCl was chosen due to its high reactivity with alcohols and its stability at higher temperatures (T_{decom} 260°C). Perfluoro ether diol (PF-diol) was selected for its low surface energy groups (–CF_2 groups). Using these two monomers, P1 polymer was synthesized. To terminate this polymer with CF_3 groups on either one side (P2) or both sides (P3), perfluoro ether mono-alcohol (PF-OH) was added. The molar ratios of –Cl and –OH are shown in **Table 4.1**.

To determine polymerization conditions, evaporation temperature of all monomers was obtained by thermal gravimetric analysis (TGA) (**Figure 4.5**). Thermal gravimetric analysis results revealed that IsoCl, PF-diol, and PF-OH evaporate at around 119°C, 110°C, and 90°C, respectively. The evaporation temperature of MEK is also around 80°C. When the IsoCl was mixed with perfluoro ether alcohols at room temperature, no reaction occurred. Therefore, the IsoCl reacted with perfluoro ether alcohols at 70°C in MEK solution.

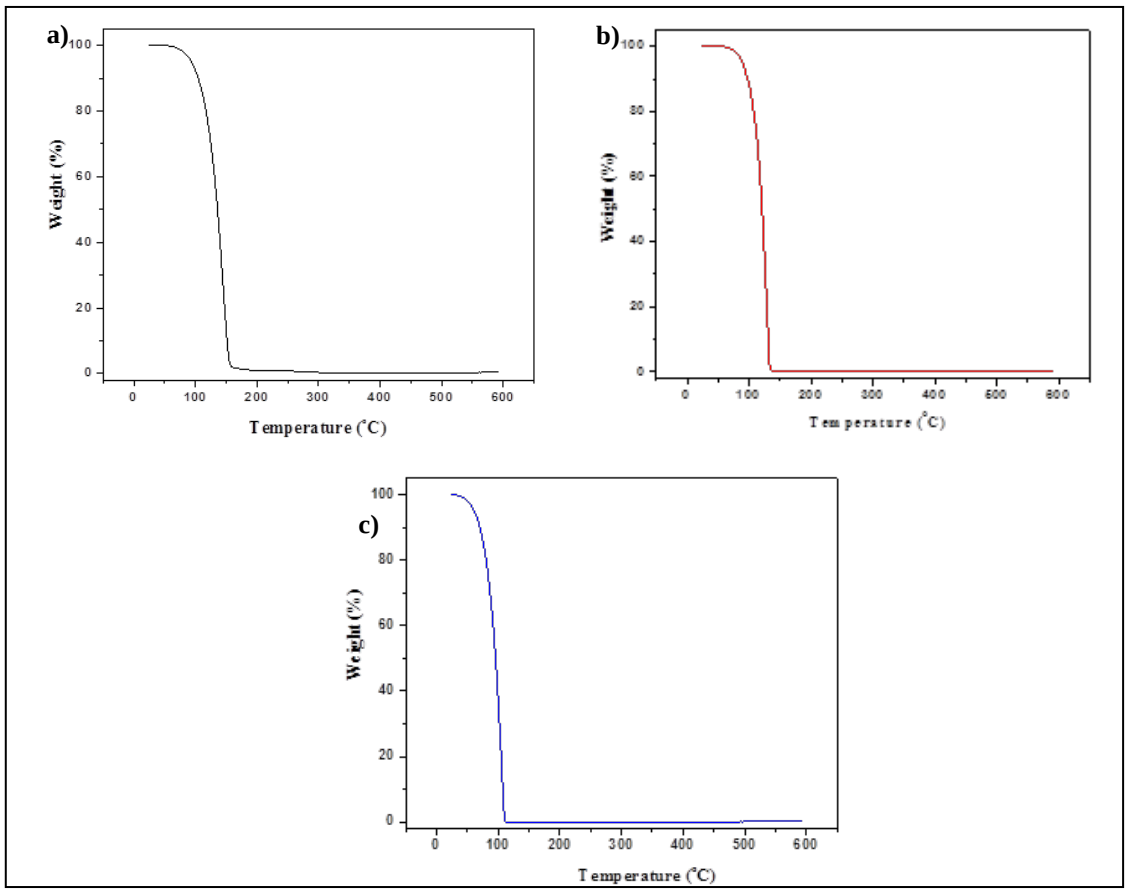

Figure 4.5. TGA results for monomers. a) IsoCl, b) PF-diol and c) PF-OH.

It is hard to obtain a high molecular weight polymer with this reaction in solution at low temperature. It is because the reaction rate strongly depends on concentration and

temperature. Melt polymerization was employed in the next step to obtain a higher molecular weight polyester. For this purpose, the solution was dried at lower temperature (50°C for 4h and 70°C for 1h) to avoid uncontrolled reaction continuation during drying. The oligomers were then reacted at elevated temperature.

To identify the melt polymerization temperature, TGA was performed to determine the composition of the product obtained during the solution process and evaporation temperatures of the product components. The TGA data is presented in **Figure 4.6**. It reveals that around 60% of the products obtained at 70°C (1h) withstand high temperatures (>350–400°C), while 40% of them evaporated at 160–175°C. It means that the former is polyester, while the latter is a mixture of monomers. Therefore, melt polymerization was performed at 150°C to continue the reaction to obtain a higher molecular weight polyester.

To determine the required duration of melt polymerization, TGA analysis was performed again on the product obtained after polymerization at 150°C for a certain period of time (**Figure 4.6**). For instance, TGA results obtained after the polymerization of P1 and P2 polyesters at 150°C for 1, 2 and 7h are presented in **Figure 4.6-a,b**. It shows that the higher molecular weight P1 and P2 polymer concentrations in the product were increased from 69% to 80% and 67% to 81%, respectively, after the polymerization was employed at 150°C for 1h. When the reactions continued for 7h, 82% of the P1 polyester and 86% of the P2 polyester in the product were obtained.

To synthesize the P3 polyester, which was terminated with the $–CF_3$ groups on both sides of the chain, melt polymerization was first employed at 150°C for 7h, then at

200°C for 5h. From the TGA analysis (**Figure 4.6-c**), it was found that the composition of the P3 polymer in the product was increased from 74% to 84% when reaction continued at 200°C for 5h. As a conclusion, polymerization goes further in melt at high temperatures. Increasing the duration of polymerization caused the low molecular weight polymer to either evaporate or react to form high molecular weight polyesters.

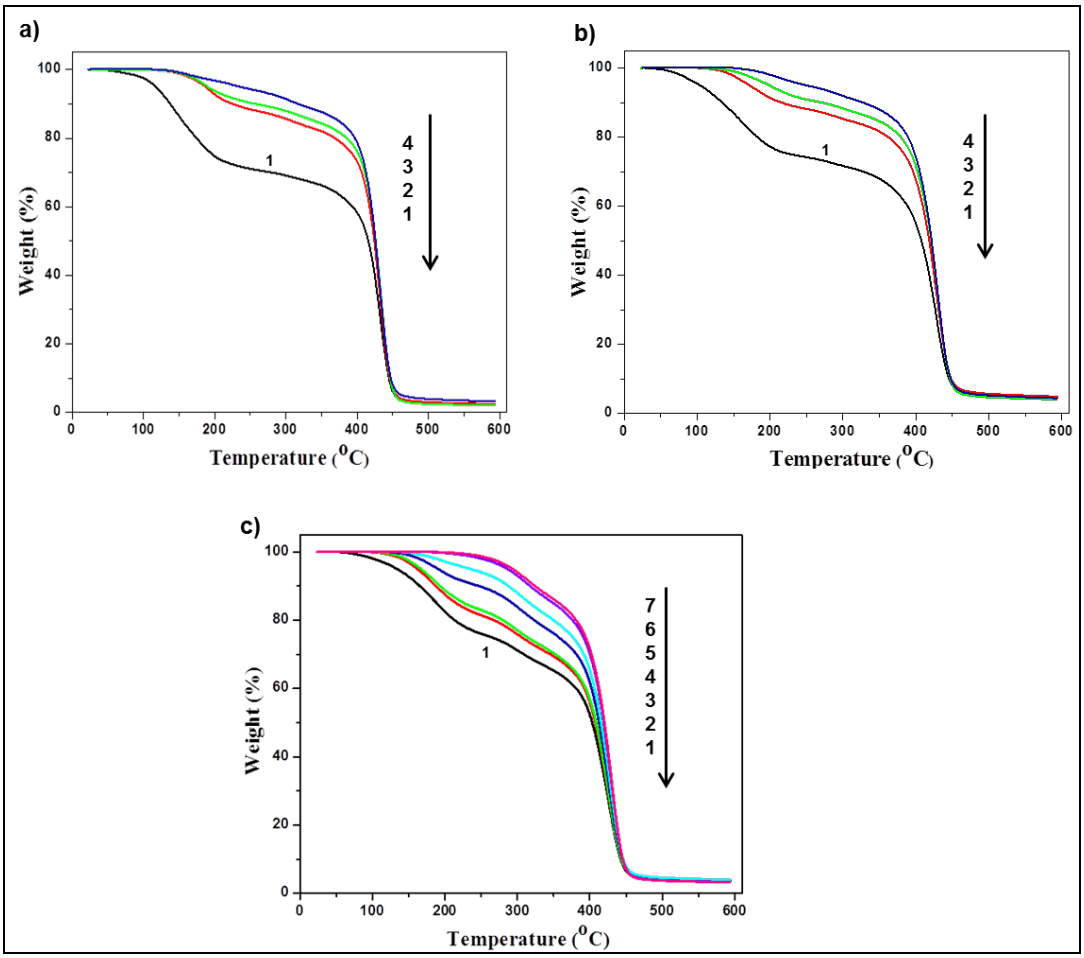

Figure 4.6. TGA results of fluorinated polyester polymers after polymerization at certain of time a) P1, b) P2and c) P3; 1)70°C for 1h; 2)150°C for 1h; 3) 150°C for 2h, 4) 150°C for 7h;5)200°C for 30min; 6) 200°C for 2.5h and 7) 200°C for 5h.

4.3.2 Structural Characterization of Fluorinated Polyester

4.3.2.1 ATR-FTIR Analysis of Fluorinated Polyesters

Attenuated total reflectance fourier transform infrared spectroscopy was performed to determine the functional groups in fluorinated polyester structures. The ATR-FTIR results of each polyester, which are shown in **Figure 4.7** and presented in **Table 4.2**, were analyzed using the Spectral Database for Organic Compounds, SDBS [36].

Table 4.2. IR absorption bands of fluorinated polyester polymers

Absorbing group and type of vibration	***P1 Polymer wavenumber (cm^{-1})***	***P2 Polymer wavenumber (cm^{-1})***	***P3 Polymer wavenumber (cm^{-1})***
-OH stretching	3465	3503	-
-CH symmetric stretching	3095- 2980	3095- 2980	3095- 2980
-OC=O stretching	1743	1743	1743
-C=O stretching in acid	1715	-	-
-C=C- stretching	1611	1611	1611
-C-O-C- symmetric stretching	1269	1270	1270
$-CF_2$ and $-CF_3$ stretching	1186-100	1186-100	1186-100
-CH bending	722	722	722

Figure 4.7 reveals that a small peak at 1715 cm^{-1}, which were attributed to carboxylic acid (-C=O) stretching, was obtained in the P1 polyester structure. The –OH

peaks at around 3500 cm^{-1} were not seen clearly in the P1 and P2 polymer structures. The most important result of the synthesis of all three fluorinated polyesters is that they possessed the ester (-OC=O) stretching and –C-O-C stretching vibrations, where the peaks were at 1749 cm^{-1} and 1269 cm^{-1}, respectively, due to acid chloride reaction with alcohol. Furthermore, $-CF_2$ and $-CF_3$ stretching vibrations appeared in the region 1200-1100 cm^{-1}[37]. C-H stretching and C=C stretching of aromatic rings in all three polymers were also detected at 2980 cm^{-1} and 1614 cm^{-1}, respectively.

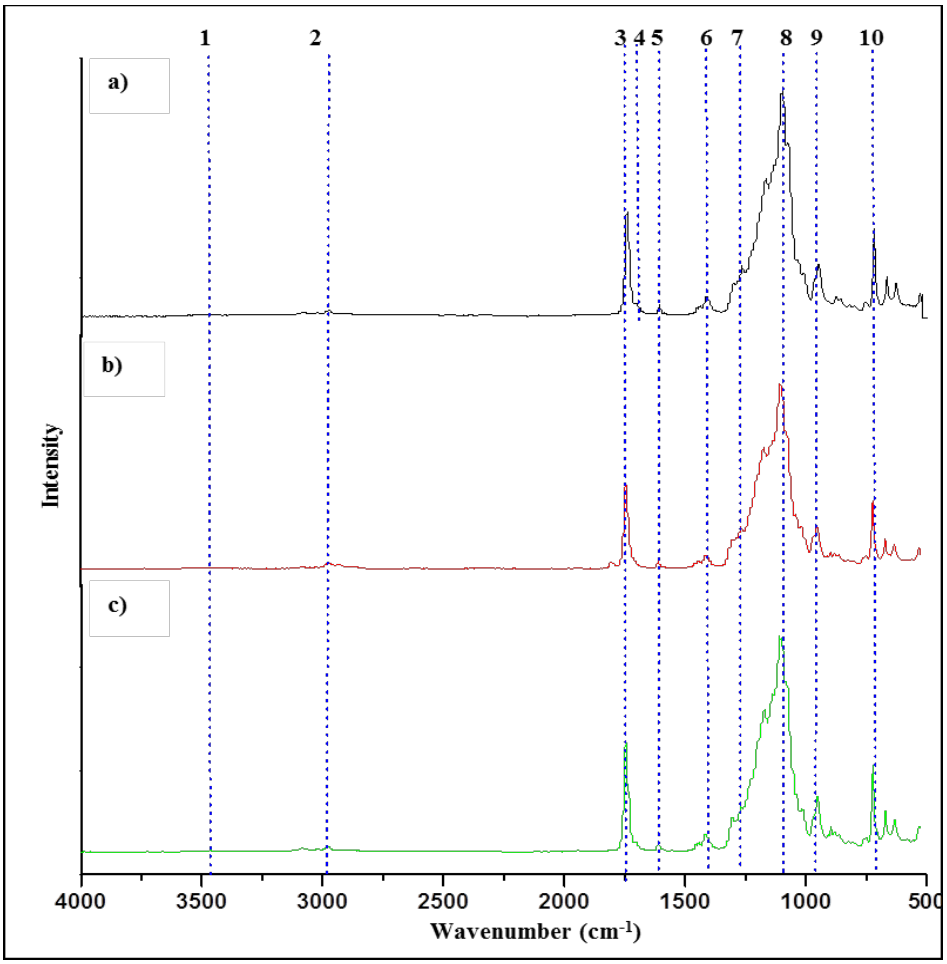

Figure 4.7. ATR-FTIR Spectra of fluorinated polyesters a)P1: P(OH-PF-oate-Iso-COOH), b) P2: P(PF-oate-Iso–oate-PF-OH) and c) P3: P(PF-oate-Iso–oate-PF). (1)-OH stretching, 3500-3450 cm^{-1}, (2) C-H symmetric stretching, 3095-2970 cm^{-1}, (3) –OC=O stretching, 1743 cm^{-1}, (4) –C=O stretching in acid, 1715 cm^{-1}, (5) -C=C- stretching, 1611 cm^{-1}, (6) –OH bending (in plane) 1414 cm^{-1}, (7) -C-O-C symmetric stretching, 1269 cm^{-1}, (8) -CF_2 and -CF_3 stretching,1186-1100 cm^{-1}, (9) -OH bending (out of plane), 953 cm^{-1}, and (10) C-H bending, 722 cm^{-1}.

4.3.2.2. ^{19}F NMR Analysis of Fluorinated Polyesters

According to the ATR-FTIR results, we determined the presence of the functional groups in the fluorinated polyesters, but we could not see significant differences among the polymer structures. To this end, NMR was performed to elucidate the structure of each polymer. **Figure 4.8, Figure 4.9**, and **Figure 4.10** display the ^{19}F NMR spectra of the P1, P2 and P3 polymers, respectively. **Figure 4.8** reveals the signals at -77.37 to -77.72 ppm (**a**) as belonging to the fluorine atom in the CF_2 groups, which were bonded to methyl ester (-O-$\underline{CF_2}$-CH_2-O-CO-) in the repeat unit. Distinctive multiple peaks at -88.88 to -91.10 ppm (**b**) are attributed to the fluorine atoms of the CF_2 groups in between ethers (–O-$\underline{CF_2}$-$\underline{CF_2}$-O) in the repeat units as well. The triplet peak at -80.72 to -80.80 ppm (**c**) belongs to the fluorine atom in the CF_2 group, which is close to the –OH end groups (-O-$\underline{CF_2}$-CH_2-OH) [38, 39]. ^{19}F NMR results confirm that P1 polyester possesses –COOH groups and –OH groups at the chain ends.

Since the P2 polyester possessed repeat units just like the P1 polymer, “a” and “b” peaks were also detected in its ^{19}F NMR data (**Figure 4.9**). The peak “**c**” was also seen in the P2 polymer structure because it was terminated with –OH groups in one side. Furthermore, perfluoro ether mono-alcohol was added to P2 polymerization to terminate it with the $–CF_3$ groups in another side. Three more peaks (**d**, **e**, and **f**) corresponding to the fluorine atoms from perfluoro ether mono-alcohol were detected. According to **Figure 4.9**, two singlet peaks, “**d**” and “**e**” at -81.92 ppm (**d**) and at -84.16 ppm (**e**), correspond to the fluorine atoms in the $–CF_3$ groups and $–CF_2$ groups bonded to ether (CF_3-CF_2CF_2-$\underline{CF_2}$-O) on the tail of polymers [40]. Another distinctive peak, “**f**” at -127.22 ppm is attributed to the fluorine atoms of the $–CF_2$ groups (CF_3-$\underline{CF_2}\underline{CF_2}$-$\underline{\ }CF_2$-O) on fluorinated tails [40].

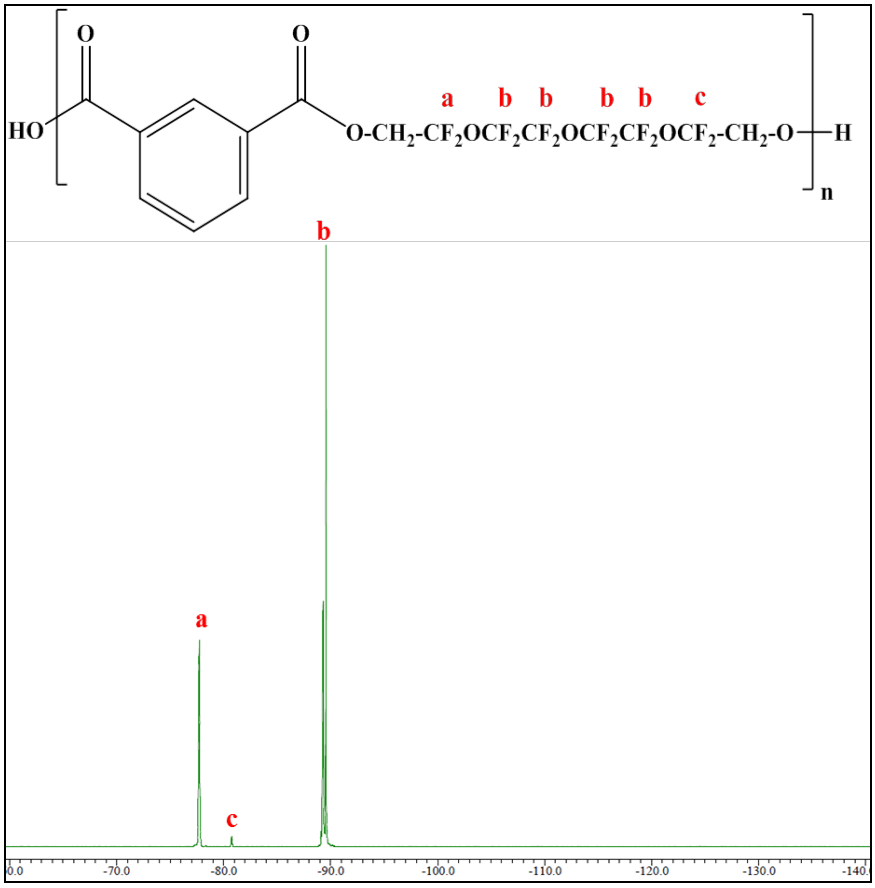

Figure 4.8. ^{19}F NMR spectra of P1 polyester.

The P3 polyester was terminated with $–CF_3$ groups in both sides using perfluoro ether mono-alcohol in excess. The three main peaks (**d**, **e**, and **f**) corresponding to the fluorine atoms in the polymer tails were detected in the P3 polyester structure (**Figure 4.10**). The P3 polyester also exhibited peak "**a**" and peak "**b**" corresponding to the fluorine atoms in the repeat units that are the same with that of the P1 polyester's as well. Interestingly, peak "**c**", which corresponds to the fluorine atoms close to the –OH end-groups was also detected in the P3 polymer structure. It is not certain whether all perfluoro ether diols reacted with the IsoCl that subsequently reacted with the mono-

alcohols. In other words, the presence of peak "**c**" in P3 shows that some of the chains terminated with -OH are not reacted with IsoCl.

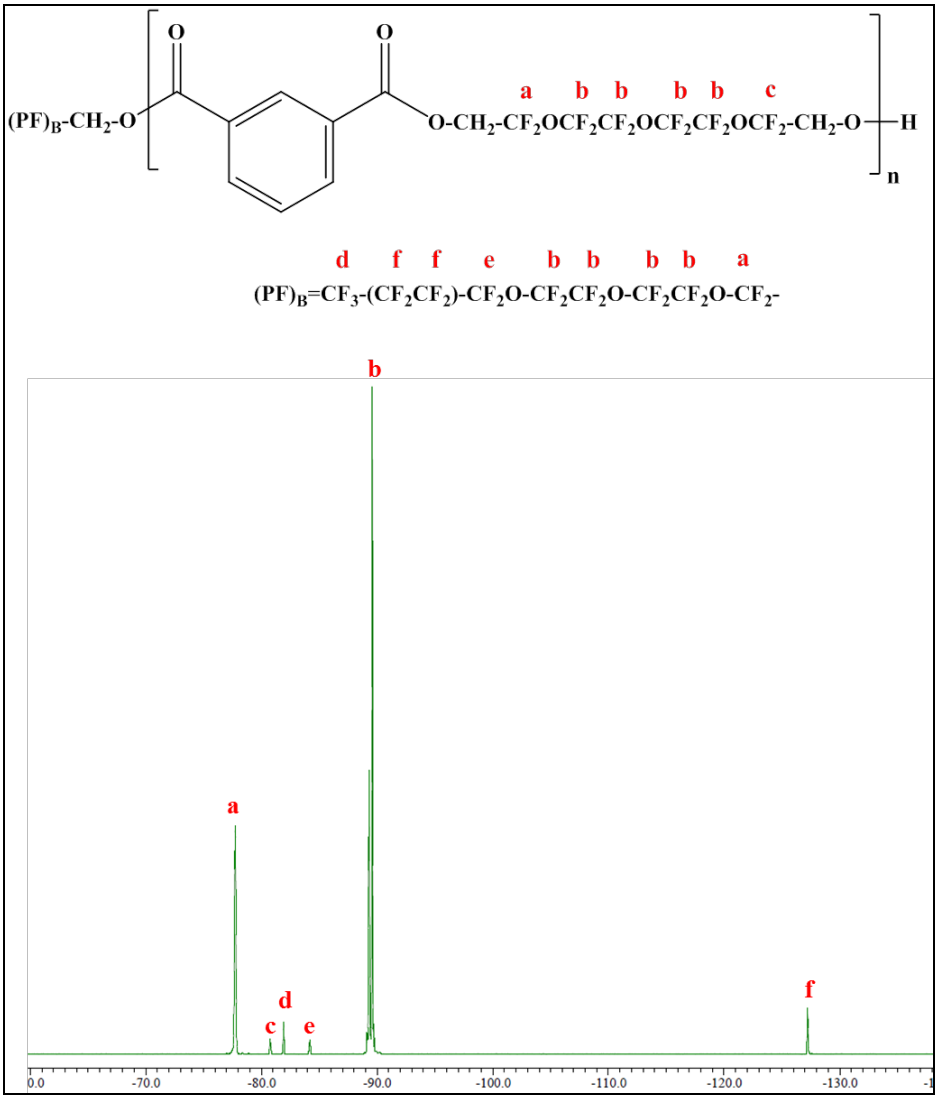

Figure 4.9. ^{19}F NMR spectra of P2 polyester.

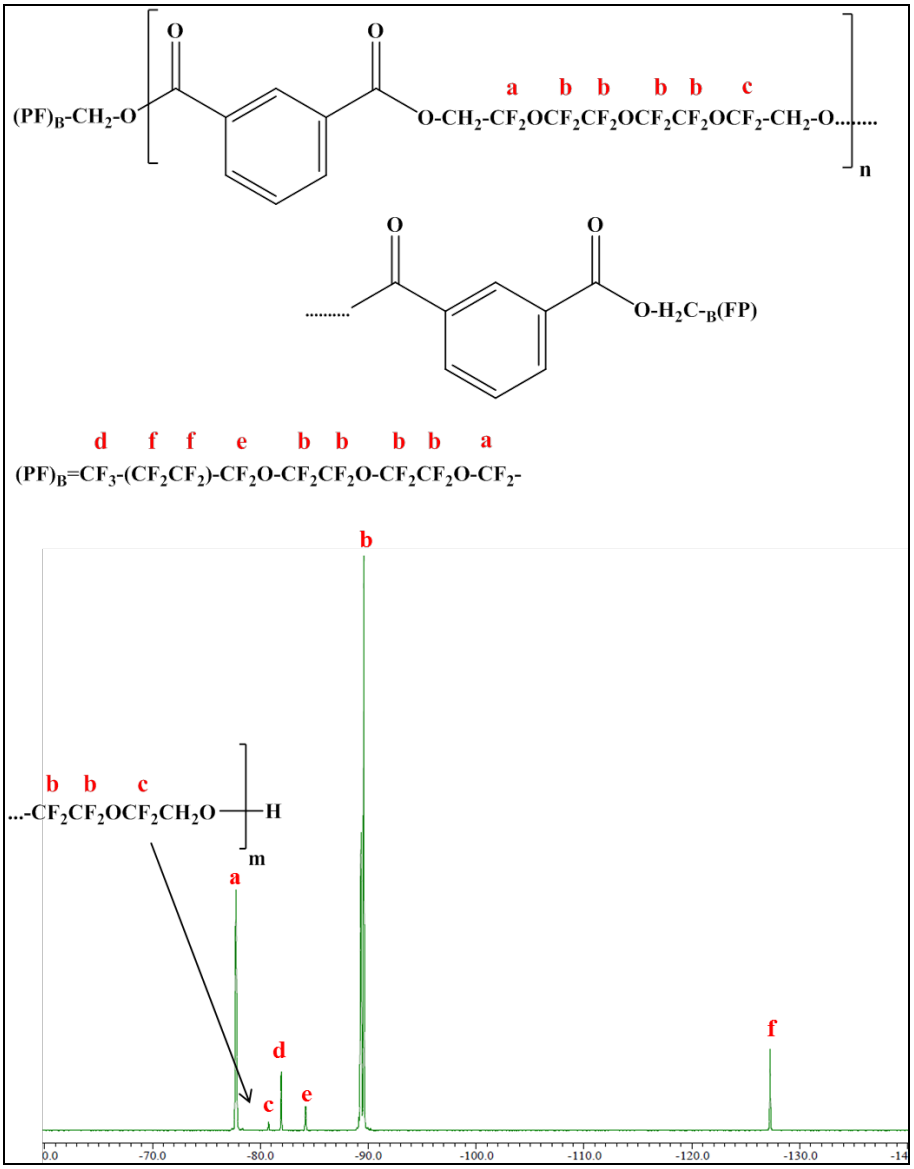

Figure 4.10. ^{19}F NMR spectra of P3 polyester.

4.3.3 Molecular Weight of Fluorinated Polyesters

4.3.3.1 GPC Analysis

Gel permeation chromatography (GPC) was performed to determine the molecular weight (MW) of fluorinated polyesters. In this analysis, polystyrene with different MWs were used as standards for calibration. All polymers were dissolved in

chloroform and were filtered before they were used in GPC. The MW and polydispersity index (PDI) of fluorinated polyesters were determined and presented in **Table 4.3**. The GPC results revealed that polymers with low MW and broad PDI values were obtained. Although the MW of all polymers was close to each other, the P2 polymer possessed more than 1.5 times broader PDI than others. This could be due to the probability of reaction of IsoCl with either mono alcohol or diol.

Table 4.3. Parameters of fluorinated polyesters.

	Polymer	M_w (g/mole)	PDI	T_g (°C)	T_f (°C)	T_f^0 (°C)	ΔH_f (J/g)	$T_{d/e}$ (°C)	Crystallinity (%)*
P1	P(OH-PF-oate-Iso-COOH)	5228	3.9	-18	55	55	27.7	411	28.0
P2	P(PF-oate-Iso–oate-PF-OH)	6221	6.8	-29	48	50	28.4	404	28.6
P3	P(PF-oate-Iso–oate-PF)	4238	4.3	-21	48	53	26.4	404	26.6

*: calculated using DCS results

4.3.4 Thermal Properties of Fluorinated Polyesters

4.3.4.1 TGA Results

The thermal stability of the fluorinated polyesters (without rinsing with water) was analyzed using TGA (**Table 4.3** and **Figure 4.6**). It appears that all fluorinated polyesters exhibit high decomposition/evaporation temperatures ($T_{d/e}$) at 407±4°C, indicating the relatively high thermal stability of the polyester due to the presence of isophthalate units in macromolecules. It was found that the stability of fluorinated

polyesters is end-group dependent. Polyesters terminated with fluorinated tails were less stable, with the decomposition temperature decreased from 411°C to 404°C. Consequently, the P1 polymer appeared to be more stable compared to its counterparts.

The effect of acidification on polymer content was also investigated. The TGA results of the P1 and P2 polyesters before and after rinsing with water are shown in **Figure 4.11**. It is evident that the content of P1 in the product was increased from 80% to 89%. In other words, higher purity P1 polymers were obtained after rinsing them with water. In the presence of water, unreacted -Cl converted to –COOH groups and hydrogen bonds were formed between the water molecules and unreacted acid (**Figure 4.12**). Low molecular weight oligomers with –Cl end groups became soluble in water during acidification, while high molecular weights did not.

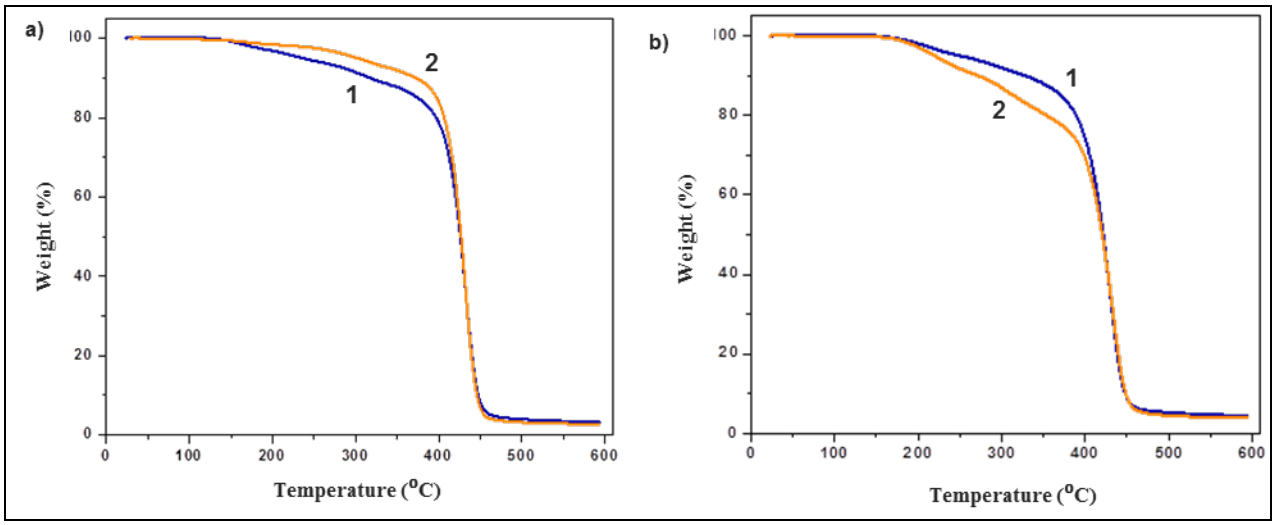

Figure 4.11. TGA results of a) P1 and b) P2 polymers (1) before and (2) after rinsing with water.

Interestingly, it was found that the amount of P2 polyester was reduced from 86% to 77% after acidification, as compared to the amount of P1 (**Figure 4.11-b**). It could be

because the amount of -Cl terminated oligomers, which were dissolved in water, were higher in the final product. Thus, when they were rinsed, they dissolved and the P2 content in the final product was reduced. Another reason is that the P2 polyester mixture may have been hydrolyzed during the rinsing with water, resulting to lower concentration of P2 in the mixture. Apart from this, the thermal stability of polyesters remains the same because the decomposition temperature of P1 and P2 did not change significantly after acidification.

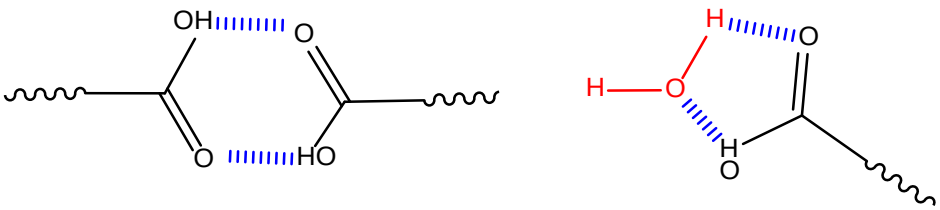

Figure 4.12. Scheme of hydrogen bonding between acid /acid and acid/ water.

4.3.4.2. DSC Results

The thermal properties of the fluorinated polyesters, such as T_g and T_f of the polymers, were determined using DSC at a heating rate of 10^0C/min under N_2. Results (**Figure 4.13**) show that all fluorinated polyesters are semi-crystalline materials. The T_g for the polyesters ranged from -18°C to -29°C, while the T_f ranged from 48°C to 55°C. This variation can be dependent on the end groups of polymers. It is observed that polyesters (P1) terminated with-OH and -COOH groups resulted in higher T_f than those of corresponding polymers with fluorinated tails (P2 and P3). It is hypothesized that this occurs because the phenyl ring is a symmetrical molecule and can pack more efficiently. On the other hand, fluorinated tails are more mobile compared to the phenyl ring and tend

to disrupt packing. Further investigation to understand the effect of end groups on T_g is needed.

The degree (percentage) of crystallinity of the fluorinated polyesters was estimated from the DSC data (**Figure 4.13**). The percentage can be calculated using the following equation:

$$\%\ crystallinity = 100\left[\frac{\Delta H_f - \Delta H_c}{\Delta H^f_{crys}}\right] \qquad (4.3)$$

where ΔH_f is the heat of fusion, ΔH_c is the heat of additional crystallization of the polymer, ΔH^f_{crys} is the heat of fusion for 100% crystalline polymer.

According to the DCS results of fluorinated polyesters (**Figure 4.13**), none of the polyesters possesses the heat of the additional crystallization ($\Delta H_c = 0$). In addition, ΔH_f for the P1, P2, and P3 polymers were found as 27.7 J/g, 28.4 J/g and 26.4 J/g, respectively. Since we could not find the ΔH^f_{crys} for the fluorinated polyesters in the literature, it was estimated from the tabulated molar contributions of the chemical groups, which constitute repeat units of fluorinated polyesters [41].

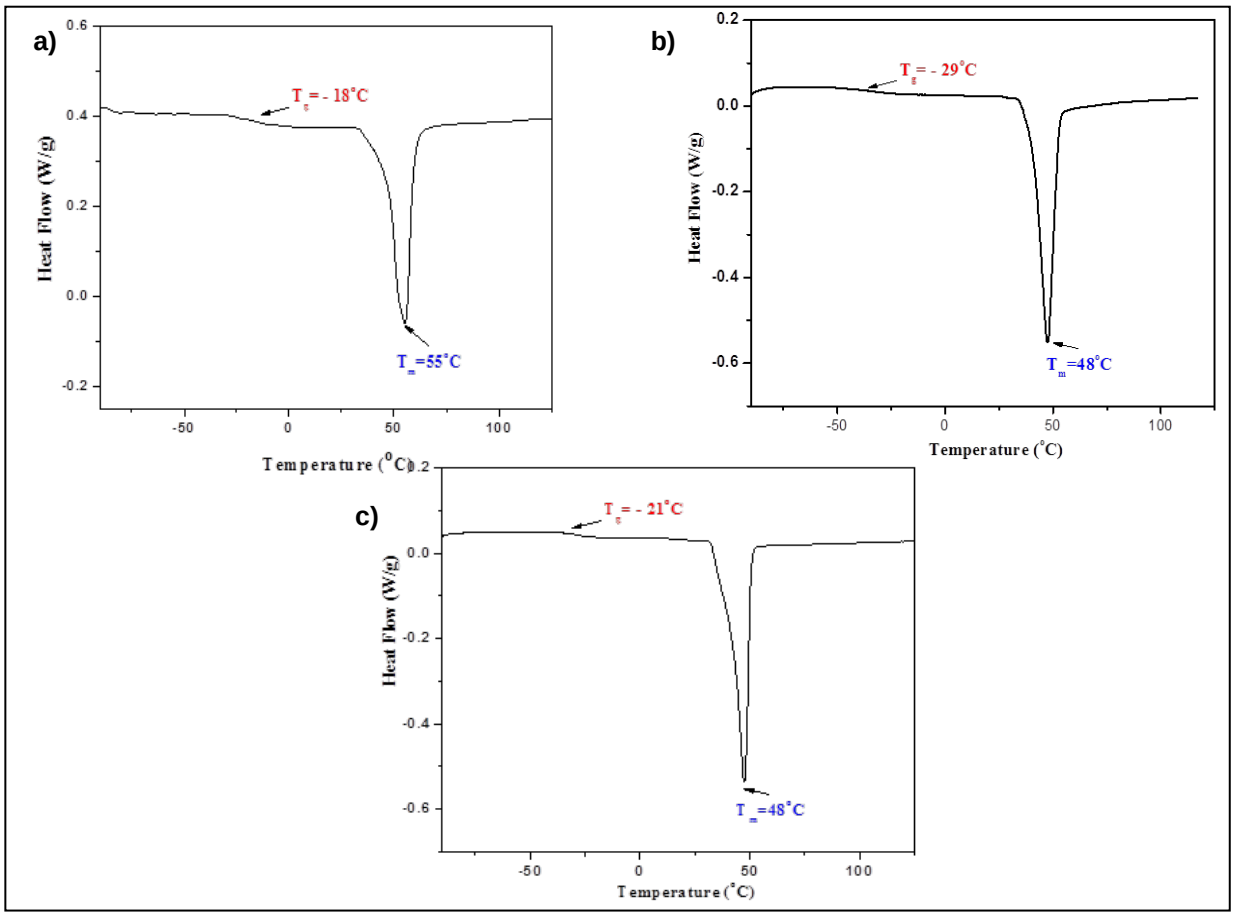

Figure 4.13. DSC results of a) P1, b) P2 and c) P3 polyesters

Herein, one ΔH_{crys}^{f} value is determined for all three fluorinated polyesters that possess the same crystallizable repeat units as shown in **Figure 4.14**, since this method ignores the end groups' effects on heat of fusion.

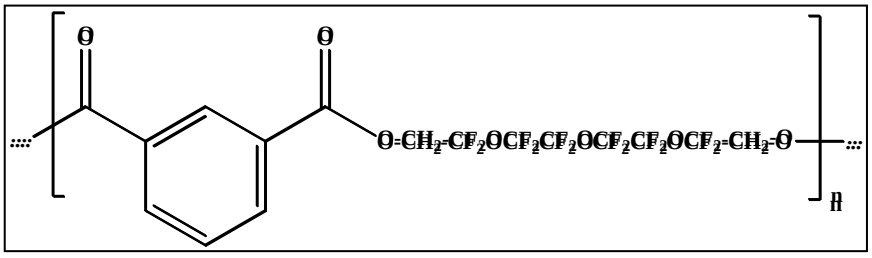

Figure 4.14. Chemical structure of repeat unit for all fluorinated polyesters.

The heats of fusion for fluorinated polyesters constituent groups at T=298K are [41]

2 CH_2 = 2x4 = 8 kJ/mole
6 CF_2 = 6x4 = 24 kJ/mole
3 O = 3x1 = 3 kJ/mole
1 -OOC-C_6H_4-COO-= 1x17= 17 kJ/mole
Total= 52 kJ/ mole
ΔH^f_{crys} **=99.2 J/g**

The ΔH^f_{crys} value was determined by multiplying the total heat of the fusion with number of repeat units in the polyester. In addition, ΔH^f_{crys} was used to calculate the degree of crystallinity for each fluorinated polyesters (**Equation 4.3**) and their crystallinity are presented in Table 4.3. It shows that the degree of crystallinity of all polymers are almost the same (P1, 28%; P2, 29%, and P3, 26.6%). In addition, the level of melting point depression in pure crystalline fluorinated polymers, ΔT_f^* is obtained using the following equation[42] to determine the end groups' effect on melting.

$$\frac{1}{\Delta T_f^*} = \frac{1}{T_f} - \frac{1}{T_f^0} = \frac{R}{\Delta H_f}\frac{M_o}{M_n} \qquad (4.4)$$

where R is the gas constant, ΔH_f is the heat of fusion per mole of crystalline mers, M_n is the molecular weight of polymer, and M_o is the total molecular weight of the end groups.

According to above approach, M_0/M_n represents the mole fraction of the end groups in the polyester. In this case, the mole fractions of the chains ends were obtained as 0.003, 0.09, and 0.28 for P1, P2, and P3 polymers, respectively. Then, T_f^o was determined and presented in Table 4.3. It shows that there are no significant differences between the T_f and T_f^o values. For the P1 polymer, temperatures are the same because it does not have any end groups. For the P2 and P3 polymers, T_f^o is higher than their T_f values. Therefore, we can conclude that the fluorinated chain ends decrease the melting point for the polyesters.

4.4. Conclusions

Three fluorinated polyesters terminated with different end groups (-COOH/-OH, -CF_3/-OH and -CF_3/-CF_3) were prepared through the polycondensation reaction of IsoCl with perfluoro ether alcohols. Polymerization was conducted in a two-stage process. The first stage of the polymerization was the solution polymerization. In this stage, low molecular weight oligomers were obtained. The second stage of polymerization was a melt-state polymerization. Both the ATR-FTIR and ^{19}F NMR characterization verified the structure of the polyesters. Apart from this, it was determined that perfluoro ether mono-alcohol used in excess did not terminate all chains of the P3 polyester with –CF_3 groups on both sides. We found that 30% of the P3 polymer chains were still terminated

with –OH end-groups. The TGA and DSC studies showed that all polymers were semi-crystalline. They were also soft at room temperature because of their lower T_g (<-10). Among fluorinated polymers, polyester terminated with –COOH and –OH groups result in higher T_f than those of corresponding polymers with fluorinated tails because phenyl ring is a symmetrical molecule that can pack efficiently, while the fluorinated tail is more mobile.

4.5. References

1. Plunkett, R. J. Tetrafluoroethylene polymers. 1941, 1941.
2. Wang, Z.; Li, W.; Zhao, X.; Zhu, D.; You, J., Self-Segregation Behavior of N-Ethyl-pentadecafluorooctanamide-Terminated Polybutylene Isophthalate and Its Effects on Film Morphology and Wettability. *The Journal of Physical Chemistry B* **2009,** *113* (46), 15204-15211.
3. Thomas, R. R.; Anton, D. R.; Graham, W. F.; Darmon, M. J.; Stika, K. M., Films Containing Reactive Mixtures of Perfluoroalkylethyl Methacrylate Copolymers and Fluorinated Isocyanates:Synthesis and Surface Properties. *Macromolecules* **1998,** *31* (14), 4595-4604.
4. Tan, H.; Guo, M.; Du, R.; Xie, X.; Li, J.; Zhong, Y.; Fu, Q., The effect of fluorinated side chain attached on hard segment on the phase separation and surface topography of polyurethanes. *Polymer* **2004,** *45* (5), 1647-1657.
5. Chapman, T. M.; Benrashid, R.; Gribbin, K. L.; Keener, J. P., Determination of Low Critical Surface Energies of Novel Fluorinated Poly(amide urethane) Block Copolymers. 1. Fluorinated Side Chains. *Macromolecules* **1995,** *28* (1), 331-335.
6. Zheng, F.; Deng, H.; Zhao, X.; Li, X.; Yang, C.; Yang, Y.; Zhang, A., Fluorinated hyperbranched polyurethane electrospun nanofibrous membrane: Fluorine-enriching surface and superhydrophobic state with high adhesion to water. *Journal of Colloid and Interface Science* **2014,** *421* (0), 49-55.
7. Synytska, A.; Appelhans, D.; Wang, Z. G.; Simon, F.; Lehmann, F.; Stamm, M.; Grundke, K., Perfluoroalkyl End-Functionalized Oligoesters: Correlation between Wettability and End-Group Segregation. *Macromolecules* **2006,** *40* (2), 297-305.
8. Ming, W.; Lou, X.; van de Grampel, R. D.; van Dongen, J. L. J.; van der Linde, R., Partial Fluorination of Hydroxyl End-Capped Oligoesters Revealed by MALDI-TOF Mass Spectrometry. *Macromolecules* **2001,** *34* (7), 2389-2393.
9. Ming, W.; Laven, J.; van der Linde, R., Synthesis and Surface Properties of Films Based on Solventless Liquid Fluorinated Oligoester. *Macromolecules* **2000,** *33* (18), 6886-6891.

10. Zhang, W.; Muller, A. H. E., Architecture, self-assembly and properties of well-defined hybrid polymers based on polyhedral oligomeric silsequioxane (POSS). *Progress in Polymer Science* **2013,** *38* (8), 1121-1162.
11. Beyou, E.; Bennetau, B.; Dunoguès, J.; Babin, P.; Teyssié, D.; Boileau, S.; Corpart, J.-M., New fluorinated polysiloxanes containing an ester function in the spacer—II. Surface tension studies. *Polymer International* **1995,** *38* (3), 237-244.
12. Lazzari, D.; Cassani, M. C.; Solinas, G.; Pretto, M., Fluoroalkyl allyl ethers: Useful building blocks for the synthesis of environmentally safer fluorinated multiblock molecules. *Journal of Fluorine Chemistry* **2013,** *156* (0), 34-37.
13. Xu, W.; An, Q.; Hao, L.; Zhang, D.; Zhang, M., Synthesis and characterization of self-crosslinking fluorinated polyacrylate soap-free latices with core-shell structure. *Applied Surface Science* **2013,** *268* (0), 373-380.
14. Cengiz, U.; Erbil, H. Y., Superhydrophobic perfluoropolymer surfaces having heterogeneous roughness created by dip-coating from solutions containing a nonsolvent. *Applied Surface Science* **2014,** *292* (0), 591-597.
15. O'Rourke Muisener, P. A. V.; Jalbert, C. A.; Yuan, C.; Baetzold, J.; Mason, R.; Wong, D.; Kim, Y. J.; Koberstein, J. T.; Gunesin, B., Measurement and Modeling of End Group Concentration Depth Profiles for w-Fluorosilane Polystyrene and Its Blends. *Macromolecules* **2003,** *36* (8), 2956-2966.
16. Kim, B. G.; Chung, J.-S.; Sohn, E.-H.; Kwak, S.-Y.; Lee, J.-C., Comb-Like Fluorinated Polystyrenes Having Different Side Chain Interconnecting Groups. *Macromolecules* **2009,** *42* (9), 3333-3339.
17. Krishnan, S.; Paik, M. Y.; Ober, C. K.; Martinelli, E.; Galli, G.; Sohn, K. E.; Kramer, E. J.; Fischer, D. A., NEXAFS Depth Profiling of Surface Segregation in Block Copolymer Thin Films. *Macromolecules* **2010,** *43* (10), 4733-4743.
18. Lee, H.; Willis, C.; Stone, C., Modeling and preparation of a super-oleophobic non-woven fabric. *Journal of Materials Science* **2011,** *46* (11), 3907-3913.
19. Genzer, J.; Efimenko, K., Recent developments in superhydrophobic surfaces and their relevance to marine fouling: a review. *Biofouling* **2006,** *22* (5), 339-360.
20. Zhao, X.; Chen, W.; Su, Y.; Zhu, W.; Peng, J.; Jiang, Z.; Kong, L.; Li, Y.; Liu, J., Hierarchically engineered membrane surfaces with superior antifouling and self-cleaning properties. *Journal of Membrane Science* **2013,** *441* (0), 93-101.
21. Jiang, R.; Fuller, T.; Brawn, S.; Gittleman, C., Perfluorocyclobutane and poly(vinylidene fluoride) blend membranes for fuel cells. *Electrochimica Acta* **2013,** *110* (0), 306-315.
22. Gugliuzza, A.; Drioli, E., A review on membrane engineering for innovation in wearable fabrics and protective textiles. *Journal of Membrane Science* **2013,** *446* (0), 350-375.
23. Zhao, Z.; Pu, H.; Chang, Z.; Pan, H., A versatile strategy towards semi-interpenetrating polymer network for proton exchange membranes. *International Journal of Hydrogen Energy* **2014,** *39* (12), 6657-6663.
24. Tang, J.; Sirkar, K. K.; Majumdar, S., Permeation and sorption of organic solvents and separation of their mixtures through an amorphous perfluoropolymer membrane in pervaporation. *Journal of Membrane Science* **2013,** *447* (0), 345-354.

25. Hauptschein, M.; O'Brien, J. F.; Stokes, C. S.; Filler, R., Fluorinated Esters. I. Esters of Perfluoro Monocarboxylic and Dicarboxylic Acids with 1,1-Dihydroperfluoroalcohols and Tetrahydroperfluoroglycols. *Journal of the American Chemical Society* **1953,** *75* (1), 87-89.
26. Mera, A. E.; Griffith, J. R.; Armistead, J. P., Linear fluoroalihatic polyesters from long-chain fluorinated diols. *Abstracts of Papers of the American Chemical Society* **1990,** *199*, 110-POLY.
27. Zhu, Q.; Han, C. C., Synthesis and crystallization behaviors of highly fluorinated aromatic polyesters. *Polymer* **2007,** *48* (13), 3624-3631.
28. Pilati, F.; Bonora, V.; Manaresi, P.; Munari, A.; Toselli, M.; Re, A.; De Giorgi, M., Preparation of poly(ethylene terephthalate) in the presence of a telechelic perfluoropolyether. *Journal of Polymer Science Part A: Polymer Chemistry* **1989,** *27* (3), 951-962.
29. Pilati, F.; Manaresi, P.; Toselli, M.; Re, A., Synthesis of poly(ethylene terephthalate) in the presence of perfluoropolyethers. II. Effect of various catalysts. *Journal of Polymer Science Part A: Polymer Chemistry* **1990,** *28* (11), 3047-3054.
30. Pilati, F.; Toselli, M.; Vallieri, A.; Tonelli, C., Synthesis of polyesters-perfluoropolyethers block copolymers. *Polymer Bulletin* **1992,** *28* (2), 151-157.
31. Levi, M.; Turri, S., Model structures of thermoplastic polyesters having regularly alternated aromatic and fluorinated segments. *Journal of Polymer Science Part A: Polymer Chemistry* **1998,** *36* (6), 939-947.
32. Reis-Nunes, R. C.; Riande, E.; Chavez, N. C.; Guzman, J., Comparative Study of the Conformational Characteristics of Partially Fluorinated Polyesters and Their Hydrogenated Counterparts. *Macromolecules* **1996,** *29* (24), 7989-7994.
33. Choi, E. J.; Hill, D. J. T.; Kim, K. Y.; O'Donnell, J. H.; Pomery, P. J., Synthesis, thermal and radiation sensitivities of fluorine containing methylene-bridged aromatic polyesters. *Polymer* **1997,** *38* (14), 3669-3676.
34. Hahn, C.; Wesselbaum, S.; Keul, H.; Muller, M., OH-functional polyesters based on malic acid: Influence of the OH-groups onto the thermal properties. *European Polymer Journal* **2013,** *49* (1), 217-227.
35. Carothers, W. H., Polymers and polyfunctonality. *Transactions of the Faraday Society* **1936,** *32*, 39-49.
36. T. Yamaji, T. S., K. Hayamizu, M. Yanagisawa and O. Yamamoto, Introduction to the Spectral Data Base.
37. Hao, L.; An, Q.; Xu, W.; Huang, L., Synthesis, film morphology and hydrophobicity of novel fluorinated polyacrylate emulsion and solution on silicon wafer. *Colloids and Surfaces A: Physicochemical and Engineering Aspects* **2012,** *396* (0), 83-89.
38. Wu, J.; Zhou, X.; Harris, F. W., Bis(perfluoro-2-n-propoxyethyl)diacyl peroxide initiated homopolymerization of vinylidene fluoride (VDF) and copolymerization with perfluoro-n-propylvinylether (PPVE). *Polymer* **2014,** *55* (16), 3557-3563.
39. Turri, S.; Barchiesi, E.; Levi, M., NMR of perfluoropolyether diols and their acetal copolymers. *Macromolecules* **1995,** *28* (21), 7271-7275.

40. Karis, T. E.; Marchon, B.; Hopper, D. A.; Siemens, R. L., Perfluoropolyether characterization by nuclear magnetic resonance spectroscopy and gel permeation chromatography. *Journal of Fluorine Chemistry* **2002,** *118* (1-2), 81-94.
41. Krevlen, D. W. V., Thermodynamic properties:calculation of the free enthalpy of reaction from group contributions. In *In Properties of Polymers*, Elsevier: Amsterdam, 1990; pp 626-639.
42. Keller, A. H., M.;Rastogi, S.; Toda, A., Barham, P.J.;Gold-beck -wood, G.;, An approach to the formation and growth of new phases with application to polymer crystallization:effect of finite size, metastability and OStwald's rule of stages. *Journal of Material Science* **1994,** *29* (10).

CHAPTER FIVE

LOW-SURFACE ENERGY POLYESTER/FLUORINATED POLYESTER BLENDED FILMS

5.1. Introduction

The blending of polymers is typically employed to generate new materials that exhibit better properties than pure polymers alone. Most of the polymer blends are immiscible and phase-separated. In this respect, the surface properties (e.g. wettability) of the blends that are functions of blend composition have attained considerable interest in scientific and industrial applications. Essentially, the composition of the blend surface has been found to be different from the one in the bulk due to the surface energy differences of the polymers forming the blend. The lower surface energy polymers segregate to the surface to enrich the air-polymer interface, resulting in vertical phase-separation. Using this phenomenon, the blending of fluorinated polymers with non-fluorinated counterparts was found to be an effective method to produce low surface energy films, including anti-fouling and self-cleaning films [1–3].

When fluorinated polymer is blended with a non-fluorinated polymer, the fluorocarbon groups due to their low surface energy, leading to oleophobic/hydrophobic surfaces, dominate the surface composition of the polymer blend [1–4]. This reduction in the surface energy is the driving force for the surface segregation of the fluorocarbon groups [5–7]. There is no such driving force for the surface segregation of polar groups since they possessed higher surface energy than their bulk, resulting in the inhibition of surface segregation [8]. It was reported in the literature that when the films were covered

with the closely packed trifluoromethyl groups (-CF_3), they exhibited the lowest surface energy (6 mN/m) [6, 9]. Consequently, numerous studies were carried out to synthesize fluorinated polymers that possessed fluorinated side chains (i.e. –CF_3 groups) to fabricate efficient oleophobic films.

To this end, this chapter describes the fabrication and understanding of oleophobic surfaces obtained by blending the fluorinated polyesters with their non-fluorinated counterparts. Specifically, we used fluorinated polyesters with -CF_3 terminated and non-CF_3 terminated chains, which have similar chemical structures, as described in **Chapter 4** to prepare blends. Herein, these fluorinated polyesters were solvent-blended with polyethylene terephthalate (PET) at various concentrations to obtain polyester films with different compositions. The surface properties, such as the morphology and wettability of films, were investigated using atomic force microscopy (AFM) and contact angle measurements, respectively.

5.2. Experimental Part

5.2.1. Materials

Polyethylene terephthalate (PET) was obtained from Unifi. The fluorinated polyesters used are described in **Chapter 4** and solvent (1,1,1,3,3,3-Hexafluoro-2-propanol (HFIP)) purchased from Oakwood Products, Inc. were used to prepare films.

5.2.2. Film Preparation

The synthesized fluorinated polyesters with non-CF_3 terminated (P1 polyester) and -CF_3 terminated chains (P2 and P3 polyesters), which have similar chemical structures,

were used to fabricate oleophobic films. Polyethylene terephthalate was blended with the fluorinated polyesters in different concentrations (5, 17, and 33 w/w % fluorinated polyesters in PET matrix) (**Figure 5.1**). Blended films were prepared on Si wafer substrate by dip coating from 3 wt% polymer blend solution in HFIP. Before the dip coating, the silicon wafers were cleaned by piranha solution using a mixture of H_2O_2 and H_2SO_4 (1:3 by volume) at 80°C for 1h, rinsed with DI water, and dried by N_2. After the deposition, the films were dried at room temperature, and they were annealed at 140°C for 3h in vacuum oven.

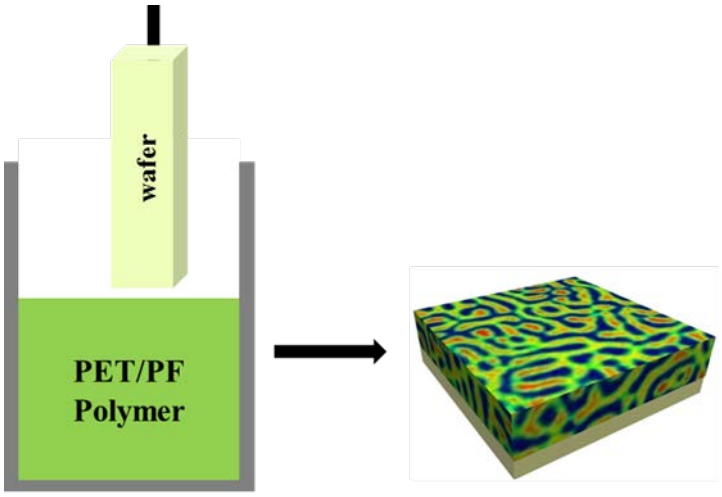

Figure 5.1. Schematic of the film formation method to generate PET/fluorinated polyester films.

In this study, the thermal properties, morphology and wettability of PET/Fluorinated polyester blends were conducted using DSC/TGA, AFM and contact angle measurements, respectively. In all analysis, results of blended films were compared with pure PET coating. The 100% uniform fluorinated polyester films were not obtained because they were dewetting during the deposition from the solution.

5.3. Results and Discussions

5.3.1. Fabrication of model PET/Fluorinated Polyester Films

Polyethylene terephthalate is one of the most common polyesters to be used in numerous applications, such as packaging, insulations, electronics, and textile. It is also well known that PET is partially wettable with water. The polymer is also highly oleophilic. To this end, to fabricate less oleophilic PET-based films, three fluorinated polyesters with different end groups (P1, P2, and P3), as shown in **Figure 4.2-4.3-4.4** (**Chapter 4**), were used as additives to PET. Specifically, a series of experiments was conducted to study the morphology and property of the PET-blended fluorinated polyester films deposited on Si wafers via dip coating. In this study, Si wafers were preferred more than glass slides due to their reflectance feature, which was required for thickness measurement of films using reflectometry and/or ellipsometry.

The fluorinated polyesters are soluble in many organic solvents (**Table 5.1**), while PET is not. It is only soluble in either HFIP or acetic acid-chloroform (1:2v/v %) mixture. Therefore, the blended polymer films were prepared by dip coating the wafers in the 3 w/v% PET/fluorinated polyester solutions in HFIP. One of the experimental challenges in this study was the volatile nature of the HFIP (bp≈60°C), which made it difficult to obtain homogeneous films. To overcome this obstacle, the polymer blend solution was contained in a vial that was at most half full. This allowed for the upper half of the vial to have a near saturated-solvent atmosphere, giving the film time to dry slowly. Dip coating was done in a close system to prevent air currents from creating streaks on the substrates by causing substrate motion and inhomogeneous drying. The prepared films were around

300±50nm in thickness using 300mm/min withdrawal rate. **Figure 5.1** displays a schematic of the film formation method to generate PET/fluorinated polyester films. Si wafers were dip coated into PET/fluorinated polyester solution with different fluorinated polymers to obtain 5, 17, and 33 w/w % of the polyester in the PET matrix.

Table 5.1. Solvents for PET and fluorinated polyesters

Polymers / **Solvents**	**PET**	**Fluorinated polyesters**
Acetone	-	+
MEK	-	+
Chloroform	-	+
Toluene	-	±
THF	-	+
Ethanol	-	-
HFIP	+	+
Acetic acid/chloroform	+	+

+ :soluble; -:insoluble; ± partially soluble

5.3.1.1. Annealing of PET/Fluorinated Polyester Films

It is obvious that the wettability of the PET/fluorinated polyester films depends on the ability of fluorinated species to segregate to the surface. The composition of the surface layer depends on the bulk compositions in the blends and in the annealing conditions, which have an influence on the physical properties of the films' surface.

Therefore, it is necessary to investigate the effects of composition and annealing conditions on the morphology and wettability of the films.

To identify the annealing condition, the thermal transition temperatures (glass-transition (T_g), melting temperature (T_f), and evaporation temperature (T_d) of the PET and fluorinated polyesters were obtained using DCS and TGA, respectively (**Table 5.2**). It revealed that all fluorinated polyesters melt at around 50±4°C and decompose at 406±4°C. In addition, PET starts melting at 230^0C (ΔH_f≈33.11J/g) and decomposing at 425^0C. It also possesses recrystallization temperature (T_c) at around 126^0C (ΔH_c≈25.85J/g), where the PET undergoes crystallization while heating in the DSC. The PET crystallization have been confirmed by several studies, which reported that the crystalline structures of PET were formed when they were annealed above its T_c [17]. In this study, PET and PET/fluorinated polyester films were annealed above T_c at 140°C for 3h under vacuum to determine the morphology changes and their effects on wettability.

Table 5.2. Thermal properties of fluorinated polyesters and PET

	T_g	T_f^a	ΔH_f^a	$\%^a$	T_c	ΔH_c	$T_f^{b,1}$	$\Delta H_f^{b,1}$	$\%^b$	T_d
P1	-18	55	27.7	28.0	-	-	-	-	-	411
P2	-29	48	28.4	28.6	-	-	-	-	-	404
P3	-21	48	26.4	26.6	-	-	-	-	-	404
PET*	67.6	-	-	-	126	27.35	238	33.77	5.2	425

[a]:fluorinated polyester polymer , [b-*]: PET polymer

5.3.2. Characterization of PET/Fluorinated Polyester Films

5.3.2.1. Characterization of PET/Fluorinated Ester Isophthaloic Acid (PET/P1) Films

A series of blended films consisting of 5, 17 and 33% (w/w) P1 polymer in PET matrix were conducted to prepare oleophobic films. Films were also annealed at 140°C for 3h.

Surface Morphology Analysis

The surface morphology of the PET and PET/P1 films before and after annealing was analyzed using atomic force microscopy (AFM). The AFM images presented in this study are dimensionally 10x10μ to observe the uniformity of films and microphase segregation of polymers. The root-mean-square (RMS) roughness was obtained using AFM software analysis. Examination of surface morphology (**Figure 5.2**) indicated that smooth and homogeneous PET and PET/P1 films were obtained without visible crystal formation. Although both PET and P1 polymer possess ester groups in their backbone structure, they are immiscible, leading to phase separation. Moreover, an increase of the concentration of P1 polymer in blends results in an increase in the size of phase-separated domains. It was found that the domain size increased from 176±33nm to 345±27nm and 546±100nm, as the concentration of P1 increased from 5wt% to 17wt% and 33wt%, respectively. **Figure 5.2** illustrates that P1 polymer content cannot influence film roughness; thus, it is independent of the P1 content.

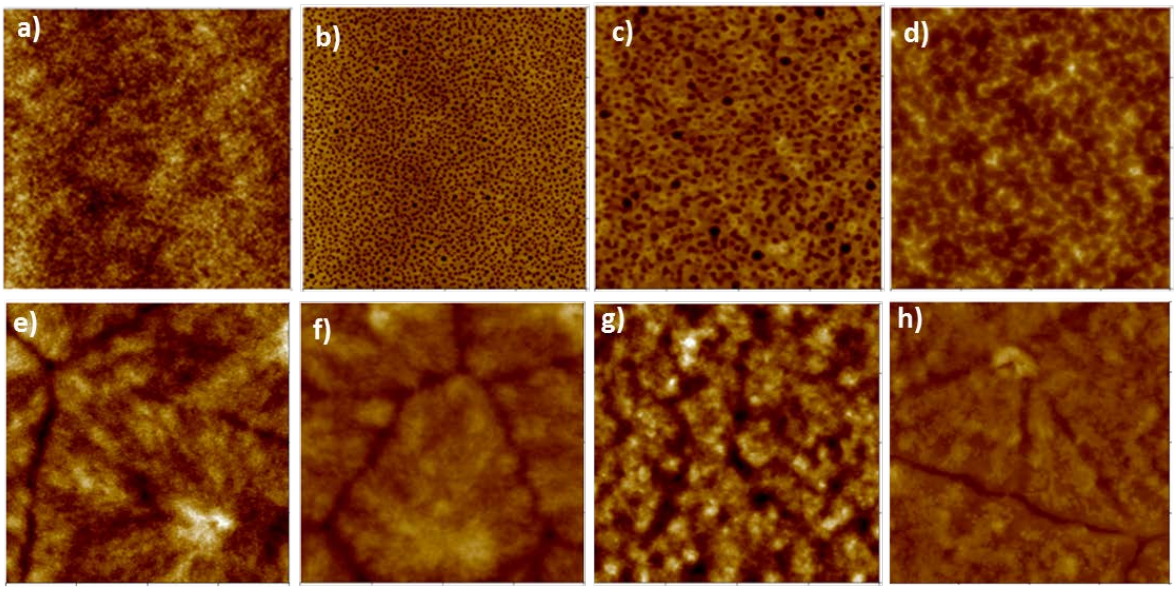

Figure 5.2. AFM images of PET and PET/P1 films (10µx10µ). Before annealing a) PET (RMS=0.3nm), b)5wt% P1 (RMS=1nm), c) 17wt% P1 (RMS=2.5nm), d) 33wt% P1 (RMS=1nm) and after annealing e)PET (RMS=6nm), f) 5wt% P1 (RMS=10nm), g) 17wt% P1 (RMS=7nm) and h) 33wt% P1 (RMS=7nm).

Figure 5.2 shows that the morphology of films after the annealing was different from that prior to the annealing. The crystalline domains were formed within both the PET and PET/P1 film surfaces because films were heated above the T_c of PET and T_f of P1. Polymer chains rearranged themselves and form crystals during the heating. The roughness of surfaces increased from 1-3nm to 6-10nm after the annealing due to the crystalline formation. Furthermore, phase separation was clearly seen in the annealed surfaces.

Wettability of PET/P1 Polymer Films

It is well known that the contact angle (CA) of liquids on films is a direct reflection of surface energy of the components of the surface. Therefore, we measured

the CA of the reference liquids, such as hexadecane and water on PET and PET/ P1 films. The results are shown in **Figure 5.3** and **Figure 5.4**, respectively. Contact angle measurements were used to determine effects of P1 content on the wettability of PET films. Results show that pure PET coating is completely wettable with hexadecane and partially wettable with water (**Figure 5.3-5.4**). It is clearly seen that the incorporation of a small amount of fluorinated species (5 wt%) into the PET results in strong increase of water and hexadecane contact angles. The CAs of hexadecane increased up to 41° and the CAs of water increased from 58° to 67°. Furthermore, the CA of water kept increasing from 67° to 76°, as the P1 polymer concentration increased from 5 wt% to 33 wt%. For hexadecane, the effect is less pronounced (44° at 33 wt%).

To date, numerous studies have been devoted to alter the wettability of the films. From those studies, it is known that the wettability of films depends on both chemical structure and surface roughness. The AFM results in this study reveal that all films possessed smooth surfaces (RMS<10nm). Thus, the influence of roughness on the wettability of films is negligible. Consequently, the variation of the contact angles of liquids is solely associated with the chemical structure of the coating surfaces. In other words, the packing of the outermost atoms on the surface influences the wettability of the films. The key issue in this case is how to pack more densely fluorocarbon groups on the outermost surfaces of the PET/P1 films to reduce surface energy, resulting in high CA of liquids on surfaces.

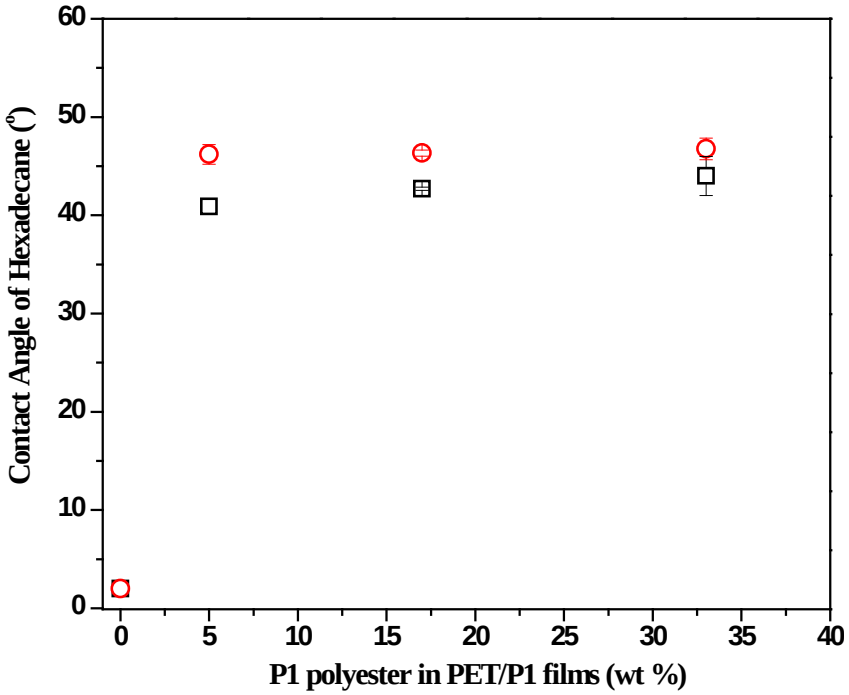

Figure 5.3. Contact angle of hexadecane on PET and PET/P1 films;

(□) before annealing and (○) after annealing at 140°C for 3h.

To investigate how annealing influences the wettability of PET/P1 films, the CAs of both hexadecane and water on surfaces were measured after annealing at 140° for 3h, as shown in **Figure 5.3** and **Figure 5.4**, respectively. Figures show that the significant increase in the CA of water on annealed samples was obtained. The angle increased from 75° to 86° when films contained 33 wt% of P1. However, there were only small changes in the CAs of hexadecane (from 44° to 46°) on the same samples. It could have happened that when the annealing treatment was performed above the T_g of films, the $–CF_2$ groups in the P1 polyester backbone had sufficient mobility to rearrange. This rearrangement resulted in the migration of chains to the outermost surface, indicating an enrichment of $–CF_2$ groups on the top. In addition, the CAs of water on annealed film surfaces increased

from 76° to 86°, increasing the amount of the P1 polymer from 5 wt% to 33 wt% in films.

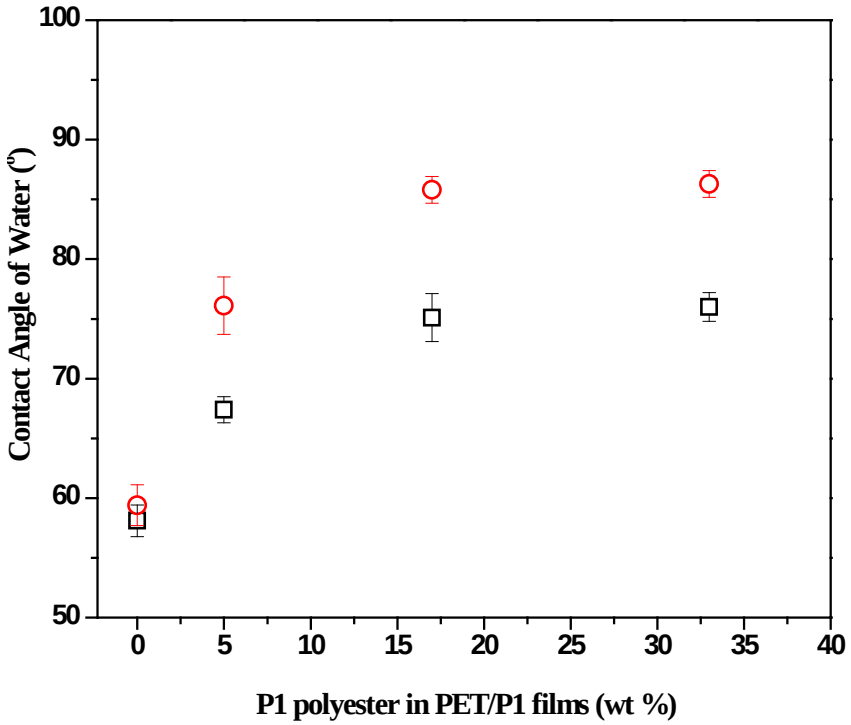

Figure 5.4. Contact angle of water on PET and PET/P1 films;

(□) before annealing and (○) after annealing at 140°C for 3h.

Apart from the CA measurements, the surface energy estimation was also used to characterize the surface of the films. The surface energy of the films plays an important role in the phenomena that occurs in the solid-liquid and solid-vapor interfaces. Knowledge of this parameter is valuable for the industrial applications of these films. The contact angle of two liquids on the surface permitted the rapid and qualitative evaluations of the surface energy of polymer films. In this study, we calculated the surface energy of PET and PET/P1 films according to the Owens-Wendt method [59] shown in **Equation 5.1**.

$$1+\cos\theta \approx 2\left[\frac{\sqrt{\gamma_s^d \gamma_1^d}+\sqrt{\gamma_s^p \gamma_1^p}}{\gamma_1}\right] \quad (5.1a)$$

$$1+\cos\theta \approx 2\left[\frac{\sqrt{\gamma_s^d \gamma_2^d}+\sqrt{\gamma_s^p \gamma_2^p}}{\gamma_2}\right] \quad (5.1b)$$

$$\gamma_s = \gamma_s^d + \gamma_s^p \quad (5.1c)$$

where γ_s and γ_l is the surface tension of the solid and liquid, respectively. The subscripts *d* and *p* correspond to dispersion and polar components of the surface tension, respectively.

Surface free energy (γ_s) and its polar (γ_s^p), as well as the dispersion (γ_s^d) components of the PET/P1 surfaces were determined using two sets of the CA measurements of water and hexadecane. The γ_l^p and γ_l^d values for each solvents were obtained from the literature (**Table 5.3**). After calculating the surface energy of the PET/P1 films, they were compared with the surface energy of pure PET films, as shown in **Figure 5.5**.

Table 5.3. The surface energy values of polar and dispersion components of liquids.

	γ_d	γ_p	γ
water	21.8	51	72.8
hexadecane	27.47	0	27.47

PET films demonstrated quite high surface energy (46 mN/m). However, the energy was reduced up to 37.6 mN/m when PET was blended with 5 wt% P1 polymer. Our results were compared with polytetrafluoroethylene (PTFE, $\gamma_s \approx 18$ mN/m), which is shown as blue line in **Figure 5.5**. It was found that PTFE possessed lower surface energy compared to PET/P1 films. It happened because PTFE consisted only fluorocarbon groups, while P1 possessed not only the fluorocarbon groups, but also the hydrocarbon groups and polar-end groups, such as -COOH and -OH in its structure.

Furthermore, **Figure 5.5** revealed that a decrease of surface energy in PET/P1 films from 37.6 mN/m to 31.8 mN/m was determined by increasing the P1 polyester concentration from 5 to 33 wt%, resulting in high amount of $–CF_2$ groups on surface-minimized surface energy of films. Annealing treatment also decreased their surface energy. For instance, the surface energy of PET/P1 (33 wt%) films was reduced from 31.8 to 26 mN/m after the annealing. Compared to the effects of the two parameters: *i) P1 polyester concentration in films* and *ii) annealing treatment* on surface energy, **Figure 5.5** shows that the annealing influenced their surface energy more predominantly than the P1 polyester concentration. It revealed that the surface energy of the annealed PET/P1 films (5 wt% P1) was (31.4 mN/m) was close to the surface energy of the PET/P1 films (33 wt% P1) that were not annealed (31.8 mN/m). The latter sample even had higher surface energy than the annealed films containing 17 wt% P1 polymer (26.3 mN/m). It could happen because the P1 polymer possessed polar end-groups –COOH and –OH. However, non-polar $–CF_2$ groups were in the backbone and have less ability to be present at the surface than the end groups.

Upon increasing the concentration of the P1 polyester in the films, not only the amount of the $-CF_2$ groups increased; the amount of the polar end-groups increased as well. Therefore, both the polar and non-polar groups influenced the surface energy of the films. On the other hand, the non-polar groups in bulk migrated through the surface during the annealing although films had low P1 concentrations.

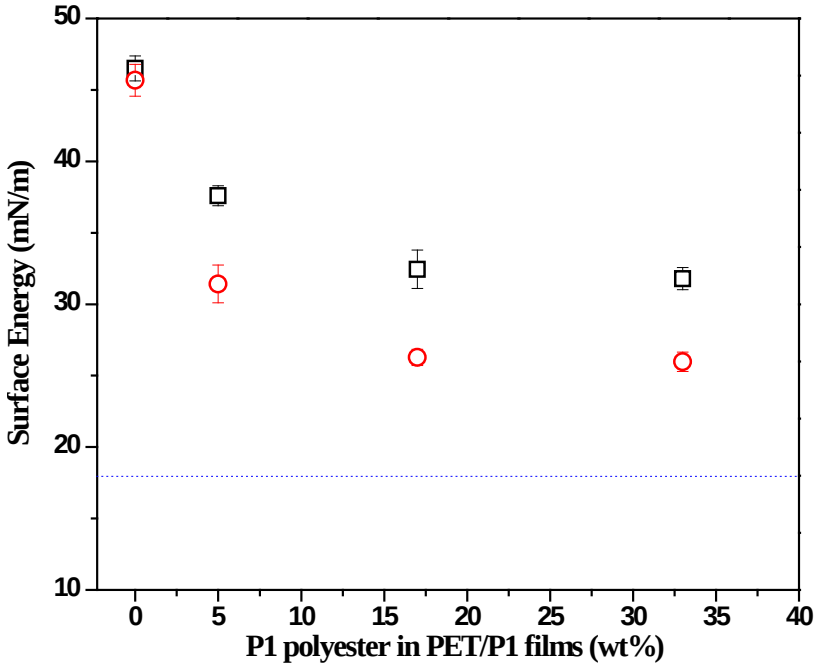

Figure 5.5. Surface energy of PET/P1 films with different concentration of P1 polymer in films; (□) before annealing and (○) after annealing at 140°C for 3h.

Therefore, film surfaces resulting in the enrichment of the $-CF_2$ groups as compared with the polar groups have lowered surface energy more during the annealing. As a conclusion, surface energy can be altered by either increasing the concentration of the P1 polyester or by annealing the films. It was found that the annealing treatment was the most efficient method to reduce surface energy.

5.3.2.2. Characterization of PET/Fluorinated Ester Isophthaloyl Polyester (PET/P2) Films

A series of blended films consisting of 5, 17, and 33% (w/w) P2 polyester in PET matrix were conducted to prepare oleophobic films. Films were annealed at 140°C for 3h.

Surface Morphology Analysis

The morphology of the PET/P2 films was determined using AFM. Results are presented in **Figure 5.6**. The images show that the PET/P2 films possessed smooth surfaces. The roughness of the surfaces was observed to be 32±5 nm. The P2 polyester is also immiscible with PET, as evident from the phase separation. The sizes of the domains in the 5 wt% and 17 wt% samples were found to be 391±81 and 410±67nm, respectively. The PET/P2 (33 wt% P2) films possessed considerably larger P2 domains (e.g., 1.3μ and 3.6μ). The sample also had highest roughness (36nm). On the other hand, the roughness of the annealed PET/P2 films was lower than before the annealing. For instance, the roughness of the films with 33 wt% P2 was found to be at 18nm.

Wettability of PET/P2 Films

The wettability of the PET/P2 polymer films was evaluated with CA measurements of hexadecane and water. **Figure 5.7** and **Figure 5.8** show that when PET was blended with P2 polyester, surface wettability was changed significantly. The PET/P2 films became partially oleophobic and highly hydrophobic, with dependence on the P2 polyester content in the films. The maximum value of the CA of hexadecane and

water reached 51° (**Figure 5.7**) and 87° (**Figure 5.8**), respectively, with 33 wt% P2 in PET films.

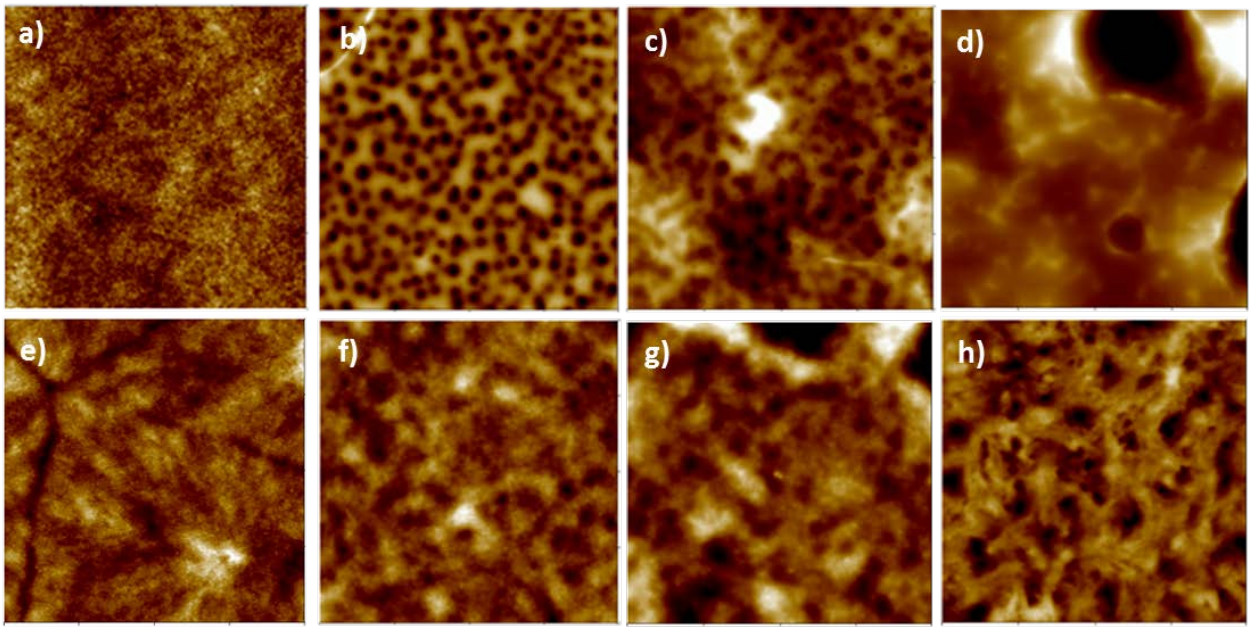

Figure 5.6. AFM images of PET and PET/P2 films (10µx10µ). Before annealing a) PET (RMS=0.3nm), b)5wt% P2 (RMS=26nm), c) 17wt% P2(RMS=33nm), d) 33wt% P2 (RMS=36nm) and after annealing e)PET (RMS=6nm), f) 5wt% P2 (RMS=10nm), g) 17wt% P2 (RMS=32nm) and h) 33wt% P2 (RMS=18nm).

To investigate how annealing influenced the wettability of the PET/P2 polyester films, the CAs of the solvents on films were also measured after annealing at 140°C for 3h. Results are shown in **Figure 5.7** and **Figure 5.8.** It was found that the CAs of water increased after annealing from 87° to 91°. The reason behind this increment of CA measurements is the enrichment of the fluorocarbon groups on the surface during annealing.

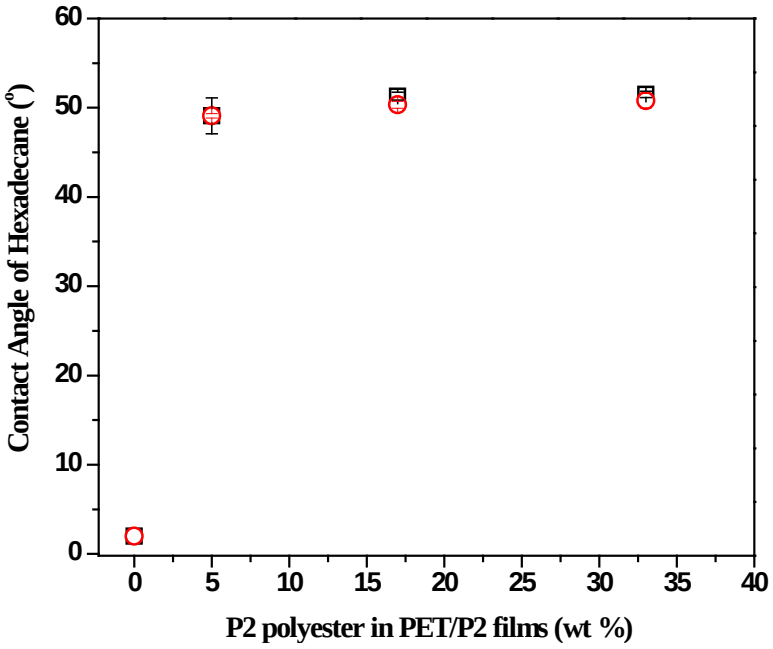

Figure 5.7. Contact angle of hexadecane on PET and PET/P2 films ;

(□) before annealing and (○) after annealing at 140°C for 3h.

Compared to the effect of P1 and P2 polyesters on the wettability of PET films, the latter polyester exhibited higher CAs measurements than the former. P1 possessed only –CF_2 groups in the backbone and polar groups at the ends, while P2 had both –CF_2 groups in the backbone and –OH and–CF_3 groups at the ends. It is well known that –CF_3 groups exhibit lowest surface energy. The mobility of polymer chains during annealing allowed both –CF_2 and –CF_3 groups to migrate to the surface. Essentially, the enrichment of –CF_3 groups on the surface decreased the surface energy of films more, resulting in high CAs of solvents on them.

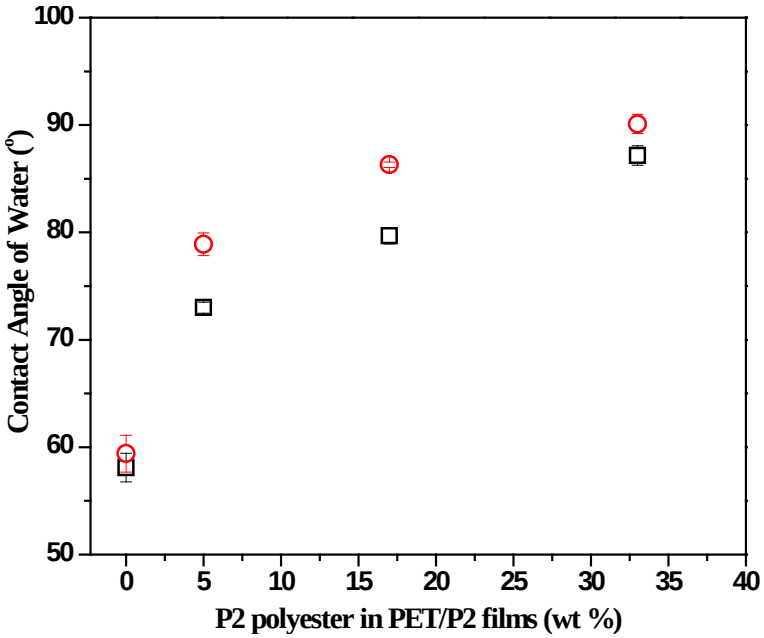

Figure 5.8. Contact angle of water on PET and PET/P2 films;

(□) before annealing and (○) after annealing at 140°C for 3h.

The surface energy of the PET/P2 films was also calculated using CA measurements, as shown in **Figure 5.9**. Apparently, incorporation of small amount of P2 polyester in PET films decreased the surface energy from 46mN/m to 33mN/m (5 wt% P2). Increasing the P2 concentration with high amounts of $–CF_2$ and $–CF_3$ groups on the surface also reduced their surface energy. The minimum surface energy, 24.7 mN/m, was obtained when the PET film contained 33 wt% P2 polyester.

Figure 5.9 illustrates that surface energy also decreased after the annealing of the PET/P2 films. It was found that the surface energy of films (5 wt% P2) reduced from 33 to 29 mN/m. It could happen because the P2 polymer possessed $–CF_3$ end-groups. During the annealing, they migrated to the surface; the surface was enriched with them, resulting in lower surface energy.

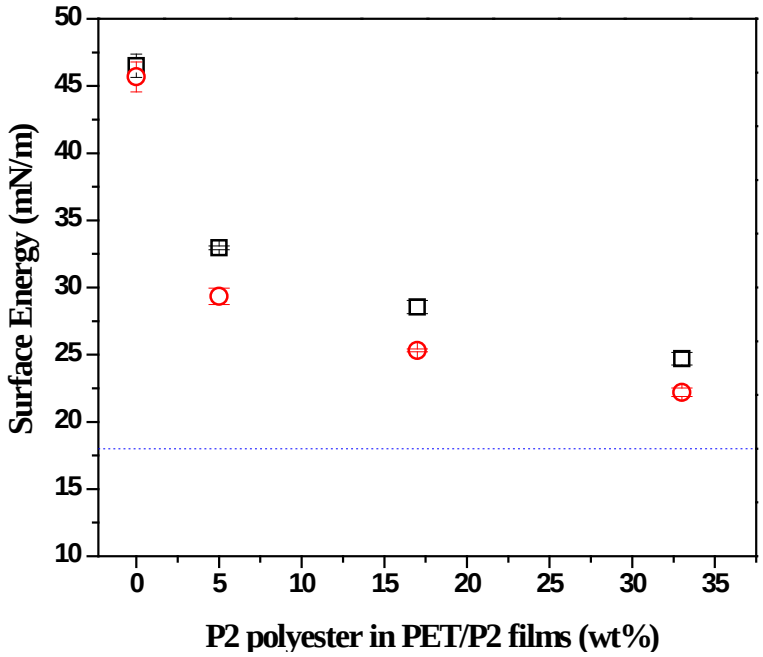

Figure 5.9. Surface energy of PET/P2 films;

(□) before annealing and (○) after annealing at 140°C for 3h.

The annealed films with 33% P2 possessed lowest surface energy (22.2 mN/m). It is also clearly seen that the annealing has more effect on the surface energy of films than the P2 polyester content. When we almost doubled the P2 content in the films (from 17 wt% to 33 wt%), the surface energy was decreased from 28.5 mN/m to 24.7 mN/m. The only reason behind this is that the annealing treatment accelerated fluorinated carbon entities' movement to the surface, lowering surface energy.

5.3.2.3. Characterization of PET/Fluorinated Diester Isophthaloyl Polyester (PET/P3) Films

A series of blended films containing 5, 17, and 33% (w/w) P3 polymer in PET matrix were conducted to prepare oleophobic films. Subsequently, they were annealed at 140°C for 3h.

Surface Morphology Analysis

Figure 5.10 shows the morphology of the PET/ P3 films before and after annealing. It can be seen that this polymer was also immiscible with PET. Again, phase separation was observed. Although the overall size of the domains increased from 548±61nm to 605±106 nm, the P3 polyester content increased from 5wt% to 17 wt%, respectively, films contained 33 wt% P3 polymer possessed large P3 domains (e.g.1.6µ and 2µ), as well. After annealing, the crystalline structures similar to PET/P1 films were also obtained in PET/ P3 films.

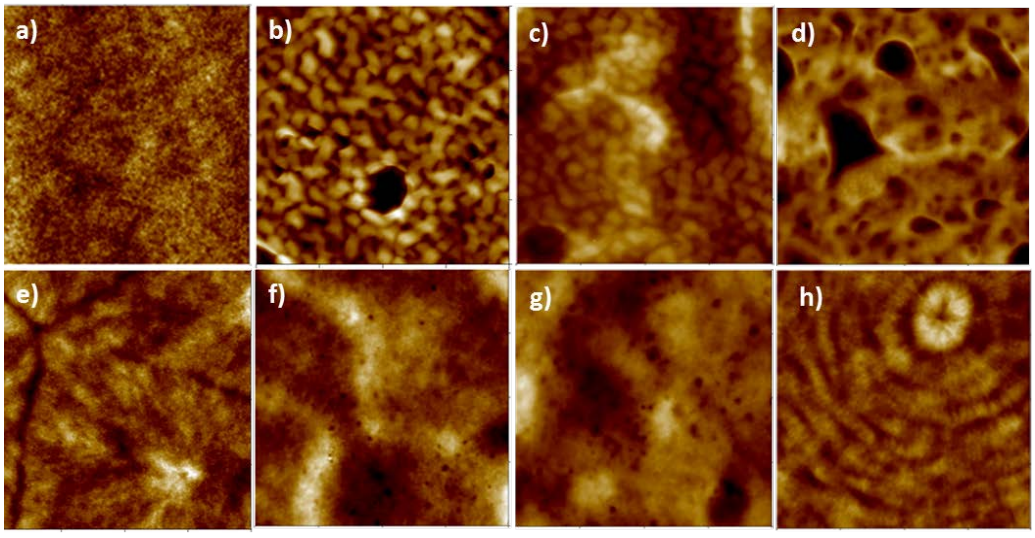

Figure 5.10. AFM images of PET and PET/P3 films (10µx10µ). Before annealing a)PET (RMS=0.3nm), b)5wt% P3 (RMS=16nm), c) 17wt% P3 (RMS=32nm), d) 33wt% P3 (RMS=31nm) and after annealing e)PET (RMS=6nm), f) 5wt% P3 (RMS=15nm), g) 17wt% P3 (RMS=25nm) and h) 33wt% P3 (RMS=9nm).

Wettability of PET/P3 Films

The contact angles of hexadecane and water on the PET/P3 films before and after annealing are shown in **Figure 5.11** and **Figure 5.12**, respectively. It is seen that the addition of P3 into the PET films influenced the CAs of water and hexadecane. The CAs of water increased from 73° to 88°, increasing P3 polymer concentration from 5 wt% to 33 wt% in the film. The CA change of hexadecane is not pronounced since it is increased from 51° to 53°.

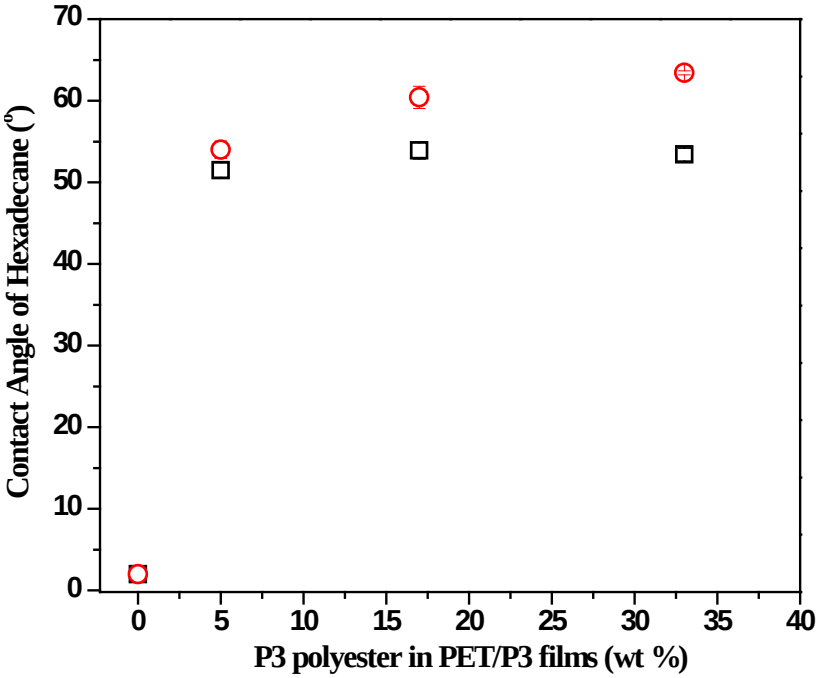

Figure 5.11. Contact angle of hexadecane on PET/P3 films,

(□) before annealing and (○) after annealing at 140°C for 3h.

As shown in **Figure 5.11** and **Figure 5.12**, the wettability of the PET/P3 films was also influenced by annealing. When the PET/P3 films were annealed at 140°C for 3h, chains became more mobile and could be reoriented. During reorientation, most of the fluorine in the films migrated to the surfaces due to their low surface energy. Concentration and closer packing of $-CF_3$ groups of P3 polyester in the outermost surface region were increased, resulting in low surface energy. As a result, the CAs of liquids increased. The maximum CAs of hexadecane and water was found to be 63° and 103°, respectively.

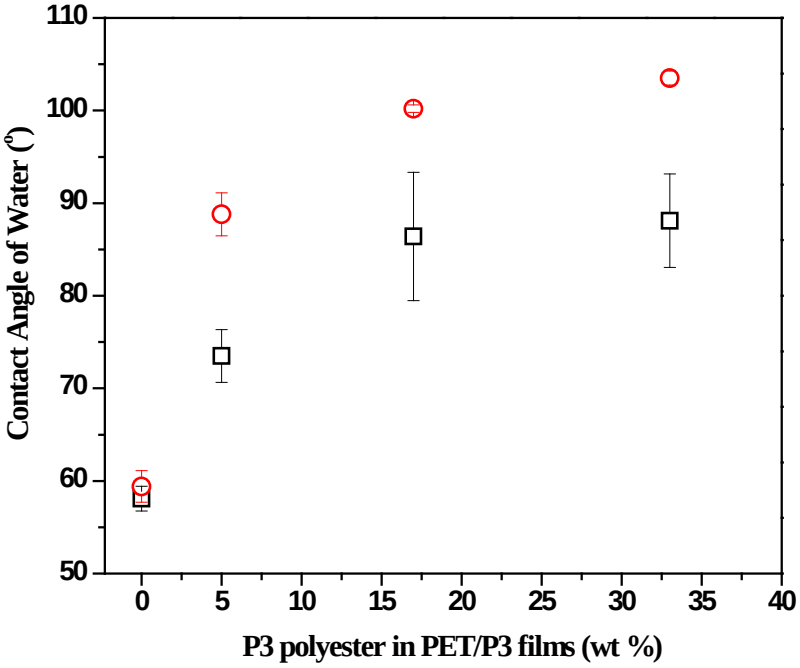

Figure 5.12. Contact angle of water on PET/P3 films,

(□) before annealing and (○) after annealing at 140°C for 3h.

The contact angle measurements of the PET/P3 films were also used to calculate surface energies. **Figure 5.13** shows that surface energy decreased upon the increase of the amount of P3 polyester in the PET/P3 films. The films with 33 wt % P3 polyester content exhibited the lowest surface energy (24 mN/m) although it was still higher than PTFE. However, after annealing the same films, their surface energy decreased more and became lower (16.5 mN/m) than PTFE because the P3 polymer possessed $-CF_3$ end-groups in both sides and film surfaces were enriched with them after annealing.

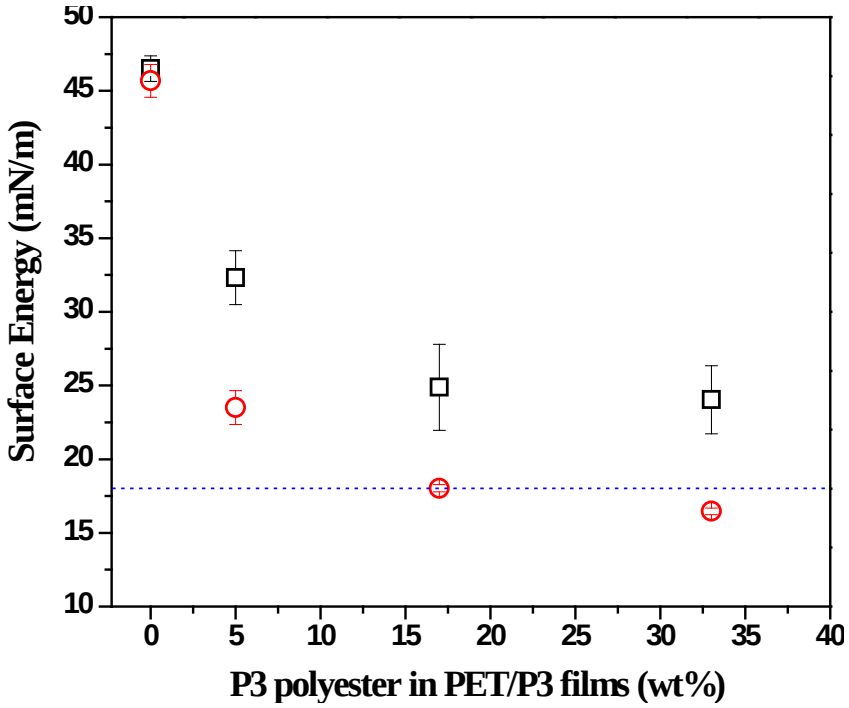

Figure 5.13. Surface energy of PET/P3 films;

before annealing and ○) after annealing at 140°C for 3h.

5.3.2.4. XPS Analysis of PET/Fluorinated Polyester Films

XPS was used to examine the composition of the outermost surface of the PET/fluorinated polyester films (max~10nm) before and after the annealing. It was

carried out on PET/Fluorinated polymeric systems consisting of 5% and 33% fluorinated polyesters in blends. Three fluorinated polyesters (P1, P2, and P3) with different end groups were used to investigate the end groups' effect on the surface composition. It was found that the XPS' survey spectra of PET/fluorinated polyester blends possessed only three characteristic peaks, namely F1s, O1s, and C1s. There was no signal indicative of the silicon wafer substrate being present. The F1s was primarily from the fluorinated polyesters. The rest were from both the PET and fluorinated polymers. The experimental F/C ratio contained the contribution of both PET and fluorinated polyesters to the overall F1s and C1s spectra. The F/C ratios of samples obtained from the XPS are presented in **Table 5.4** and **Table 5.5**.

Table 5.4.C/F atomic ratios for PET/Fluorinated polyester films (5 wt %).

	2:1 PET/P1		**2:1 PET/P2**		**2:1 PET/P3**	
degree	**before annealing**	**after annealing**	**before annealing**	**after annealing**	**before annealing**	**after annealing**
0	4.69	2.18	2.66	1.41	1.71	1.39
30	4.75	2.23	2.54	1.30	1.64	1.34
60	3.08	1.7	1.92	0.70	1.10	1.00

Table 5.5.C/F atomic ratios for PET/Fluorinated polyester films (33 wt%).

	PET/P1		**PET/P2**		**PET/P3**	
degree	**before annealing**	**after annealing**	**before annealing**	**after annealing**	**before annealing**	**after annealing**
0	1.27	1.42	1.05	1.1	0.91	0.76
30	1.29	1.19	1.05	1.09	0.93	0.72
60	1.32	1.08	0.99	0.8	0.86	0.65

The molar concentration of fluorinated polyesters at the outer surface was calculated based on the elemental F/C ratio from the survey spectra using the following formula [15]:

$$\left(\frac{F}{C}\right)_{XPS} = \frac{X_{PF}F_{PF}}{X_{PF}C_{PF} + X_{PET}C_{PET}} \qquad (5.2a)$$

$$X_{PF} + X_{PET} = 1 \qquad (5.2b)$$

where X_{PF} and X_{PET} is the molar concentration of fluorinated polyesters (PF) and PET at the surface, respectively, and $F_{PF,}$ $C_{PF,}$ and C_{PET} are the atomic concentrations in the fluorinated polyester and PET polymers, respectively.

In this study, three incident angles (0°, 30°, and 60°) were used. The detector line of sight is perpendicular to the sample at 0°. Depth from the surface decreased with each increased incident angle. For instance, the composition of 10 nm depth from the coating surface was examined when the angle was 0°; while 4-6 nm and/or 1-3 nm depth from the surface was analyzed if the angle was 30° and/or 60°, respectively[15]. Fluorinated polyester concentration as a function of depth from the surface before and after annealing is presented in **Figure 5.14** (5% PF in blend) and **Figure 5.15** (33% PF in blend). The C/F atomic ratios were obtained using XPS. XPS results display that the surfaces were enriched with fluorinated polyesters instead of PET. It is seen that the content of fluorine decreased with each increase of depths from the surface. For instance, PET/P1 films (**Figure 5.15**) exhibited 89% coverage of 1-3nm depths of the surface (60°), while it was

only covered 80% of films in 10 nm depths (0°). It means that outermost surface is the densest with fluorinated species.

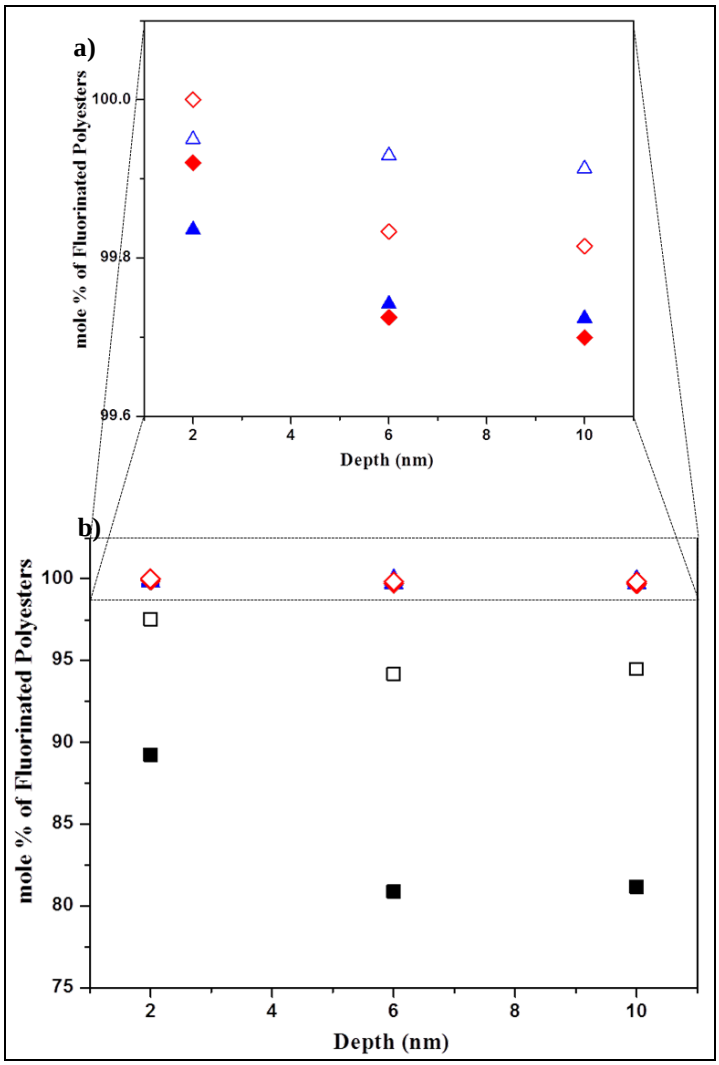

Figure 5.14. Surface concentration of fluorinated polyesters (5%) with different end-groups in blends (solid) before and after annealing at 140°C for 3h (empty). □)P1 (OH/COOH); Δ)P2 (CF_3/COOH) and ◊)P3(CF_3/ CF_3).

The effect of the end groups of fluorinated polyesters on the surface coverage was also investigated. It was found that when the blended films contained 5% fluorinated

polyesters, the PET/P1 films exhibited 89% coverage with the P1 polymer terminated with –OH and –COOH groups. It is expected because P1 polyester has fluorocarbon groups (-CF_2) in the backbone of the polymer. Therefore, PET/P1 surface was enriched with both the CF_2 groups and the polar end- groups of P1 polymer when it migrated to the surface.

The P2 and P3 polymers possessed long fluorinated tails in one side and both sides, respectively. These tails contain –CF_3 entities, which have the lowest surface energy. When these polyesters were blended with PET, the mobile fluorine tails migrated to the surface easily and enriched it completely. Thus, P2 and P3 polyesters covered almost 100% of the PET/P2 and PET/P3 coating surfaces, respectively (**Figure 5.14, a**). The P3 polymer exhibited the highest coverage on the surface.

The degree of fluorinated polyester enrichment at the surface depends on fluorinated polyester concentrations in blends. When the blended films possessed 33 wt % P1, surface was fully covered with P1 (**Figure 5.15**), while 89% of P1 coverage was obtained if 5% P1 was used (**Figure 5.14**). However, it is not the case for the P2 and P3 polymers because they always fully covered surfaces even if 5 wt% of them was blended with PET. It was concluded that if the fluorinated polyester did not have fluorinated tails, it was better to use high concentration in blends to obtain fully fluorocarbon groups coverage on the surface. Conversely, if the polyester was terminated with fluorinated tails, lower amounts of them in blends were enough to cover the surface completely.

Annealing also influenced the composition of fluorinated polyesters at the surface. It is well known that at room temperature, soft segments of polymers (fluorinated

polyesters) are above glass transition temperature, T_g; thus, they are more mobile than stiff segments (PET) being generally glassy. It is expected that the mobility of the stiff segments was increased with annealing polymeric blends above their T_g. During annealing, PET stiff segments also reordered and allowed fluorinated segments movement through the surface to minimize system energy. To investigate the effects of annealing on surface composition, PET/Fluorinated polyester films were annealed at 140°C for 3h under vacuum. Subsequently, XPS analysis was conducted.

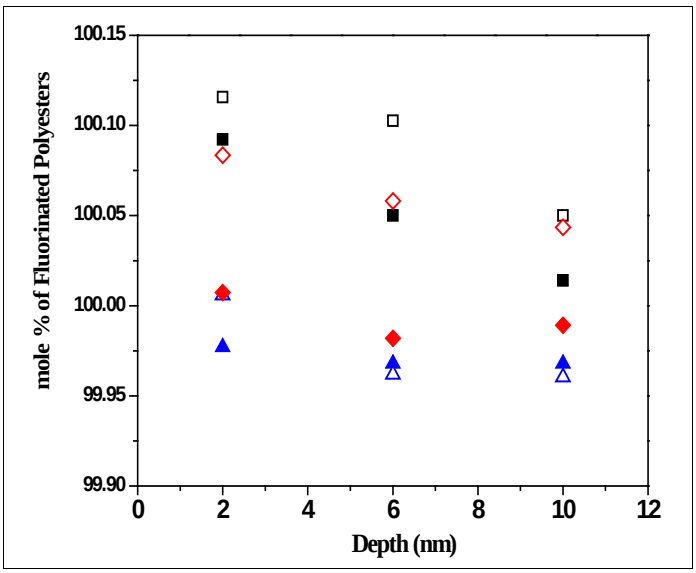

Figure 5.15. Surface concentration of fluorinated polyesters (33%) with different end-groups in blends (solid)before and after annealing at 140°C for 3h (empty). □) P1 (OH/COOH); Δ)P2 (CF_3/COOH) and ◊)P3(CF_3/ CF_3).

As seen in **Figure 5.14** and **Figure 5.15**, fluorine concentration at the surface changed with annealing. As low concentration of fluorinated polyester was used in blends, fluorocarbon groups concentration increased after annealing at all depths. Specifically, for PET/P1 films, 89% of the surface was covered with P1, but when they

were annealed, 98% of the surface was covered with it. For other polymers, 100% coverage was obtained as well.

Interestingly, the surface energy of the annealed films was different for each PET/fluorinated polyester films although all annealed surfaces were fully covered with fluorocarbon groups. The reason for possessing different surface energies for each PET/fluorinated polyester films is the type of fluorocarbon groups that covered the surfaces. For instance, the PET/P1 films were fully covered with only $–CF_2$ groups, while $–CF_2$ and $-CF_3$ groups fully covered the PET/P2 and PET/P3 surfaces. In addition, it was well known that $-CF_3$ groups exhibited lowest surface energy. Among them, the PET/P3 films possessed the lowest surface energy, even lower than the PTFE.

5.3.2.5. The Effects of the End Groups of Fluorinated Polyesters on Wettability

The wettability of surfaces is dependent only on a few nanometers of films. The wettability of PET-coating surfaces can be altered by changing the structure of surfaces with the change of their surface energy. As detailed above, the CAs of both water and hexadecane rose sharply with each increase of fluorinated polyester content in the PET films. Based on these results, we also found that the wettability of PET/fluorinated polyester films depended not only on the concentration of fluorinated polymers in films, but also on the end groups of fluoro polymers. To investigate how the end groups of fluorinated polyester influence the wettability of films, the CAs of hexadecane and water on PET/fluorinated polyester systems consisting of 67 wt% PET and 33 wt% fluorinated polyesters are shown in **Figure 5.16** and **Figure 5.17**, respectively.

These figures revealed that although the end groups of the P1 polymer were polar, the CA of both water and hexadecane on the PET/P1 film significantly increased in comparison with the pure PET film. This is a result of the presence of $-CF_2$ groups in the polymer backbone, resulting in the lower surface energy of films as compared to hydrocarbons.

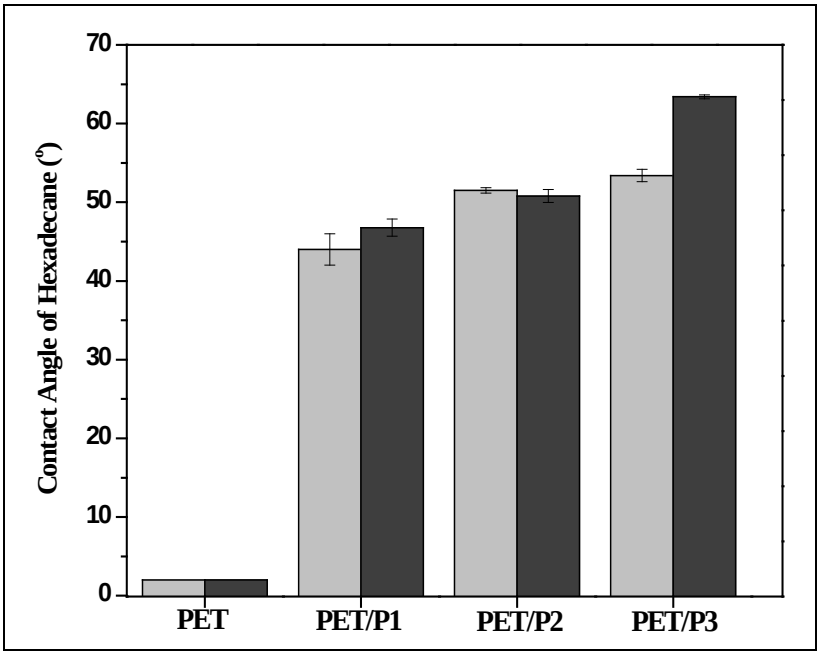

Figure 5.16. Contact angle of hexadecane on PET/Fluorinated polyester films (33w/w %); □) before annealing, □) after annealing.

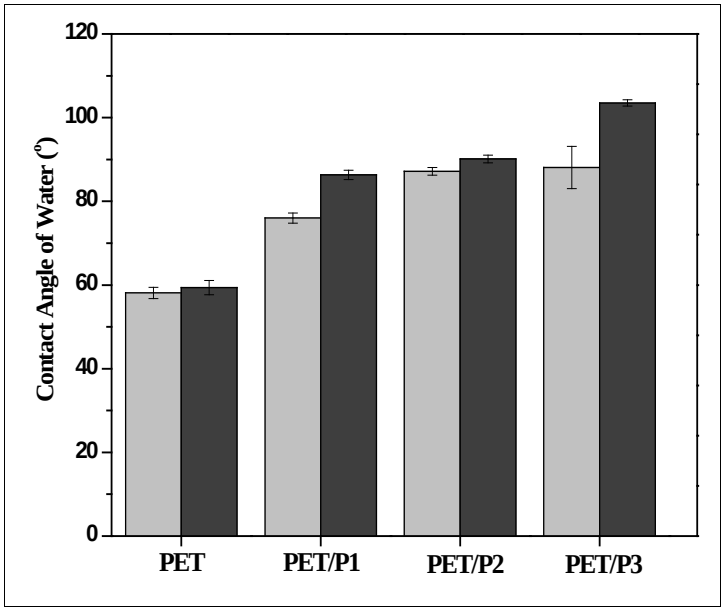

Figure 5.17. Contact angle of water on PET/Fluorinated polyester films (33w/w %); □) before annealing, □) after annealing.

When the P2 and P3 polyesters were blended with PET, the PET/P3 films exhibited the highest values of CA of liquids in comparison with others due to their possession of -CF_3 end groups in both sides, resulting in lowest surface energy of film surface. It was also seen clearly that all PET/fluorinated polyester films had a higher contact angle for water after being annealed at 140°C for 3h. For hexadecane, the effect was lesser. Apart from the contact angle measurements, the surface energy of PET/fluorinated polyester films (33 w/w%) were compared and presented in **Figure 5.18**. It shows that the addition of fluorinated polyesters into the PET blends significantly reduced its surface energy. In this study, P3 was terminated –CF_3 groups in both sides; thus, the PET/P3 films exhibited lowest surface energy. As detailed above, surfaces were enriched with fluoro-carbon groups since fluorinated entities migrated to the surface

during the annealing treatment. Therefore, the PET/P3 films exhibited not only the lowest surface energy among the annealed blended films, but also lower than PTFE, shown as blue line in **Figure 5.18**.

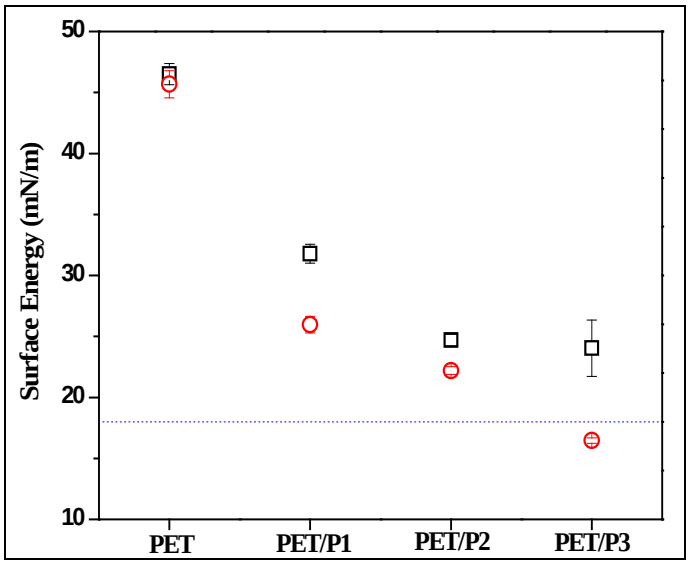

Figure 5.18. Surface energy of PET/Fluorinated polyester films (33w/w%). □) before annealing and ○) after annealing at 140°C for 3h.

5.4. Conclusions

The oleophobic films were fabricated from the blends of the PET polymer with three fluorinated polyesters terminated with different end groups (-COOH, -OH, and -CF_3) in different concentrations. It was found that the wettability of the surface depends on the end groups of fluorinated polyesters, their compositions in the blend, and annealing treatment. From the CA measurements of water and hexadecane, the P3 polymer terminated with –CF_3 groups in both sides exhibited the lowest wettability. XPS analysis was performed to quantify the concentration of the fluorinated polyester at the surface. Fluorinated species were denser at the surface than in the bulk. As the fluorinated

content was increased in the blends, the surface was enriched more with fluorine. Furthermore, surface concentration was changed with annealing. Even at low concentration of fluorinated polyester blends, all fluorinated species migrated to the surface during annealing, resulting in a higher concentration of fluorine on the surface. Therefore, all fluorinated polyesters exhibited 100% coverage on the surfaces after annealing.

5.5. References

1. Boker, A.; Herweg, T.; Reihs, K., Selective Alteration of Polymer Surfaces by Thermal Cleavage of Fluorinated Side Chains. *Macromolecules* **2002,** *35* (13), 4929-4937.
2. Iyengar, D. R.; Perutz, S. M.; Dai, C.-A.; Ober, C. K.; Kramer, E. J., Surface Segregation Studies of Fluorine-Containing Diblock Copolymers. *Macromolecules* **1996,** *29* (4), 1229-1234.
3. Shull, K. R.; Kramer, E. J., Mean-field theory of polymer interfaces in the presence of block copolymers. *Macromolecules* **1990,** *23* (22).
4. Dai, K. H.; Kramer, E. J.; Shull, K. R., Interfacial segregation in two-phase polymer blends with diblock copolymer additives: the effect of homopolymer molecular weight. *Macromolecules* **1992,** *25* (1), 220-225.
5. Bongiovanni, R.; Di Meo, A.; Pollicino, A.; Priola, A.; Tonelli, C., New perfluoropolyether urethane methacrylates as surface modifiers: Effect of molecular weight and end group structure. *Reactive and Functional Polymers* **2008,** *68* (1), 189-200.
6. Honda, K. M., M.; Otsuka, H.;Takahara, A., Molecular aggregation structure and surface properties of poly(fluoroalkyl acrylate) thin films. *Macromolecules* **2005,** *38* (13).
7. Owens, D. K.; Wendt, R. C., Estimation of the surface free energy of polymers. *Journal of Applied Polymer Science* **1969,** *13* (8), 1741-1747.
8. Hutchings, L., Stimuli responsive surface segregation of well-defined end-functionalized polymers. *Polymer Reprints* **2009,** *50* (1).
9. Lau, W. W. Y.; Burns, C. M., Effect of temperature and molecular weight on the rate of spreading of polystyrene melts on plane soda lime glass surfaces. *Journal of Polymer Science: Polymer Physics Edition* **1974,** *12* (2), 431-439.
10. Lee, H.; Archer, L. A., Functionalizing polymer surfaces by surface migration of copolymer additives: role of additive molecular weight. *Polymer* **2002,** *43* (9), 2721-2728.
11. Tanaka, K.; Takahara, A.; Kajiyama, T., Surface Molecular Aggregation Structure and Surface Molecular Motions of High-Molecular-Weight Polystyrene/Low-Molecular-Weight Poly(methyl methacrylate) Blend Films. *Macromolecules* **1998,** *31* (3), 863-869.

12. Jones, R. A. L., *Polymers at surfaces and interfaces*. Cambridge University Press: Cambridge, 1999.
13. Mason, R.; Jalbert, C. A.; O'Rourke Muisener, P. A. V.; Koberstein, J. T.; Elman, J. F.; Long, T. E.; Gunesin, B. Z., Surface energy and surface composition of end-fluorinated polystyrene. *Advances in Colloid and Interface Science* **2001,** *94* (1-3), 1-19.
14. Walheim, S.; Boltau, M.; Mlynek, J.; Krausch, G.; Steiner, U., Structure Formation via Polymer Demixing in Spin-Cast Films. *Macromolecules* **1997,** *30* (17), 4995-5003.
15. Ton-That, C.; Shard, A. G.; Daley, R.; Bradley, R. H., Effects of Annealing on the Surface Composition and Morphology of PS/PMMA Blend. *Macromolecules* **2000,** *33* (22), 8453-8459.
16. Wang, C.; Krausch, G.; Geoghegan, M., Dewetting at a Polymer:Polymer Interface: Film Thickness Dependence. *Langmuir* **2001,** *17* (20), 6269-6274.
17. O., B. Characterization of macromolecular layers grafted to polymer surfaces. Clemson University, Clemson, 2008.

CHAPTER SIX

THE EFFECT OF THE MOELCULAR WEIGHT OF FLUORINATED POLYESTERS ON THE WETTABILITY OF SURFACES

6.1. Introduction

The fabrication of oleophobic PET films was presented in **Chapter 5**. It was determined that the blends of oleophilic PET with fluorinated polyesters with different end groups repelled not only water, but also oils to some extent. It was found that an increase in the concentration of fluorinated polyesters in blends increased the water and oil repellency as well. Furthermore, it was discovered that annealing the blended film surfaces above the T_g and T_c of each component led to the migration of $–CF_2$ and $–CF_3$ groups to the surface, resulting to decreased water/oil wettability. According to the results shown in **Chapter 5**, it was also found that among the three fluorinated polyesters, PET blended P3 polyester, which was terminated with $–CF_3$ end groups, exhibited the highest repellency. Even though oil repellent films were prepared, the question comes to mind whether the oil repellency of the most successful films (PET/P3) could be further improved or not.

The wettability of the polymer-blended surfaces depends on the surface composition and surface orientation of polymeric chains. The surface composition of polymer-blended films is different between bulk and surface due to the surface energy, molecular weights, miscibility of components in blends, and diffusion rate of the migrating components [1-4]. The amount of migration of additives and their migration directions depend on the aforementioned key parameters. Among these key parameters,

the surface energy differences between the components in polymer blends is the main driving force to migrate additives to the surface [5-7].

Another driving force for migration and surface segregation is the molecular weight differences of the components in blends [8-13]. One of the schools of thought suggests that when the polymer chains are at the air-polymer interface, they could be compressed along the direction perpendicular to the films' surface, resulting in limited number of polymer chain conformations on the surface. It decreases the conformational entropy of polymer chains at the surface as compared with that of a polymer chain in the bulk (**Figure 6.1**) [8]. The conformational entropy penalthy, which is a difference in the conformational entropy of polymers at the surface and in the bulk, depends on the molecular weight of polymers in blends [8].

High molecular weight components in the blends experience a larger entropy penalty at the surfaces as compared to the low molecular weight ones [8, 14-16]. As a result, surface is typically enriched with lower molecular weight macromolecules to maintain the least surface energy [5, 17, 18]. This phenomenon has been confirmed by Ralf Mason *et al.* who reported that low molecular weight fluorinated polystyrene polymer exhibited higher surface enrichment of fluorinated end groups of styrene than the high molecular weight chains [5]. However, contrary observations were also reported in the literature. Keiji *et al.* demonstrated that the surface of the high molecular weight polystyrene/low molecular weight poly(methyl methacrylate) blended films (HM-PS/LM-PMMA) were enriched with LM-PMMA. Even PMMA possessed higher surface energy than HM-PS [8]. Similar results were also obtained when LM poly(L-lactic acid)

(PLLA) polymer was blended with HM-PS. Jung *et al.* also found the higher surface energy PLLA to be segregated to PS/PLLA –air interface. As a result, surface energy effect was overcome by molecular weight derived entropy effect [19].

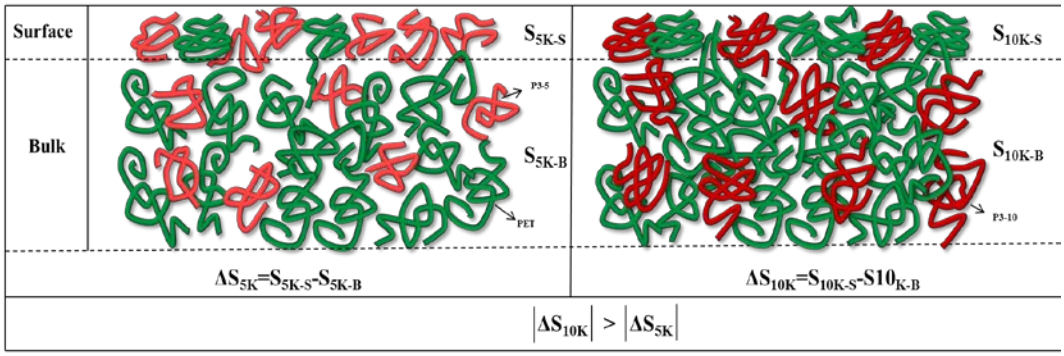

Figure 6.1. Scheme of the surface arrangement of P3-5 and P3-10. Their entropy changes between the surface and bulk [19].

These studies encouraged us to investigate how the molecular weights of P3 polyesters in PET matrix influence surface wettability. In this study, we synthesized two batches of P3 polyesters, which are terminated with two $-CF_3$ end groups possessing two molecular weights (P3-5 : M_w ≈5380 g/mole and P3-10: M_w ≈10,000 g/mole). The fluorinated polyesters were blended with PET at various concentrations to obtain low surface energy PET-based films. Hereby, contact angle measurements of water and hexadecane were conducted to determine the wettability of film surfaces. Furthermore, the morphology of the films was studied using atomic force microscopy.

6.2. Experimental Part

6.2.1. Synthesis of Perfluoro Diester Isophthaloyl Polyesters (P3)

Perfluoro diester isophthaloyl, P3 polyesters (**Figure 6.2**), were synthesized via the condensation reaction of IsoCl with perfluoro ether alcohol(s). Details are shown in **Figure 4.1** (**Chapter 4**).

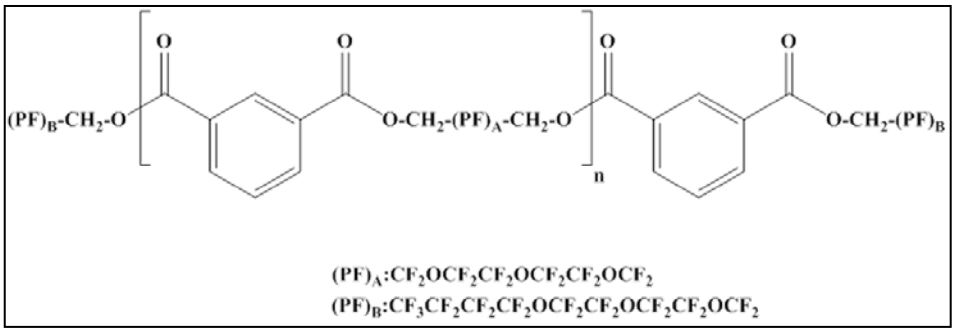

Figure 6.2. Chemical structure of P3 polyester.

6.2.3. Film Preparation

The synthesized P3 polyesters with different molecular weights, M_w (5.38K and 10K), were blended with polyethylene terephthalate (PET) at different concentrations. The films were prepared according to the procedure detailed in **Chapter 5**.

6.3. Results and Discussions

6.3.1. Structural Characterization of P3 Polyesters with Different Molecular Weights

A series of experiments were conducted to synthesize P3 polyesters. Although the same amount of monomers (perfluoro ether di- and mono alcohols and IsoCl) and the

same procedure were used in these processes, P3-5 (M_w= 5.38K) and P3-10 (M_w= 10K) polyesters with different molecular weight were obtained. The reason behind the synthesis of the different molecular weights of P3 polyesters is that all monomers were used as received in this study. None of them were purified before the synthesis of the P3 polyesters. In our work, we used different batches/stocks of monomers; therefore, purity of monomers could not be same. We suggest that the level of impurity of monomers influences polymerization, as well as the molecular weight of polymers.

As we synthesized P3 polyesters with two different M_w, we decided to investigate how the molecular weight of P3 influenced the wettability and morphology of the PET/P3 films. For this purpose, first we characterized both P3-5 and P3-10K polyesters. After that, they were blended with PET, and the wettability of the obtained films was analyzed.

6.3.2. Characterization of P3 Polyesters

6.3.2.1. ATR-FTIR Analysis of P3 Polyesters

The functional groups of P3-5 and P3-10 polyesters were determined using ATR-FTIR as shown in **Figure 6.3**. It reveals that both P3 polyesters possessed the ester (-OC=O) stretching and –C-O-C stretching vibrations, where they peak at 1749 cm^{-1} and 1269 cm^{-1}, respectively. In addition, carboxylic acid (-C=O) stretching (1715cm^{-1}) was not found in both spectrums. It means that either all acid chloride groups reacted with perfluoro ether alcohols or very small amount of acid chloride, which was not detectable in ATR-FTIR, could not react with alcohol. In addition, both polymers possessed -CF_2 and -CF_3 stretching peaks, which were detected in the region at 1186–1100 cm^{-1}. The C-

H stretching and C=C stretching of aromatic rings also appeared at 2980 cm^{-1} and 1614 cm^{-1}, respectively. According to ATR-FTIR, the P3-5 and P3-10 polyesters possess the same chemical structures.

6.3.2.2. ^{19}F NMR Analysis of P3 Polyesters

The ^{19}F NMR spectrums of the P3-5 and P3-10 polyesters are shown in **Figure 6.4** and **Figure 6.5**, respectively. It is clearly seen that the NMR spectra of both polymers are almost the same. Both polymers possessed signals at around -77 ppm (a) belonging to the fluorine atom in the CF_2 groups, which were bonded to methyl ester (-O-$\underline{CF_2}$-CH_2-O-CO-) in the repeat units.

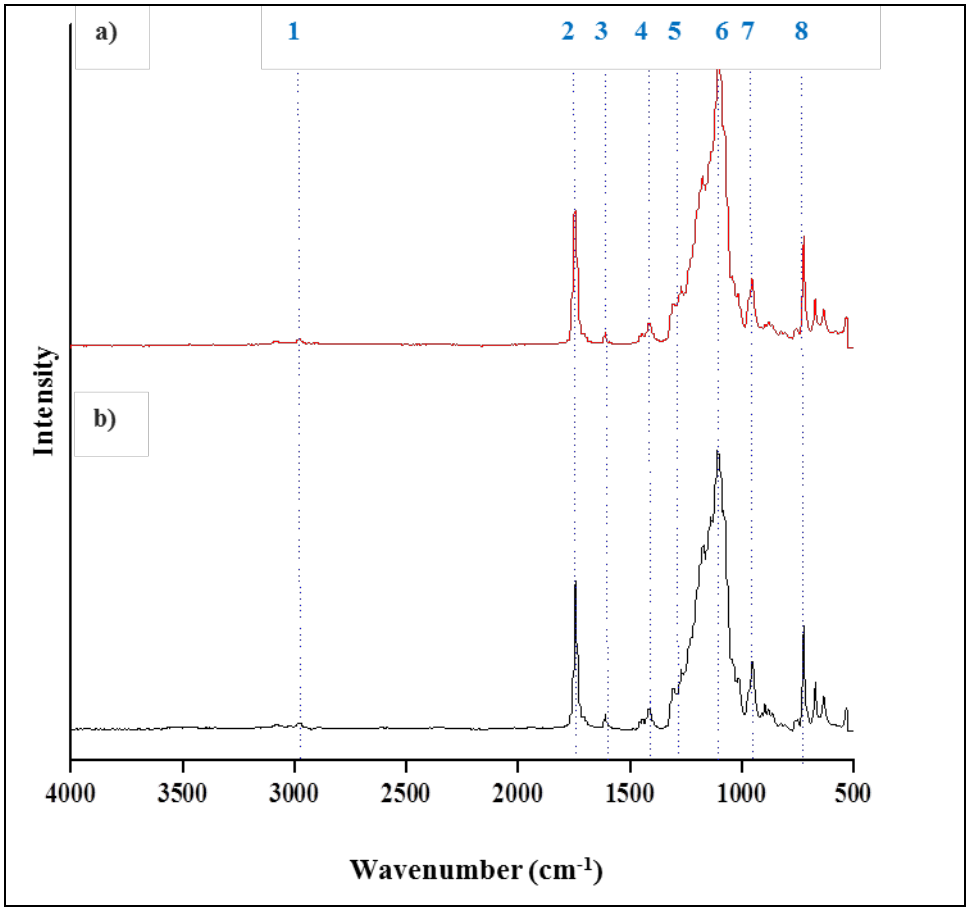

Figure 6.3. ATR-FTIR Spectra of P3 polymers a) P3-5; b) P3-10 (1) C-H symetric stretching, 3095-2970 cm^{-1}, (2) –OC=O stretching, 1743 cm^{-1}, (3) -C=C- stretching, 1611 cm^{-1}, (4) –OH bending (in plane) 1414 cm^{-1}, (5)-C-O-C symmetric stretching, 1269 cm^{-1}, (6) -CF_2 and -CF_3 stretching,1186-1100 cm^{-1}, (7)-OH bending (out of plane), 953 cm^{-1}, and (8)C-H bending, 722 cm^{-1}.

They also have distinctive multiple peaks at -88 to -91 ppm, which (b) are attributed to the fluorine atoms of the CF_2 groups in between ethers (–O-$\underline{CF_2}$-$\underline{CF_2}$-O) in their repeat units. A singlet peak at around -81 ppm (d) belongs to the fluorine atoms in the –CF_3 groups. The broad singlet peak at around -84 ppm corresponds to the –CF_2 groups bonded to ether (CF_3-CF_2CF_2-$\underline{CF_2}$-O) on the fluorinated tail of polymers (e). Another distinctive peak at -127.22 ppm is attributed to the fluorine atoms of the –CF_2 groups (CF_3-$\underline{CF_2}\underline{CF_2}$-$\underline{\ }$$CF_2$-O) on the fluorinated tails (f).

The difference between the NMR spectrum of these two polymers is only a triplet peak at around -80.5 to -80.9 ppm (c), which corresponds to the fluorine atoms in the CF_2 group, which is close to the –OH end groups (-O-$\underline{CF_2}$-CH_2-OH). This peak was only obtained in low M_w of the P3 polyester (P3-5). It means that some of the chains in the P3-5 polyesters were terminated with the –OH groups instead of the CF_3 groups although perfluoro mono-alcohol was used in excess. This result clearly indicates that during the synthesis of the P3-5, less pure IsoCl with more impurities was employed.

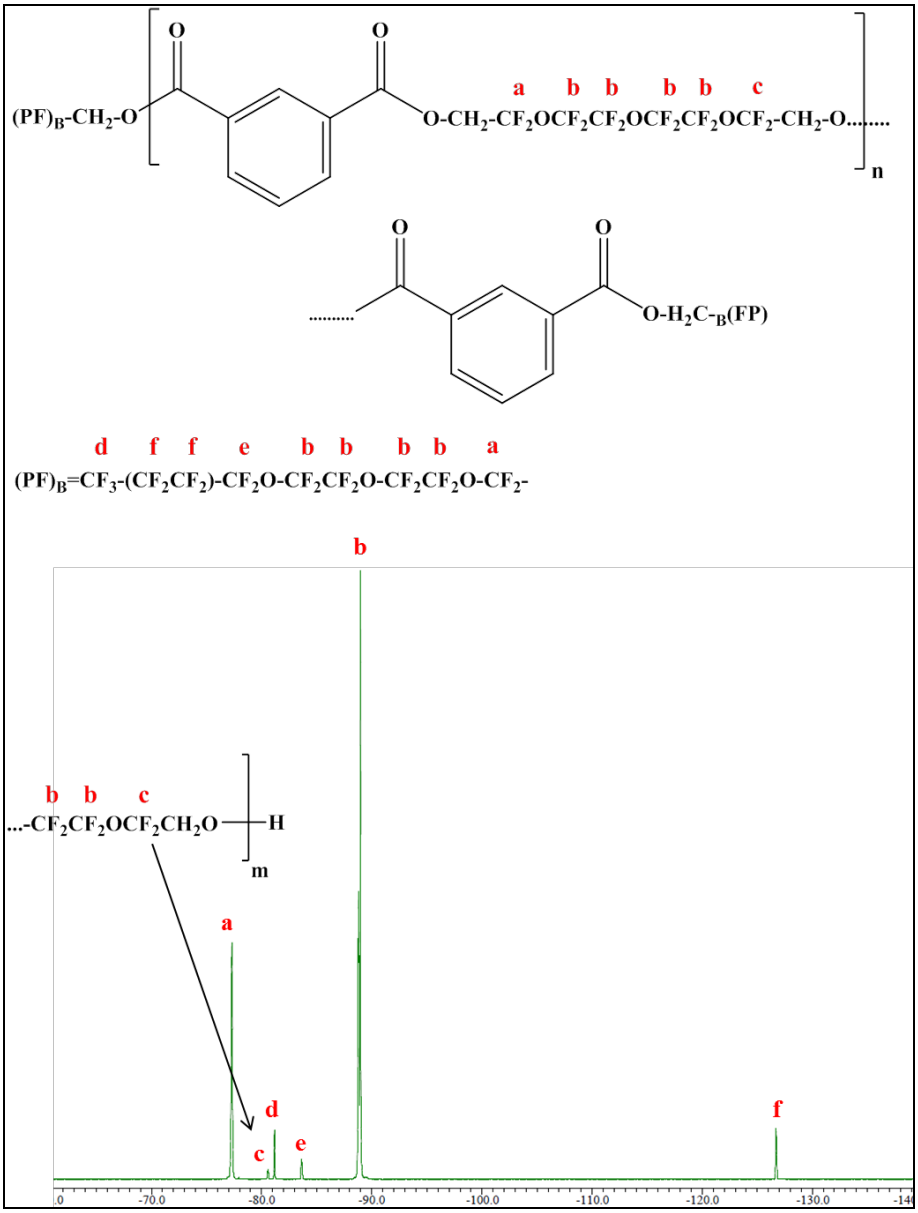

Figure 6.4. ^{19}F NMR spectra of P3-5 polyester.

According to NMR results, we concluded that both the P3-5 and P3-10 polyesters had virtually similar chemical structures. The only difference between these two was that all chains in the high M_w of the P3 polyester were terminated with the CF_3 groups, while their low counterparts possessed some small number of the –OH end groups. We

considered that those chains terminated with –OH do not segregate to the surface because of their higher surface energy.

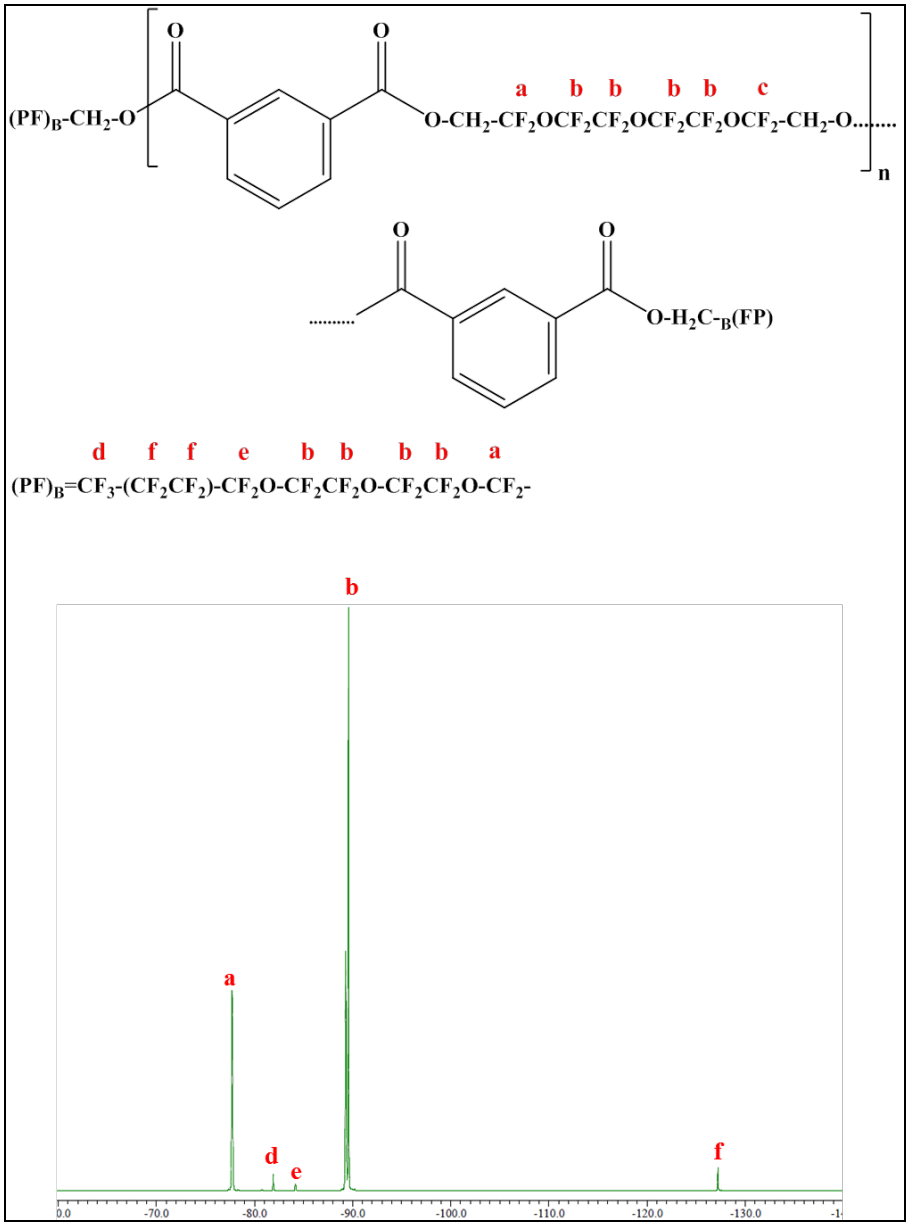

Figure 6.5. ^{19}F NMR spectra of P3-10 polyester.

6.3.2.3. Thermal Properties of P3 Polyesters

DSC Analysis

The thermal properties of the P3 polyesters, such as T_g and T_f , were determined using differential scanning calorimetry (DSC) at a heating rate of 10^0C/min under N_2. Results are summarized in **Table 6.1**. The glass transition temperatures of polymers were from -25°C (P3-5) to -16°C (P3-10), and the melting temperature was from 48°C (P3-5) to 51°C (P3-10). This variation is dependent on the molecular weight of polymers. It was found that higher M_w P3-10 polyester possesses higher T_g and T_f compared to the lower M_w. The dependence of T_g on molecular weight is explained by the theoretical analysis of Fox and Flory [20, 21]. It indicates that the relationship between T_g and molecular weight M_w is related to the glass temperature of polymers with infinite molecular weight, $T_{g,\infty}$ [22]:

$$T_g = T_{g,\infty} - \frac{K}{(\alpha_R - \alpha_G)M} \qquad (6.1)$$

where K is a constant depending on the polymer, and α_R and α_G are volume expansion coefficients of polymers in rubbery and glassy states. According to Equation 6.1, P3-10 polyesters should possess higher T_g.

The melting point depression in pure crystalline fluorinated polymers is also connected to the M_w [23]. The fusion temperature of polymers with infinite molecular weight, T_f^o is obtained as follows:

$$\frac{1}{T_f} - \frac{1}{T_f^o} = \frac{R}{\Delta H_f}\frac{M_o}{M_w} \qquad (6.2)$$

$$\frac{1}{T_{f-5K}} - \frac{1}{T_{f-10K}} = \frac{R}{\Delta H_f}\left[\frac{M_o}{M_{w-5K}} - \frac{M_o}{M_{w-10K}}\right] \qquad (6.3)$$

where R is the gas constant, ΔH_f is the heat of fusion per mole of crystalline mers, M_w is the molecular weight of polymer, and M_o is the total molecular weight of P3 polyesters.

Table 6.1. Parameters of P3 polyesters and PET polymer

	M_w	PDI	T_g	T_f^a	ΔH_f^a	$\%^a$	T_c	ΔH_c	$T_f^{b,1}$	$\Delta H_f^{b,1}$	$\%^b$	T_d
P3-5	5380	10.4	-25	48	29.7	30	-	-	-	-	-	403
P3-10	10000	10	-16	51	25.9	26.1	-	-	-	-	-	411
PET	-	-	67.6	-	-	-	126	27.35	238	33.77	5.2	425

[a]:P3 polyesters, [b]:PET polymer

According to the above approach, M_0/M_w represents the mole fraction of the end groups in polyesters. Although they possessed the same end groups, the mole fractions of the chain ends are 0.22 and 0.11 for (P3-5) and (P3-10), respectively, due to the different molecular weights. According to Equation 6.3, calculated T_f should be increased by just 1.1^0C when the molecular weight of P3 polyesters is doubled. In fact, we obtained a small difference of 3^0 between the T_f of P3-5 and T_f of P3-10.

The heat of the fusion (ΔH_f) of the P3-5 and P3-10 polyesters were found to be at 29.7 J/g and 25.9 J/g, respectively. With this data, the degree of the crystallinity of P3 polyesters was calculated using **Equation 4.3** in **Chapter 4**. It was determined that P3-5

possessed 30% crystallinity, while P3-10 had 26% (Table 6.1), making their crystallinities very close.

TGA Analysis

The thermal stability of the P3 polyesters was also analyzed using TGA (**Table 6.1**). It appeared that both polymers exhibited high decomposition temperatures (T_d) at 407±4°C, indicating the relatively high thermal stability of the polymers due to the presence of isophthalate units in macromolecules. In addition, it was concluded that the stability of fluorinated polyesters was not dependent on the molecular weight of polymers.

6.3.3. Preparation of PET/P3 Polyester Films

A series of oleophobic polyester films were prepared by dipping cleaned Si wafers into 3 w% of PET blended with P3-5 and P3-10 polyesters in HFIP solution. Each solution consisted of different concentrations of P3 polyesters. After the film formation, the wettability of the PET/P3 film surfaces was determined using the contact angle measurements of hexadecane and water. With these experiments, the effects of the molecular weight of P3 polyesters in PET matrix on surface morphology and wettability were also investigated and compared to pure PET films.

6.3.4. Characterizations of PET/P3 Polymer Films

6.3.4.1. Surface Morphology Analysis

In **Chapter 5**, it was reported that the blends of PET and P3 polyesters were immiscible. Therefore, phase separation was observed. Herein, AFM was performed to

analyze the influence of the molecular weight of P3 polyesters on the surface morphology of PET/P3 films. **Figure 6.6** and **Figure 6.7** show the present topographical (left column) and phase images (right column) of films prepared by blending PET with P3-5 and P3-10 polyesters, respectively. In the images, we observed that the dark circular and cylindrical P3 domains are distributed in the light PET matrix. It was found that the size of the P3 domains increased with each increase in P3 concentration.

It is clearly seen that the location of the dark domains of P3 on the topographical images corresponds to the lower phase values of the phase images. However, phase inversion was observed by AFM when 20% P3-10 was present in the blend (**Figure 6.7**). **Figure 6.6** shows that the continuous domains of the PET-rich invert to a dispersed phase and P3 phase turn into a continuous phase on the surface. At the increase of the P3 concentrations to more than 20%, phase inversion was seen as well.

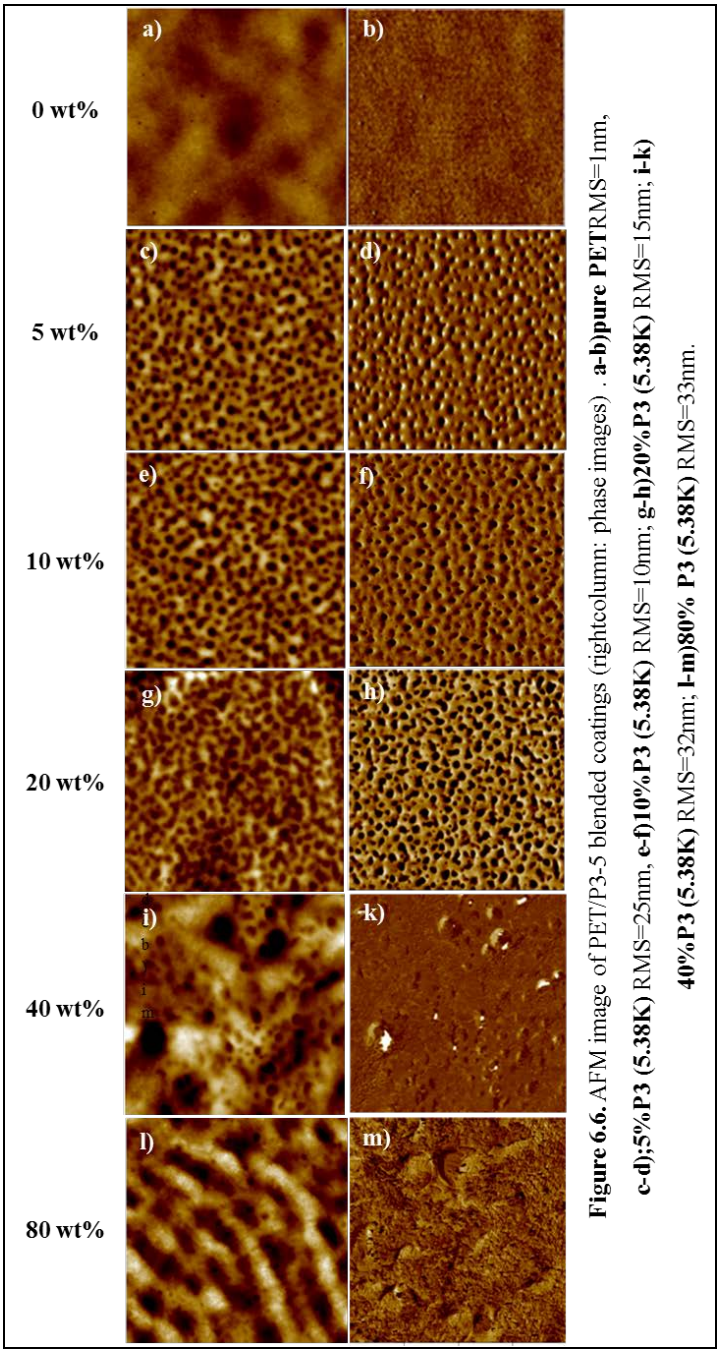

Figure 6.6. AFM image of PET/P3-5 blended coatings (rightcolumn: phase images) . **a-b)pure PET**RMS=1nm, **c-d);5%P3 (5.38K)** RMS=25nm, **e-f)10%P3 (5.38K)** RMS=10nm; **g-h)20%P3 (5.38K)** RMS=15nm; **i-k) 40%P3 (5.38K)** RMS=32nm; **l-m)80% P3 (5.38K)** RMS=33nm.

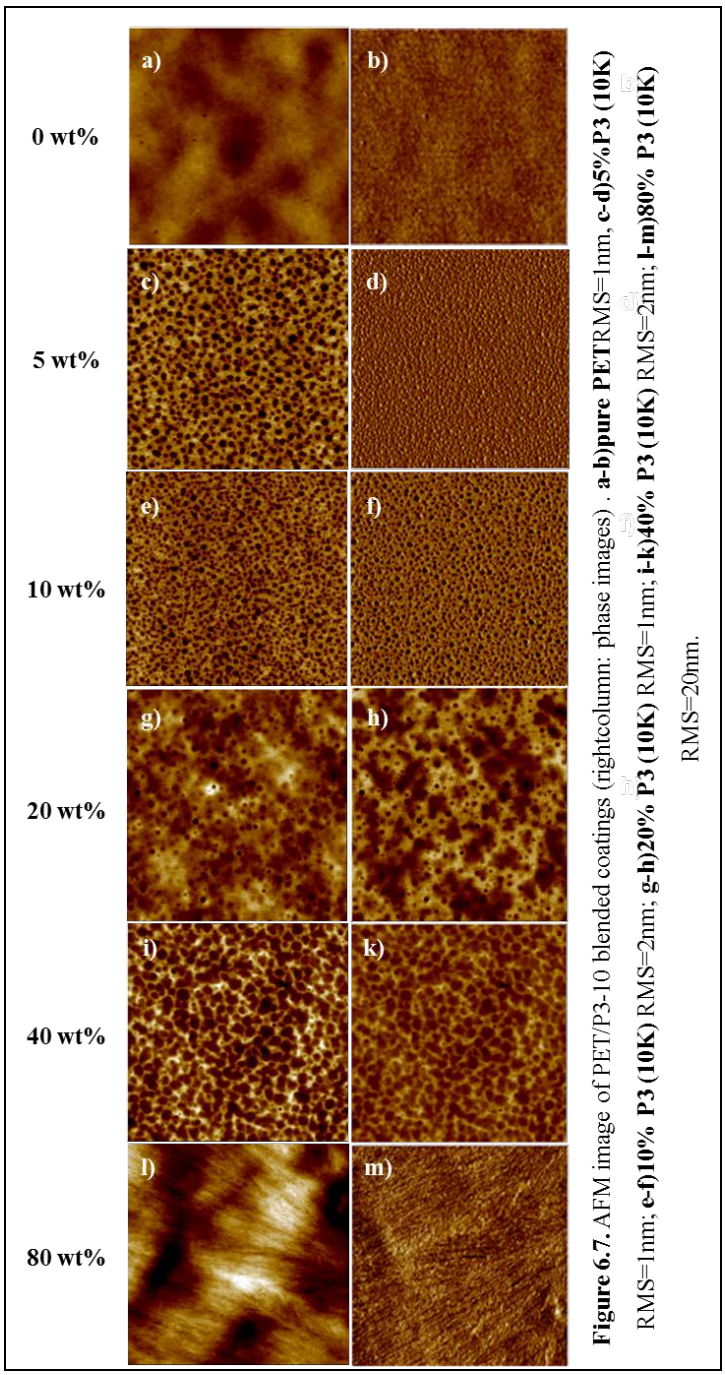

Figure 6.7. AFM image of PET/P3-10 blended coatings (rightcolumn: phase images) . **a-b)pure PET**RMS=1nm, **c-d)5%P3 (10K)** RMS=1nm; **e-f)10% P3 (10K)** RMS=2nm; **g-h)20% P3 (10K)** RMS=1nm; **i-k)40% P3 (10K)** RMS=2nm; **l-m)80% P3 (10K)** RMS=20nm.

The average sizes of the P3 domains in the topographical and phase images were calculated using the AFM results (**Table 6.2-6.3**). To estimate the surface area fraction of the P3 domains from the AFM phase images, the bearing ratio, which provides the area

percentage of surface features, were determined. The results are summarized in **Table 6.2** and **Table 6.3**.

Table 6.2. The Size of P3-5 of domains and their surface coverage

M_w of P3 = 5.38K	**5%**	**10%**	**20%**	**40%**
diameter of P3 domains in topographical image (nm)	293±64.9	330±88.2	340±97.4	644±321
diameter of P3 domains in phase image (nm)	279±63.7	319±62.1	384±42	-
total area of P3 (μ^2)	12.74	12.85	33.85	77.35
P3 area/ total area (%)	**12.74**	**12.85**	**33.85**	**77.35**

Table 6.3. The Size of P3-10 of domains and their surface coverage

M_w of P3 = 10K	**5%**	**10%**	**20%**	**40%**
diameter of P3 domains in topographical image (nm)	162+42.6	210+49.7	124.+32.3	474±58
diameter of P3 domains in phase image (nm)	171±34.3	242±54.5	-	474±58
total area of P3 (μ^2)	18.14	19.89	59.33	47.80
P3 area/ total area (%)	**18.14**	**19.89**	**59.33**	**57.72**

It was found that an increase in the amount of P3 polyesters in PET resulted in high surface coverage. When films possessed more than 40 wt% P3, surfaces were completely covered with them (**Figure 6.8**). It was expected since the XPS results of the P3 polyesters detailed in **Chapter 5** revealed that the PET/P3 films were completely covered with $-CF_2$ and $-CF_3$ groups, even if the films possessed 33 wt% P3 polyester (**Figure 5.19**).

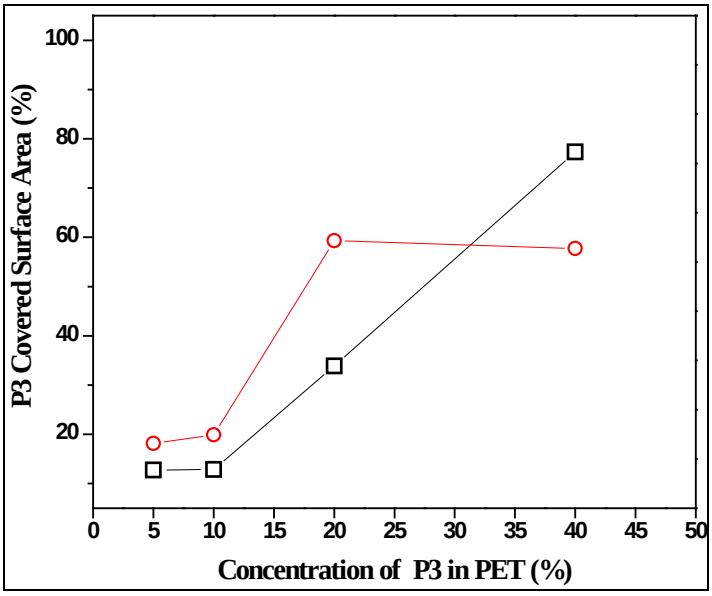

Figure 6.8. The percentage of P3 covered surface area. □) P3-5 and ○)P3-10.

6.4.3.2. Characterization Wettability of PET/P3 Films

In the synthesis of fluorinated polyesters, P3 was a key part of our strategy for the fabrication of oleophobic surfaces due to their low surface energy. Thus, P3-5 and P3-10 polyesters were blended with PET at different concentrations to make PET material oleophobic. Then, the CAs of hexadecane (**Figure 6.9**) and water (**Figure 6.10**) were measured to quantify the wettability changes on the PET/P3 surfaces triggered by two main parameters, *i) concentration of P3 in films, ii) molecular weight of P3 polyesters*.

As seen in the figures, hexadecane wet the PET, while the CA of water on PET was around 60°, which is in agreement with the studies reported in the literature [24, 25]. Incorporation of a small amount of fluorinated species (5 wt %) into the oleophilic PET films resulted in strong increase of water and hexadecane contact angles. It can be clearly seen that all of the PET/P3 films have a higher contact angle for water, which steadily

increases with each increase of the fluorinated species concentration in blends. For hexadecane, the effect is less pronounced when the P3 concentration is increased.

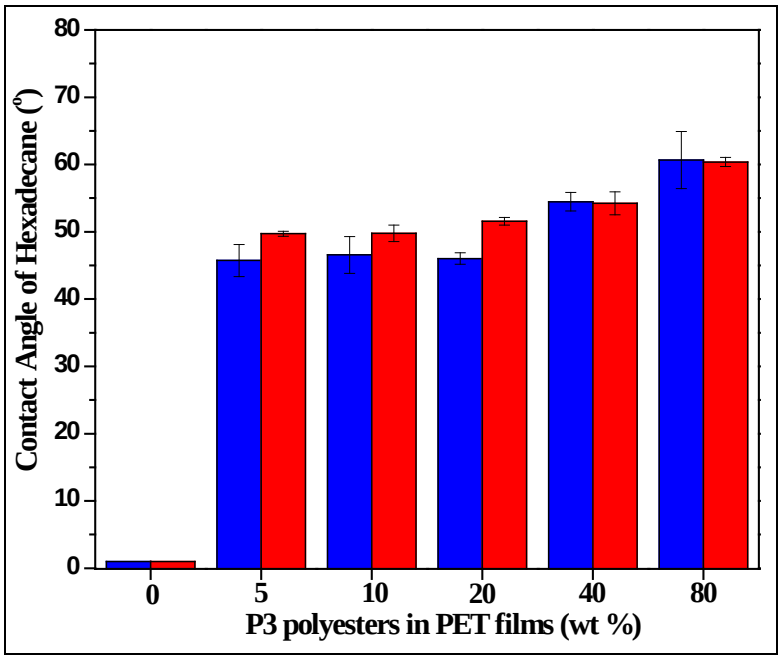

Figure 6.9. Contact angle of hexadecane on PET/ P3 films. (□)P3-5; (□) P3-10.

As seen in **Figure 6.10**, the higher values of the CA of water were obtained for the sample containing P3-5 at low concentrations rather than P3-10. **Figure 6.10** shows that short polymer chains can migrate more easily through the bulk PET films than higher molecular weight to reach the surface. This was expected because the confinement of a polymer chain on the surface may reduce conformational entropy. Small molecules on the surface have reduced conformational entropy penalty compared to the larger molecules. On the other hand, for high concentration of P3-blended films, the CA of water was increased by increasing the M_w. This happened since the P3-10 polymer demonstrates higher surface enrichment of the $-CF_3$ groups, resulting in lower surface

energy. Consequently, the end groups of the polymer dominantly influenced the contact angle of water instead of the molecular weight of polyesters when they were used at high concentrations.

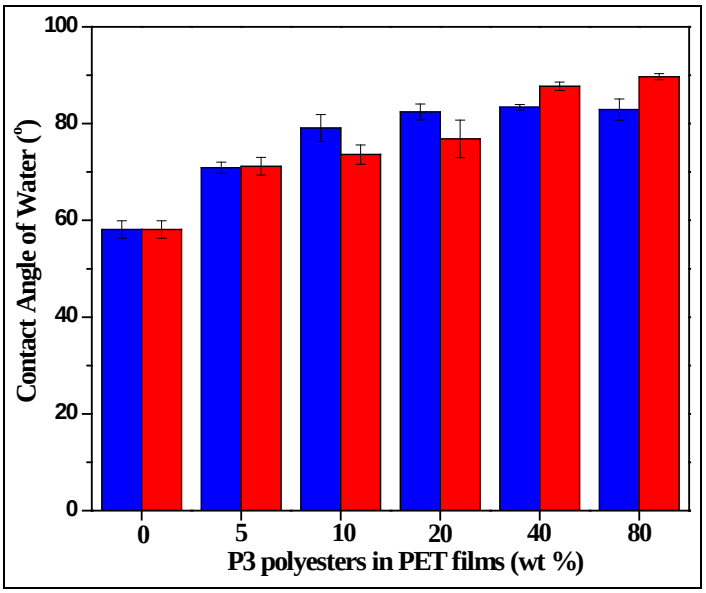

Figure 6.10. Contact angle of water on PET/ P3 films. (■)P3-5; (□) P3-10.

The Cassie and Baxter model shown in **Equation 6.4** was utilized to determine the relations between the contact angle measurements and the content of P3 polyesters in films. It is known that the Cassie and Baxter model describes the apparent contact angle of liquid θ_{CB} on a composite surface when a liquid droplet does not entirely wet the surface [26].

$$\cos\theta_{CB} = f_{P3}\cos\theta_{Y-P3} + f_{PET}\cos\theta_{Y-PET} \qquad (6.4)$$

where $\theta_{Y\text{-}P3}$, $\theta_{Y\text{-}PET}$ are Young contact angles of solvents on pure, homogeneous, smooth P3 and PET surfaces, respectively, and f_{P3}, f_{PET} are area fractions of the component surfaces.

For this calculation, f_{P3} and f_{PET} of the component surfaces were determined using AFM analysis (**Table 6.2** and **Table 6.3**). On the other hand, the $\theta_{Y\text{-}P3}$ was not obtained by contact angle measurements due to the dewetting of pure P3 polyester films. Therefore, we assumed the same value for $\theta_{Y\text{-}P3}$ for both P3-5 and P3-10. Approximately 90° for water and 60° for hexadecane were chosen, since they were close to the CA values obtained when 80% P3 polyesters were used. Based on these assumptions, the θ_{CB} of hexadecane and water for both P3 polyesters were calculated using **Equation 6.4**. The CA of hexadecane (**Figure 6.11**) and water (**Figure 6.12**) obtained from the Cassie-Baxter model were also compared with the experimental data obtained by contact angle measurements.

According to the model, it is suggested that by increasing the P3 coverage area, the CAs of hexadecane and water increased significantly. Data revealed that P3-5 exhibited possessed higher contact angles than P3-10 due to their high surface coverage area on the film surfaces with increasing concentration. However, in reality, the contact angles did not vary as much as predicted by the Cassie-Baxter model. The addition of low amount of P3 polyesters (5%) into the PET matrix exhibited higher repellency than the one predicted by **Equation 6.4**.

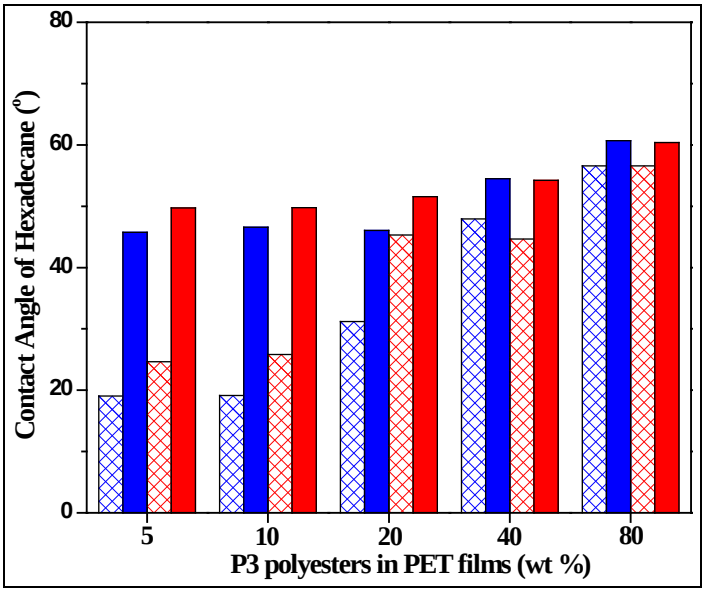

Figure 6.11. Contact angle of hexadecane on PET/ P3 films. (□)P3-5; (□) P3-10.mesh: θ_{CB} from Cassie-Baxter model, solid: experimental data.

This happened because surfaces became enriched with $–CF_2$ and $-CF_3$ groups even at low concentrations. In reality, the PET phase observed on the AMF images is covered with nanolayers of P3. The XPS results reported in **Chapter 5** suggest that the surface were almost completely covered with P3 polyesters (>85% coverage) even when 5% P3 was used (**Figure 5.19**).

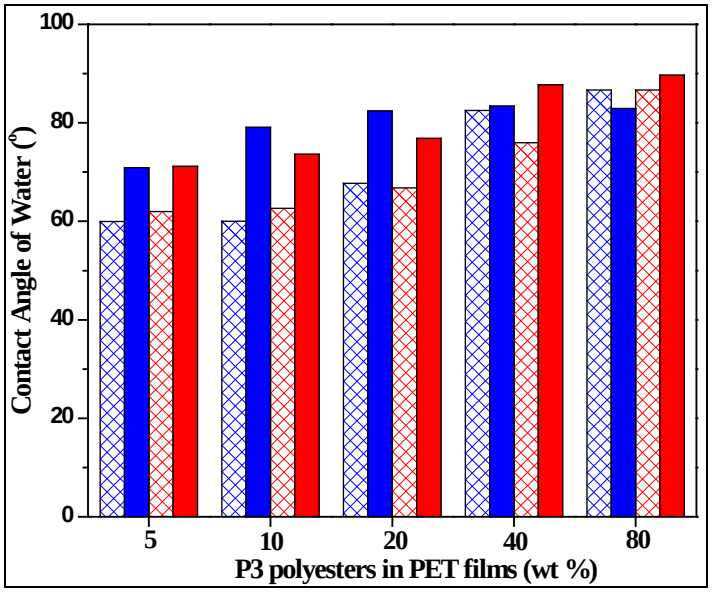

Figure 6.12. Contact angle of water on PET/ P3 films. (□)P3-5; (□) P3-10. mesh: θ_{CB} from Cassie-Baxter model, solid: experimental data.

The surface energy of the blended films that possessed different M_w (5.38K and 10K) of P3 was also calculated using **Equation 5.1** in **Chapter 5**. As compared to the surface energy of two P3 polyesters in blended films, as shown in **Figure 6.13**, it was found that P3-5 polyester possessed lower surface energy than P3-10 at low concentrations. However, at high concentrations, P3-10K exhibited lower surface energy due to the possession of high content of $–CF_2$ and $–CF_3$ groups. Again, it was understood that end groups are more effective than the molecular weight of polyesters when high concentrations of P3 were used. The surface energy of PET/P3 films were also compared with PTFE. **Figure 6.13** indicates that blended films are more wettable with water and oils than PTFE, since the latter exhibits the lowest surface energy.

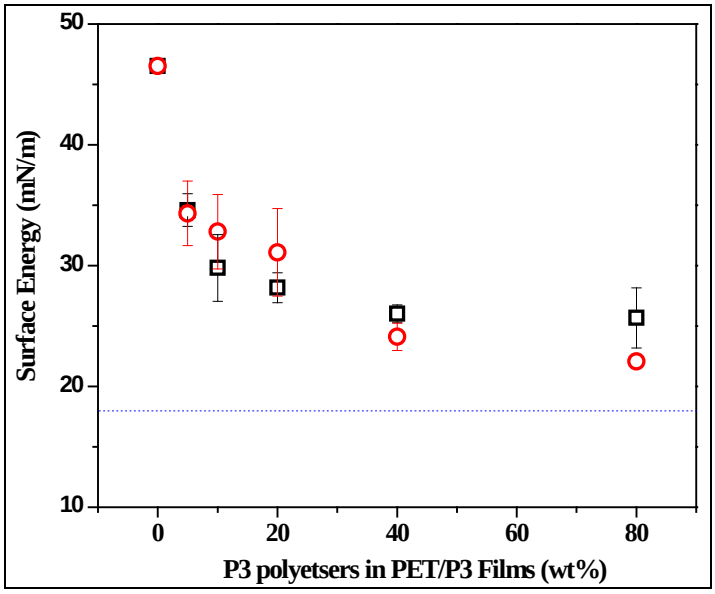

Figure 6.13. Surface energy of PET/P3. (□) P3-5; (○) P3-10 and (----)PTFE.

6.5. Conclusions

Perfluoro diester isophthaloyl polymers, P3 of two different M_w (5.38K and 10K), were synthesized through the polycondensation reaction of IsoCl with perfluoro ether alcohols and the effects of the molecular weight of P3 polyester additives on the wettability of PET/P3 films were evaluated. It was found that the wettability of the surface depends on both the *P3 polyester compositions* and *their molecular weights* in the blend. Contact angle measurement results indicate that an increase of any P3 polyester concentrations in PET films resulted in higher CA in both water and hexadecane. In addition, at low concentrations, P3-5 polyesters migrated to the surface easily due to their less entropy penalty, resulting in more surface coverage. Subsequently, it leads to more water and oil repellency. On the other hand, P3-10 polyesters in blends reduced the

wettability of the surface more than the lower ones when they were used at high concentrations

6.6. References

1. Opdahl, A.; Phillips, R. A.; Somorjai, G. A., Effect of Bulk Miscibility on the Surface Composition of Polypropylene/Poly(ethylene-co-propylene) Blends. *Macromolecules* **2002,** *35* (11), 4387-4396.
2. Artyushkova, K.; Fulghum, J. E., Quantification of PVC–PMMA polymer blend compositions by XPS in the presence of x-ray degradation effects. *Surface and Interface Analysis* **2001,** *31* (5), 352-361.
3. Affrossman, S.; Kiff, T.; O'Neill, S. A.; Pethrick, R. A.; Richards, R. W., Topography and Surface Composition of Thin Films of Blends of Poly(methyl methacrylate) and Poly(ethylene oxide). *Macromolecules* **1999,** *32* (8), 2721-2730.
4. Quinn, A.; Tjipto, E.; Yu, A.; Gengenbach, T. R.; Caruso, F., Polyelectrolyte Blend Multilayer Films:Surface Morphology, Wettability, and Protein Adsorption Characteristics. *Langmuir* **2007,** *23* (9), 4944-4949.
5. Mason, R.; Jalbert, C. A.; O'Rourke Muisener, P. A. V.; Koberstein, J. T.; Elman, J. F.; Long, T. E.; Gunesin, B. Z., Surface energy and surface composition of end-fluorinated polystyrene. *Advances in Colloid and Interface Science* **2001,** *94* (1-3), 1-19.
6. Kajiyama, T.; Tanaka, K.; Takahara, A., Surface Segregation of the Higher Surface Free Energy Component in Symmetric Polymer Blend Films. *Macromolecules* **1998,** *31* (11), 3746-3749.
7. Budkowski, A.; Klein, J.; Steiner, U.; Fetters, L. J., Diblock copolymers attached to homopolymer surfaces and interfaces. *Macromolecules* **1993,** *26* (10), 2470-2478.
8. Tanaka, K.; Takahara, A.; Kajiyama, T., Surface Molecular Aggregation Structure and Surface Molecular Motions of High-Molecular-Weight Polystyrene/Low-Molecular-Weight Poly(methyl methacrylate) Blend Films. *Macromolecules* **1998,** *31* (3), 863-869.
9. Hill, M. J.; Barham, P. J.; Keller, A.; Rosney, C. C. A., Phase segregation in melts of blends of linear and branched polyethylene. *Polymer* **1991,** *32* (8), 1384-1393.
10. Hill, M. J.; Barham, P. J.; Keller, A., Phase segregation in blends of linear with branched polyethylene: the effect of varying the molecular weight of the linear polymer. *Polymer* **1992,** *33* (12), 2530-2541.
11. Dai, K. H.; Kramer, E. J.; Shull, K. R., Interfacial segregation in two-phase polymer blends with diblock copolymer additives: the effect of homopolymer molecular weight. *Macromolecules* **1992,** *25* (1), 220-225.
12. Bongiovanni, R.; Di Meo, A.; Pollicino, A.; Priola, A.; Tonelli, C., New perfluoropolyether urethane methacrylates as surface modifiers: Effect of molecular weight and end group structure. *Reactive and Functional Polymers* **2008,** *68* (1), 189-200.

13. Mounir, E. L. S. A.; Takahara, A.; Kajiyama, T., Effect of Chain End Group-Substrate Interaction on Surface Molecular Motion of Polystyrene Ultrathin Films. *Polym J* **1999,** *31* (6), 550-556.
14. Tretinnikov, O. N.; Ohta, K., Surface Segregation in Stereochemically Asymmetric Polymer Blends. *Langmuir* **1998,** *14* (4), 915-920.
15. Jalbert, C.; Koberstein, J. T.; Yilgor, I.; Gallagher, P.; Krukonis, V., Molecular weight dependence and end-group effects on the surface tension of poly(dimethylsiloxane). *Macromolecules* **1993,** *26* (12), 3069-3074.
16. Miccio, L. A.; Liano, R.; Schreiner, W. H.; Montemartini, P. E.; Oyanguren, P. A., Partially fluorinated polymer networks: Surface and tribological properties. *Polymer* **2010,** *51* (26), 6219-6226.
17. Iyengar, D. R.; Perutz, S. M.; Dai, C.-A.; Ober, C. K.; Kramer, E. J., Surface Segregation Studies of Fluorine-Containing Diblock Copolymers. *Macromolecules* **1996,** *29* (4), 1229-1234.
18. Lau, W. W. Y.; Burns, C. M., Effect of temperature and molecular weight on the rate of spreading of polystyrene melts on plane soda lime glass surfaces. *Journal of Polymer Science: Polymer Physics Edition* **1974,** *12* (2), 431-439.
19. Lim, J. Y.; Hansen, J. C.; Siedlecki, C. A.; Hengstebeck, R. W.; Cheng, J.; Winograd, N.; Donahue, H. J., Osteoblast Adhesion on Poly(l-lactic Acid)/Polystyrene Demixed Thin Film Blends: Effect of Nanotopography, Surface Chemistry, and Wettability. *Biomacromolecules* **2005,** *6* (6), 3319-3327.
20. Fox, T. G.; Flory, P. J., Second-Order Transition Temperatures and Related Properties of Polystyrene. I. Influence of Molecular Weight. *Journal of Applied Physics* **1950,** *21* (6), 581-591.
21. Fox, T. G.; Flory, P. J., The glass temperature and related properties of polystyrene. Influence of molecular weight. *Journal of Polymer Science* **1954,** *14* (75), 315-319.
22. Sperling, L. H., Introduction to physical polymer science. Wiley Subscription Services, Inc., *A Wiley Company*: New York, 1986; Vol. 27, p 439 pp.
23. Keller, A.; Hikosaka, M.; Rastogi, S.; Toda, A.; Barham, P. J.; Goldbeck-Wood, G., An approach to the formation and growth of new phases with application to polymer crystallization: effect of finite size, metastability, and Ostwald's rule of stages. *Journal of Materials Science* **1994,** *29* (10), 2579-2604.
24. Burtovyy, O. Synthesis and Characterization of Macromolecular Layers Grafted to Polymer Surfaces. Clemson University, Clemson, 2008.
25. Cassie, A. B. D.; Baxter, S., Wettability of porous surfaces. *Transactions of the Faraday Society* **1944,** *40* (0), 546-551.

CHAPTER SEVEN

EXPLORATORY STUDY OF THE EFFECTS OF ANNEALING TEMPERATURE ON THE WETTABILITY OF THE FLUORINATED POLYESTER BLENDED SURFACES

7.1. Introduction

In this work, oleophobicity of PET films was obtained using two approaches *i) PET was blended with fluorinated polyesters with different end groups to repel water and oils* (**Chapter 5**) and it was found that among the three fluorinated polyesters, PET-blended P3 polyester, which was terminated with $–CF_3$ end groups, exhibited the highest water/oil repellency; *ii) The oleophobicity of PET films was improved by blending with the P3 polyesters of different molecular weights.* Results shown in **Chapter 6** revealed that at low concentrations, the low molecular weight of P3-5 (5.38K) polyesters exhibited higher oil. However, at high concentrations, the surface became enriched with high molecular weight of P3-10 (10K) polyesters. In addition, it was found that annealing the blended film surfaces above the T_g and T_c of each component resulted in the migration of $–CF_2$ and $–CF_3$ groups to the surface, leading to the reduction of water/oil wettability (**Chapter 5**).

In this chapter, we investigated how the annealing temperature influences the wettability of PET/fluorinated polyester films. For this purpose, two different temperatures 140°C and 250°C which are above the T_c and T_f of pure PET, were used. These temperatures were chosen since PET/fluorinated polyesters may be utilized in industry. While PET materials are produced via the melt extrusion process at high

temperatures (>230^{0}C), fluorinated polyesters are easily co-extruded with PET due to their low melting temperatures. To this end, PET/P3 films with different molecular weights used in **Chapter 6** were annealed at 140°C and at 250°C, which is used for the melt extrusion process. Then, the CA of water and hexadecane on measurements were conducted to determine the wettability of films. Furthermore, AFM was utilized to analyze the morphology changes after annealing.

7.2. Experimental Part

7.2.1. Synthesis of Perfluoro Diester Isophthaloyl Polyesters (P3)

Perfluoro diester isophthaloyl polyesters with different molecular weights M_w (P-5: 5.38K and P3-10: 10K) were synthesized via the condensation reaction of IsoCl with perfluoro ether alcohol(s) detailed in **Figure 4.1** (**Chapter 4**). Their structural characterizations were detailed in **Chapter 6**.

7.2.3. Preparation of PET/P3 Polyester Films

A series of oleophobic polyester films were prepared by dipping cleaned Si wafers into 3 w% PET blended with either P3-5 or P3-10 polyesters (PET/P3) in HFIP solution, as detailed in **Chapter 5**. After films formation, they were annealed at 140°C for 3h or 250°C for 30 min. In a model study, PET/P3 films that contained 40% P3 polyesters with different M_w (5.38K and 10K) were used to determine their morphology by AFM analysis. Furthermore, the wettability of PET/P3 film surfaces was determined by the contact angle measurements of hexadecane and water. With these experiments, the

effects of annealing temperatures on the aforementioned properties of PET/P3 films were also investigated.

To determine the thermal properties of PET/P3 blends, PET chips and fluorinated polyesters were dissolved in HFIP solution in vials and then dried until constant weight was reached. After that, they were annealed at 140°C for 3h and 250°C for 30 min.

7.3. Results and Discussions

7.3.1. Characterizations of PET/P3 Polymer Films

7.3.1.1. Model Study

TGA Analysis of Dry PET/P3 Films

Thermal gravimetric analysis experiments were conducted to determine the degradation temperature of PET/P3-5 and PET/P3-10 films after annealing. In these experiments, dry films from PET/P3 blended solution were obtained after the evaporation of HFIP for two weeks. Then, they were annealed at 140°C for 3h and 250°C for 30 min. The TGA results of the annealed blended films that possessed 40% P3 polyesters are presented in **Table 7.1**. Compared to the TGA results of annealed pure components, the degradation temperatures of blended films were in between the temperature of PET and P3 polyesters. It was found that the T_d of PET/P3-5 and PET/P3-10 films were around 411±1°C.

DSC Analysis Dry PET/P3 Films

DCS was utilized to determine the T_g and T_f of PET/P3-5 and PET/P3-10 films. The degree of crystallinity of films was also calculated using **Equation 4.3** (**Chapter 4**), and compared to that of pure components (**Table 7.1**).

Before analyzing the blended films, the thermal transitions of P3 and PET films before and after annealing at 140°C and 250°C were investigated. The DSC results of the P3-5 and P3-10 films after annealing shown in **Figure 7.1** and **Figure 7.2**, respectively, reveal that the annealing temperature could not influence the T_f of the P3 films. For instance, when P3-5 (48°C) and P3-10 (51°C) were annealed at 250°C for 30 min, their T_f was found to be at 48°C and 53°C, respectively.

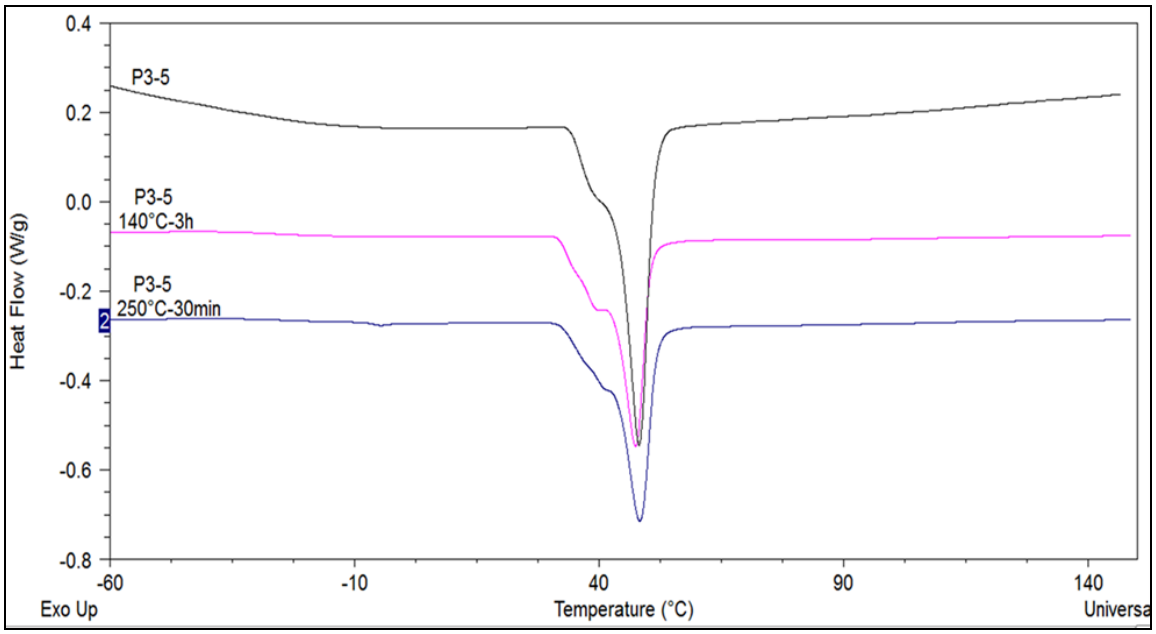

Figure 7.1. DSC results of P3-5 polyester films before and after annealing at 140°C for 3h and 250°C for 30 min.

Table7.1. Thermal properties of P3 polyesters and PET Films

	T_g	T_f^a	ΔH_f^a	$\%^a$	T_c	ΔH_c	$T_f^{b,1}$	$\Delta H_f^{b,1}$	$T_f^{b,2}$	$\Delta H_f^{b,2}$	$\%^b$	T_d
P3(5.38K)	-25	48	29.70	30.0	-	-	-	-	-	-	-	403
P3(5.38K)[c]	-	47	21.90	22.1	-	-	-	-	-	-	-	404
P3(5.38K)[d]	-	48	21.31	21.5	-	-	-	-	-	-	-	405
PET/P3-5[c] (60/40%)	-	49	8.26	20.8	-	-	-	-	-	-	-	410
PET/P3-5[d] (60/40%)	-	48	8.88	22.4	-	-	-	-	-	-	-	415
P3(10K)	-16	51	25.90	26.1	-	-	-	-	-	-	-	411
P3(10K)[c]	-	48	21.60	21.8	-	-	-	-	-	-	-	409
P3(10K)[d]	-	53	20.65	20.8	-	-	-	-	-	-	-	409
PET/P3-10[c] (60/40%)	-	49	9.08	22.9	-	-	-	-	-	-	-	412
PET/P3-10[d] (60/40%)	-	51	7.70	19.4	-	-	-	-	-	-	-	412
PET	53	-	-	-	-	-	238	33.81	-	-	24.2	425
PET[c]	-	-	-	-	126	0.31	184	3.82	238	37.1	29.0	423
PET[d]	46	-	-	-	91	2.86	143	0.54	231	26.42	17.2	424

[a]: P3 polyester parts in films; [b]:PET parts in films; [c]:annealing at 140°C for 3h and [d] : annealing at 250°C for 30 min

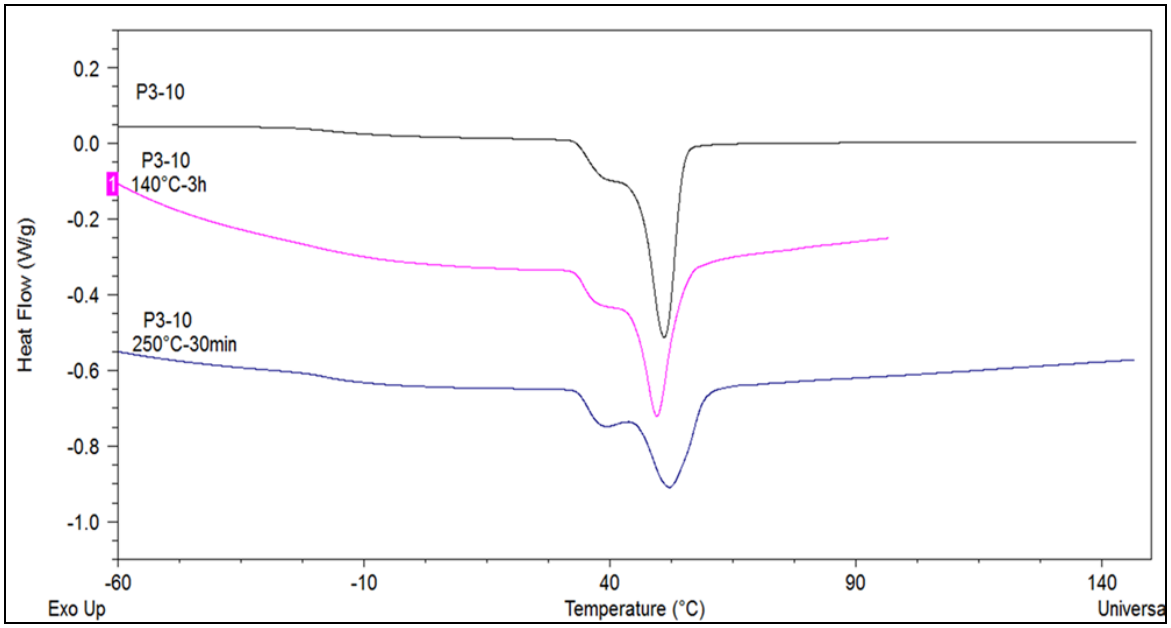

Figure 7.2. DSC results of P3-10 polyester films before and after annealing at 140°C for 3h and 250°C for 30 min.

The thermal properties of pure PET material obtained from the solution are different from PET chips. **Figure 7.3** reveals that PET chips start melting at 238^{0}C (ΔH_f≈33.77J/g) and decomposing at 425^{0}C. It also possesses recrystallization temperature (T_c) at around 126^{0}C (ΔH_c≈27.35J/g), where the PET undergoes crystallization while heating in the DSC. However, for PET films, although we could not obtain any T_c, their glass transition and melting regions are at 53^{0}C and 238^{0}C, respectively. It reveals that PET chains have enough time to reorient during the evaporation of the solvent. On the other hand, the thermal property of PET films significantly changed after the annealing. Recrystallization of PET films occur again at 126°C and 91°C when they were annealed at 140°C for 3h and 250°C for 30 min, respectively. In addition, two T_f of PET were determined after annealing at 140°C for 3h. When they were annealed at 140°C, the

different sizes of crystalline structures formed and melted at different temperatures. However, when they were annealed at 250°C above T_m, one melting temperature was determined.

The effect of annealing temperature on the degree of crystallinity of P3 and PET films was investigated. After the annealing at 140°C for 3h and 250°C for 30 min, samples were removed from the oven and then they were stored at room temperature. As shown in **Table 7.1**, the degree of crystallinity of P3-5 was decreased from 30% to 22.1% and 21.5% when they were annealed at 140°C for 3h and 250°C for 30 min, respectively. For P3-10 films, it decreased from 26.1% to 21.8% and 20.8% as well. In contrast to P3 films, the degree of crystallinity of PET was increased from 24.2 % to 29% after annealing at 140°C for 3h; whereas, it decreased to 17.2% when it was annealed at 250°C for 30 min (**Table 7.1**). Results reveal that the crystallinity of PET films increased when they were annealed above T_c as compared to above T_f. It happened because the thermal history of samples annealed above T_f was erased. When samples were removed from the oven and they were cooled down at room temperature, a common thermal history of films was created.

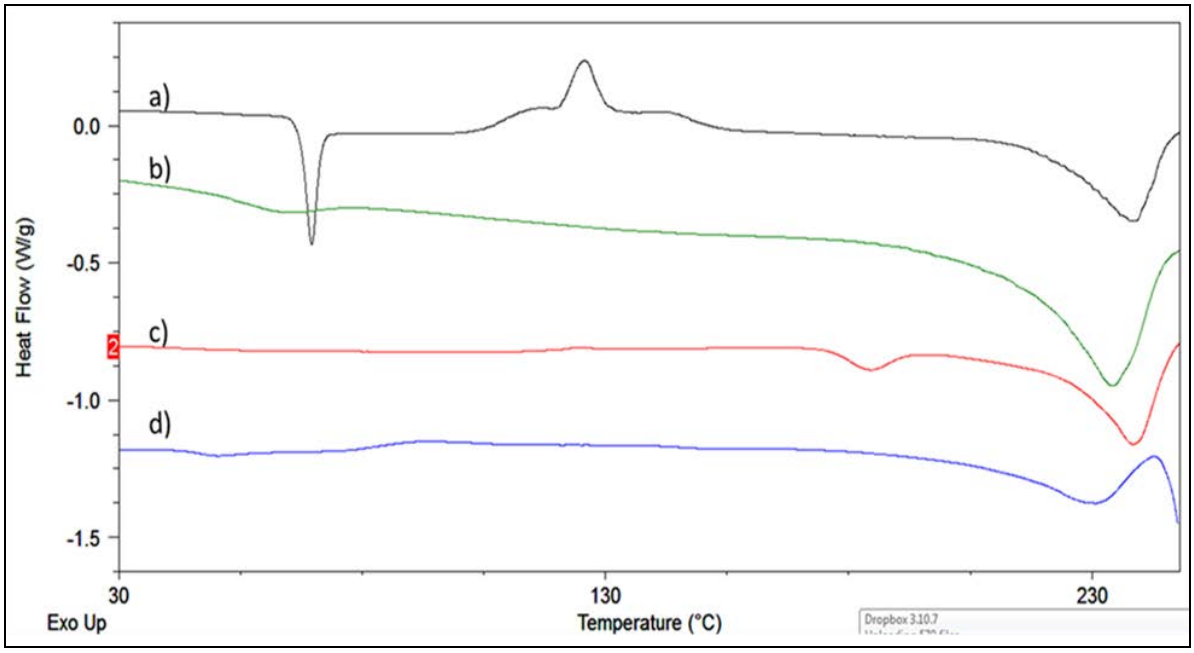

Figure 7.3. DSC results of (a) PET chip; and PET film (b) before (c-d) after annealing at (c) 140°C and (d) 250°C.

After pure components were analyzed, the thermal property of annealed PET/P3-5 and PET/P3-10 films, which contained 40% P3, was also determined. Furthermore, they were compared with pure components annealed at the same conditions. For DCS analysis, annealed PET/P3 samples were only heated up to 150°C due to the evaporation of small amount of P3 polyesters, resulting in DCS contaminations. Therefore, only melting temperatures of P3 polyester domains in PET/P3 films were analyzed. **Figure 7.4** and **Figure 7.5** show the T_f of the P3-5 and P3-10 domains in PET after annealing at 140°C for 3h. Compared with annealed pure PET and P3 polyesters, it was found that the T_f of P3-5 and P3-10 domains were similar to the pure P3 polyesters. In addition, the degree of crystallinity of the P3 domains for PET/P3-5 and PET/P3-10 films were

calculated as 20.8% and 22.9%, respectively which were very close to the their pure annealed components, 22.1% (P3-5) and 21.8% (P3-10).

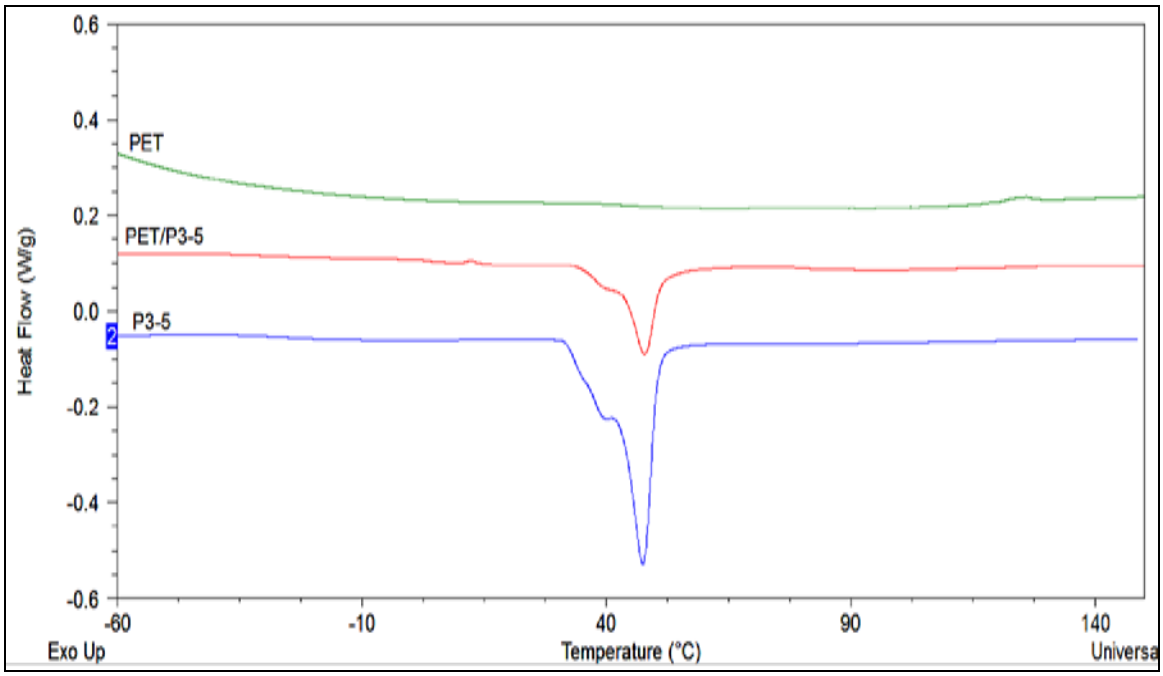

Figure 7.4. DSC results of PET, PET/P3-5 (40%) and P3-5 films after annealing at 140°C for 3h.

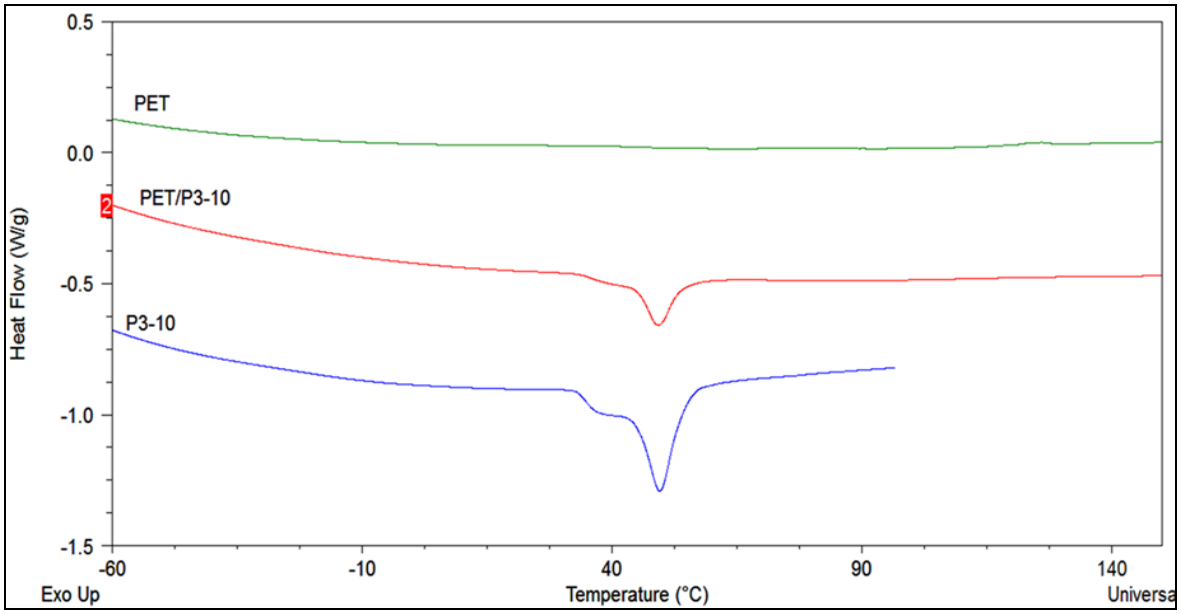

Figure 7.5. DSC results of PET, PET/P3-10 (40%) and P3-10 films after annealing at 140^0C for 3h.

The DCS results of PET/P3-5 and PET/P3-10 (40%) after annealing at 250°C for 30 min are shown in **Figure 7.6** and **Figure 7.7**, respectively. Again, the T_m of P3-5 and P3-10 domains in PET are close to their pure components. Figures revealed that blending with PET could not influence the thermal properties of P3 polyesters. In addition, the PET/P3 with low M_w (5.38K) and high M_w (10K) possessed 19.4% and 22.4% crystallinity, respectively. As a result, annealing treatment affects the thermal property of films. However, there is no significant effect of annealing temperature on it.

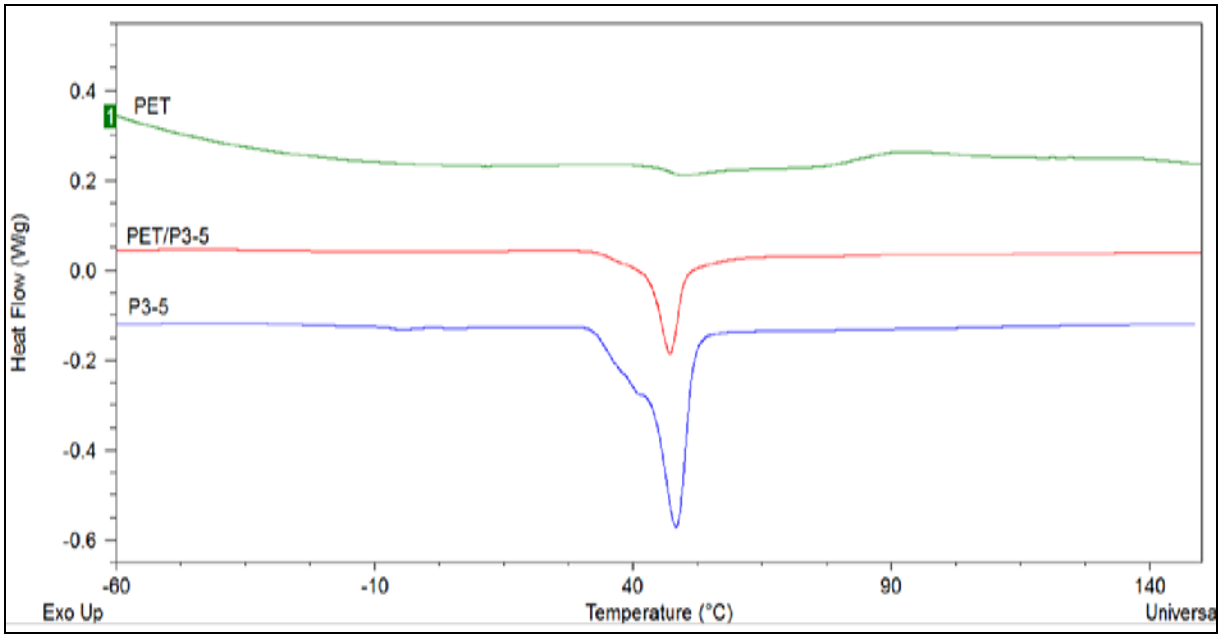

Figure 7.6. DSC results of PET, PET/P3-5 (40%) and P3-5 films after annealing at 250°C for 30min.

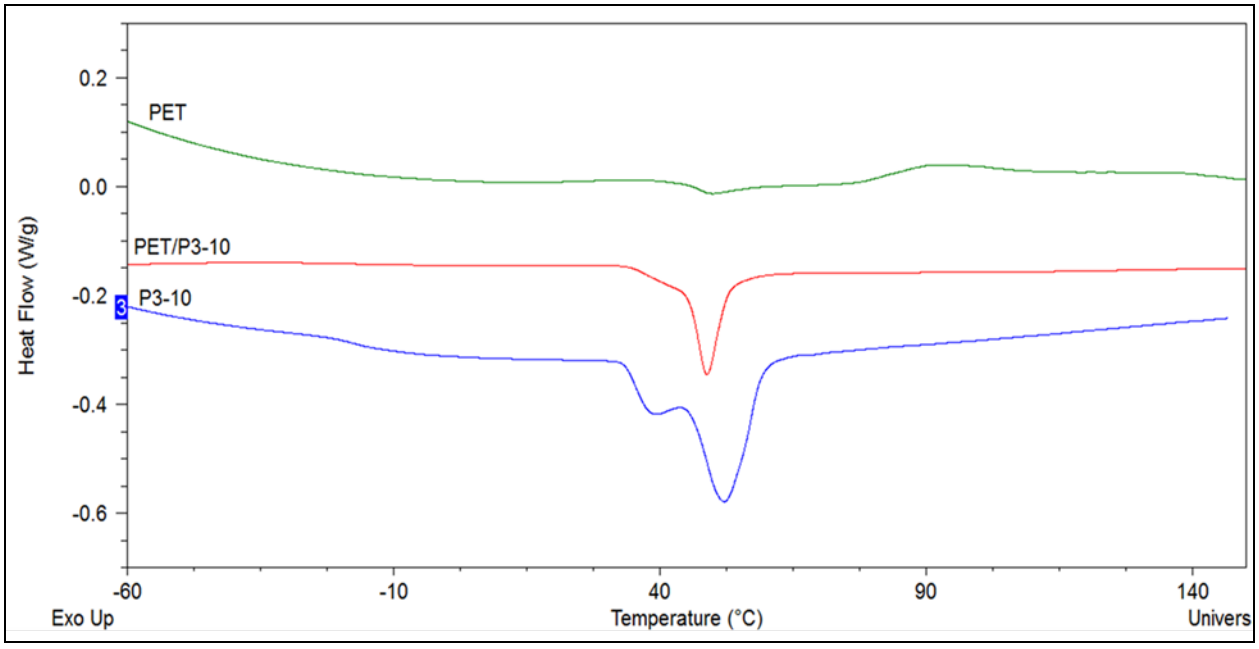

Figure 7.7. DSC results of PET, PET/P3-10 (40%) and P3-10 films after annealing at 250°C for 30min.

Surface Morphology Analysis

In **Chapter 6**, it was determined that the blends of PET and P3 polyesters were immiscible. Therefore, phase separation was observed. Herein, AFM was performed to analyze the influence of annealing temperature on the surface morphology of PET/P3 films deposited on Si wafers. **Figure 7.8** and **Figure 7.9** show the morphology of films prepared from the blending of PET with P3-5 and P3-10, respectively. All samples contained 40% P3 polyesters. The bright domains correspond to the PET matrix and the dark colors correspond to the P3 domains that can be visualized in the form of droplets as a disperse phase (**1st column**).

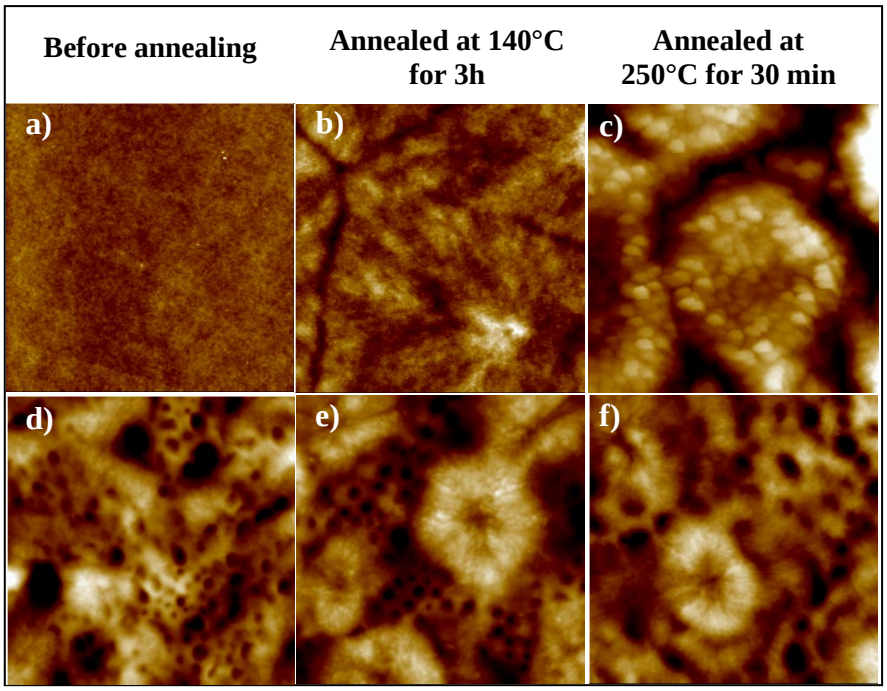

Figure 7.8. AFM image of PET/P3 (M_w=5.38K) blended films (10µ x 10µ). a-c)pure PET (a)RMS=1nm, b)RMS=6nm, c)RMS=104nm); d-f)40%P3-5 (d) RMS=32nm, e) RMS=40nm, f) RMS=26nm).

Furthermore, it was reported in the literature that annealing polymer-blended films at a temperature higher than the T_g and T_c of the polymer components produced significantly different structures than that annealed at temperatures below the T_g of the polymer components.[1–3] Therefore, PET/P3 films were annealed at 140°C, which is higher than the T_g and T_c of the P3 and PET polymers, respectively (**2nd column**). We also investigated the morphology changes when PET/P3 films were annealed for 30 min at 250°C above the melting temperature of PET (238°C), as shown in **Figure 7.8** and **Figure 7.9** (**3rd column**). It is clearly seen that annealing has a significant effect on blend morphology. After annealing, well-developed crystalline structures are seen on the films' surfaces. Indeed, DSC data presented above directly support the AFM results. Furthermore, upon crystallization from the melt, spherulitic structures were obtained. It was also found that increasing the crystallization temperatures produced larger spherulites.

Characterization Wettability of PET/P3 Films

A series of contact angle measurements were conducted to investigate the effects of annealing temperature on the wettability of PET/P3 films. In the model study, PET was blended with P3 polymers with different M_w (5.38K and 10K). All samples, which contained 40% P3 polyesters, were deposited on wafers. It is well known that the surface segregation of fluorinated polymer in blends was influenced by the heat treatment. Annealing enhanced the rate of the migration of fluorinated species to the surface [3, 4].

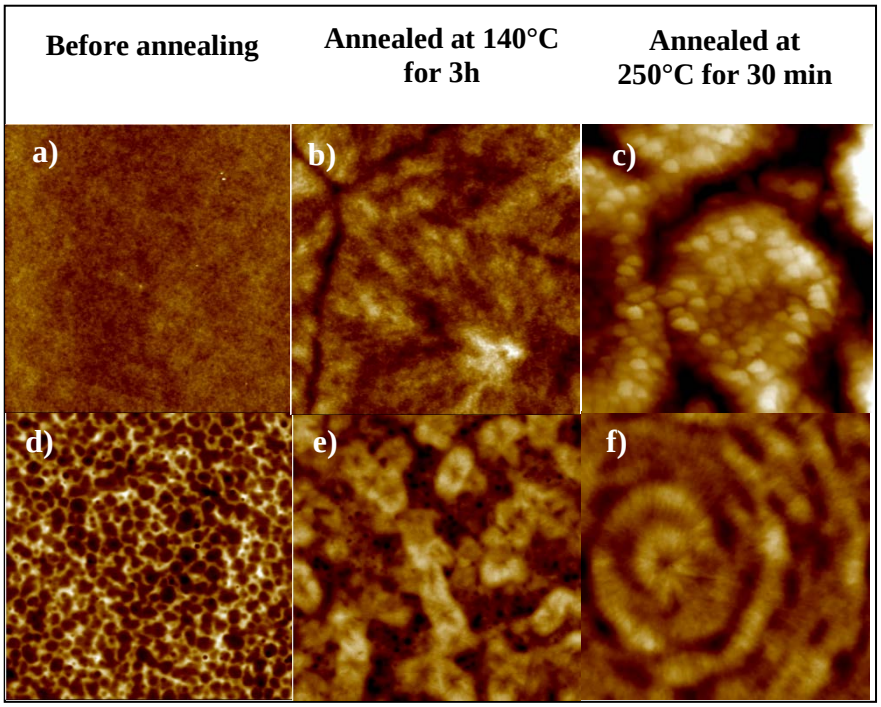

Figure 7.9. AFM image of PET/P3 (M_w=10K) blended films (10μ x 10μ). a-c)pure PET (a)RMS=1nm, b)RMS=6nm, c)RMS=104nm); d-f)40%P3-10 (c) RMS=2nm, d) RMS=23nm, f) RMS=16nm);

Therefore, PET/P3-5 and PET/P3-10 films were annealed at 140°C for 3h and at 250°C for 30 min under vacuum. Both temperatures are above the T_gs of both polymers. The contact angle measurements of water and hexadecane on the annealed samples are illustrated in **Figure 7.10** and **Figure 7.11**, respectively. It was found that the CA of water increased significantly after the annealing. It indicated that during the annealing above T_g, polymer chains reoriented, resulting in the migration of the fluorocarbon groups ($-CF_2$, $-CF_3$) to the surface. Thus, a concentration and closer packing of fluorocarbon groups in the topmost surface region increased, resulting in lower surface energy. When the PET/P3-5 and PET/P3-10 films were annealed at 140°C for 3h, the CA

of water on the former and latter films increased from 83°C to 105°C and 88°C to 101°C, respectively.

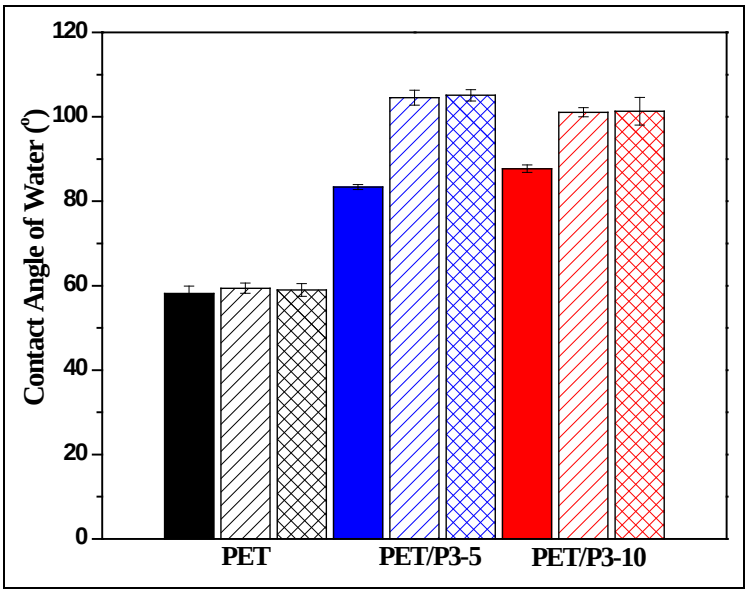

Figure 7.10. CA of water on (■) PET, (□) PET/P3-5 (40%) and (□)PET/P3-10 (40%) films. (□) before annealing, ▨) annealed at 140° C for 3h and ▩) annealed at 250°C for 30min.

However, annealing temperature could not significantly influence the CA of water. For instance, the CA of water on PET/P3-5 films was found to be at 105° and 106° after annealing at 140°C for 3h and 250°C for 30min, respectively. For hexadecane measurements, PET/P3-5 films possessed higher CAs of hexadecane after annealing at 140°C for 3h; whereas, for PET/P3-10 films, CAs of hexadecane decreased from 54° to 52°. In addition, while annealing at 250°C, the CA of hexadecane on PET/P3-5 samples decreased from 55° to 52°, while for PET/P3-10 films, it increased from 54° to 57°.

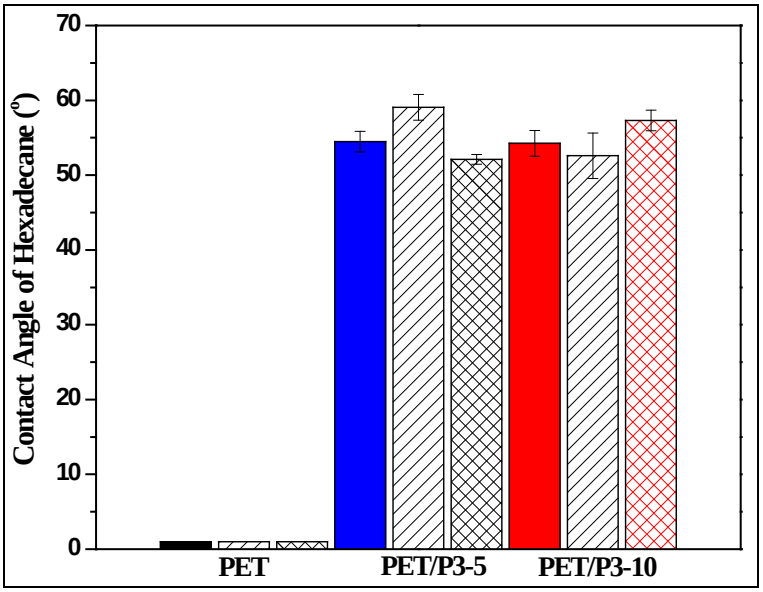

Figure 7.11. CA of hexadecane on on (■) PET, (□) PET/P3-5 (40%) and (□)PET/P3-10 (40%) films. (□) before annealing, ▨) annealed at 140° C for 3h and ▩) annealed at 250°C for 30min.

7.3.1.2. Characterization of PET/P3 Films With Different Concentrations

It is well known that the fluorinated polymers, due to their low surface energy, were essential components for repelling liquids. According to the model study, we found that the incorporation of 40% P3 polyesters into oleophilic PET matrix exhibited high hexadecane and water repellency. In the following, we discuss how the concentration of P3 polyesters (5.38K and 10K) influenced the physical properties of blended films when they were annealed. Therefore, PET/P3 films with different concentrations were prepared and then analyzed.

7.3.2 Thermal Properties of Annealed Dry Films

7.3.2.1 TGA Analysis

A series of TGA experiments were conducted to determine the degradation temperature of PET/P3 films with different concentrations (5, 10, 20, 40, and 80%). Herein, before TGA analysis, all films were annealed at 140°C for 3h and 250°C for 30 min. The TGA results of blended films possessed low (5.38K) and high molecular weight (10K). P3 polyesters are presented in **Table 7.2** and **Table 7.3**, respectively. The degradation temperatures of blended films are in between the degradation of pure components. It was found that the average of the T_d of the films was around 412±3°C.

7.3.2.2 DSC Analysis

A series of DSC experiments were utilized to determine the T_g and T_f of PET/P3-5 and PET/P3-10 films in different concentrations. The DSC results for all blended films are shown in **Appendix A** (140°C) and **Appendix B** (250°C). The degree of crystallinity of PET/P3-5 and PET/P3-10 samples was also calculated using **Equation 4.3** in **Chapter 4** and compared to pure components (**Table 7.2** and **Table 7.3**).

Figure 7.12 and **Figure 7.13** show the degree of crystallinity of the annealed PET/P3 films with different concentration of P3-5 and P3-10, respectively. The blue lines in the figures represent the crystallinity of the pure P3 components before annealing.

Table7.2. Thermal properties of PET/ P3-5 films

	T_g	T_f^a	ΔH_f^a	$\%^a$	T_d
P3 (5.38K)	**-25**	**48**	**29.7**	**30.0**	403
PET/P3[c] (95/5 %)	-	57	0.50	10.10	415
PET/P3[c] (90/10 %)	-	49	0.77	7.78	413
PET/P3[c] (80/20 %)	-	47	1.92	9.70	410
PET/P3[c] (60/40 %)	-	49	8.26	20.80	410
PET/P3[c] (20/80 %)	-	48	17.75	22.41	409
P3[c]	-	**47**	**21.9**	**22.10**	404
PET/P3[d] (95/5 %)	-	49	0.86	17.37	414
PET/P3[d] (90/10 %)	-	50	1.15	11.62	415
PET/P3[d] (80/20 %)	-	50	1.19	6.00	412
PET/P3[d] (60/40 %)	-	48	8.88	22.42	415
PET/P3[d] (20/80 %)	-	47	13.56	17.12	415
P3[d]	-	**48**	**21.31**	**21.50**	405

[a]: P3 polyester parts in films; [b]:PET parts in films; [c]:annealing at 140°C for 3h and [d] : annealing at 250°C for 30 min

Table7.3. Thermal properties of PET/ P3-10 films

	T_g	T_f	ΔH_f^a	$\%^a$	T_d
P3 (10K)	**-16**	**51**	**27**	**26.14**	411
PET/P3[c] (95/5 %)	-	54	0.33	6.85	413
PET/P3[c] (90/10 %)	-	52	1.71	17.27	414
PET/P3[c] (80/20 %)	-	52	2.12	10.71	412
PET/P3[c] (60/40 %)	-	49	9.08	22.93	412
PET/P3[c] (20/80 %)	-	50	6.20	7.83	410
P3[c]	-	**48**	**21.60**	**21.81**	409
PET/P3[d] (95/5 %)	-	49	0.23	4.65	415
PET/P3[d] (90/10 %)	-	51	0.33	3.33	415
PET/P3[d] (80/20 %)	-	51	2.25	11.36	412
PET/P3[d] (60/40 %)	-	51	7.70	19.40	412
PET/P3[d] (20/80 %)	-	49	14.1	17.80	410
P3[d]	-	**53**	**20.65**	**20.80**	409

[a]: P3 polyester parts in films; [b]:PET parts in films; [c]:annealing at 140°C for 3h and [d] : annealing at 250°C for 30 min.

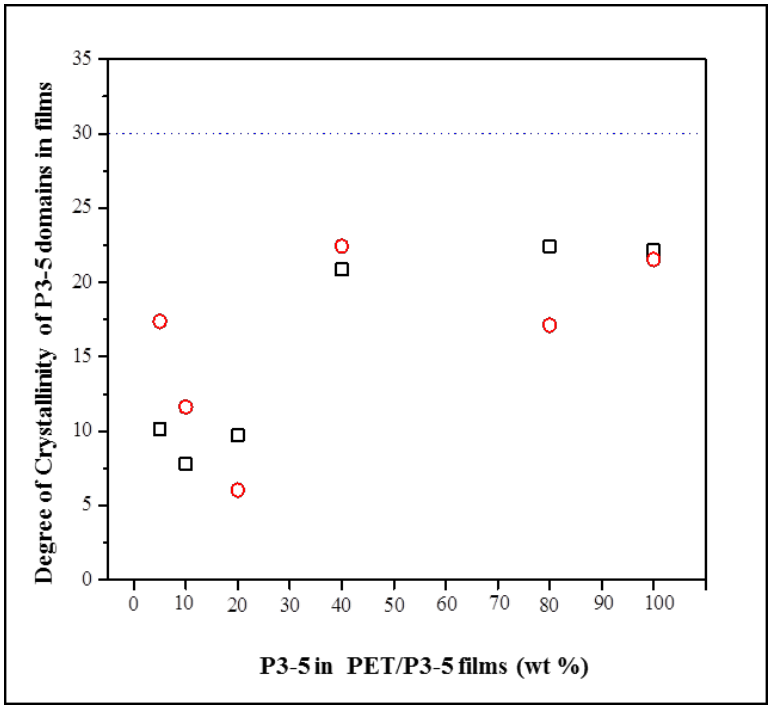

Figure 7.12. Degree of crystallinity of P3-5 (5.38K) domains in PET/P3-5 films (%). □)140°C for 3h and ○)250°C for 30min . The blue line represents the crystallinity of pure components before annealing.

Figure 7.12 illustrates that when PET/P3-5 films were annealed at 140°C for 3h, the degree of crystallinity in P3-5 domains increased from 10.1% to 22.4%, with an increased concentration of P3 in blends from 5% to 80%. On the other hand, for low concentration of P3-5, the degree of crystallinity increased with each increase of the annealing temperature, while for high concentration, the degree of crystallinity decreased.

When the P3-10 was used in films, the crystallinity of P3 domains in PET/P3-10 was also determined. **Figure 7.13** illustrates that the degree of P3 crystallinity was increased from 6.9% to 7.8%, with an increase in the concentrations from 5% to 80% in blends, while they were annealed at 140°C. The effect of annealing conditions on the

crystallinity of highly concentrated P3-10 films (80%) was also obtained. When the films were annealed at 140°C for 3h and 250°C for 30 min, the degree of P3 crystallinity in blends was found to be at 7.8% and 17.8%, respectively.

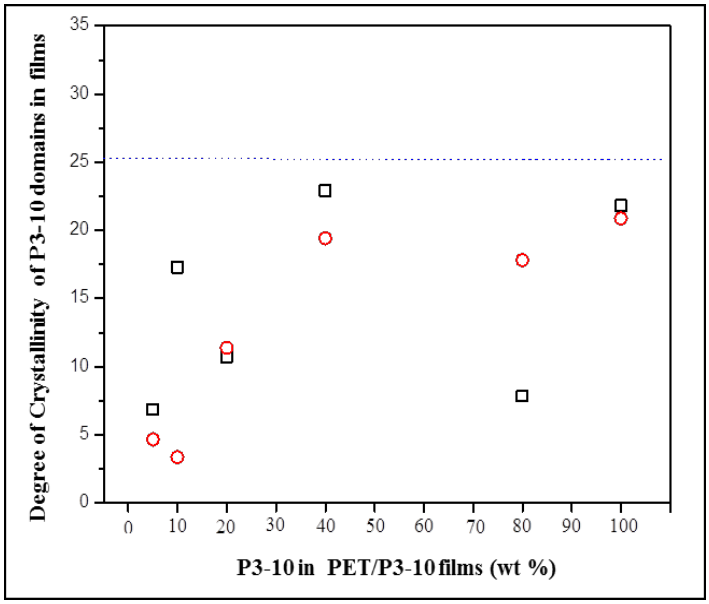

Figure 7.13. Degree of crystallinity of P3-10 (10K) domains in PET/P3-5 films (%). □)140°C for 3h and ○)250°C for 30min . The blue line represents the crystallinity of pure components before annealing.

7.3.2.3. Surface Morphology Analysis of PET/P3 Films

AFM imaging was performed to analyze the influence of annealing temperature on the surface morphology of PET/P3 films. **Figure 7.14** and **Figure 7.15** show the morphology of films prepared by blending PET with P3-5 and P3-10 polyesters, respectively. The surface morphology of the films before annealing are illustrated in the 1st column. It is clearly seen that the P3 domains (dark colors) were distributed into the PET matrix (light domains). As a result, phase separation occurs. Furthermore, a level of

phase separation increased with each increase in the concentration of P3 polyesters in films.

The morphology of the blend series of PET/P3-5 and PET/P3-10 films after annealing at 140°C for 3h and 250°C for 30 min is presented in the 2nd and 3rd columns in **Figure 7.14** and **Figure 7.15**, respectively. It is clearly seen that annealing has a significant effect on blend morphology. After annealing, well-developed crystalline structures are seen on the films' surfaces. Furthermore, upon crystallization from the melt, spherulitic structures are obtained. They became visible with increase in the concentration of fluorinated polymer, with more than 20% P3 in blends for both polymers (**Figure 7.14** and **Figure 7.15 (o-p, s-t)**). It was also found that increasing the crystallization temperatures produced larger spherulites.

7.3.2.4. Wettability of PET/ P3 Films at Different Concentrations

A series of experiments were conducted to investigate the effect of P3 concentration in blends on the wettability of PET/P3 films. For this purpose, P3-5 and P3-10 polyesters were blended with PET at different concentrations. The contact angle measurements of hexadecane and water on PET/P3 samples are illustrated in **Figure 7.16** and **Figure 7.17**, respectively. It was found that the CA of water and hexadecane increased with each increase of the P3 concentration in blends.

It is well known that polymer chains become more mobile during annealing, leading to the migration of the fluorocarbon groups (-CF_2, -CF_3) to the surface. Thus, the topmost surface region was enriched with a concentration and closer packing of the fluorocarbon groups, resulting in lower surface energy. Therefore, the wettability of the

surfaces could be altered during annealing. In addition, to determine the annealing effect on the CA measurements, PET/P3-5 and PET/P3-10 films were annealed at 140°C for 3h and at 250°C for 30 min under vacuum.

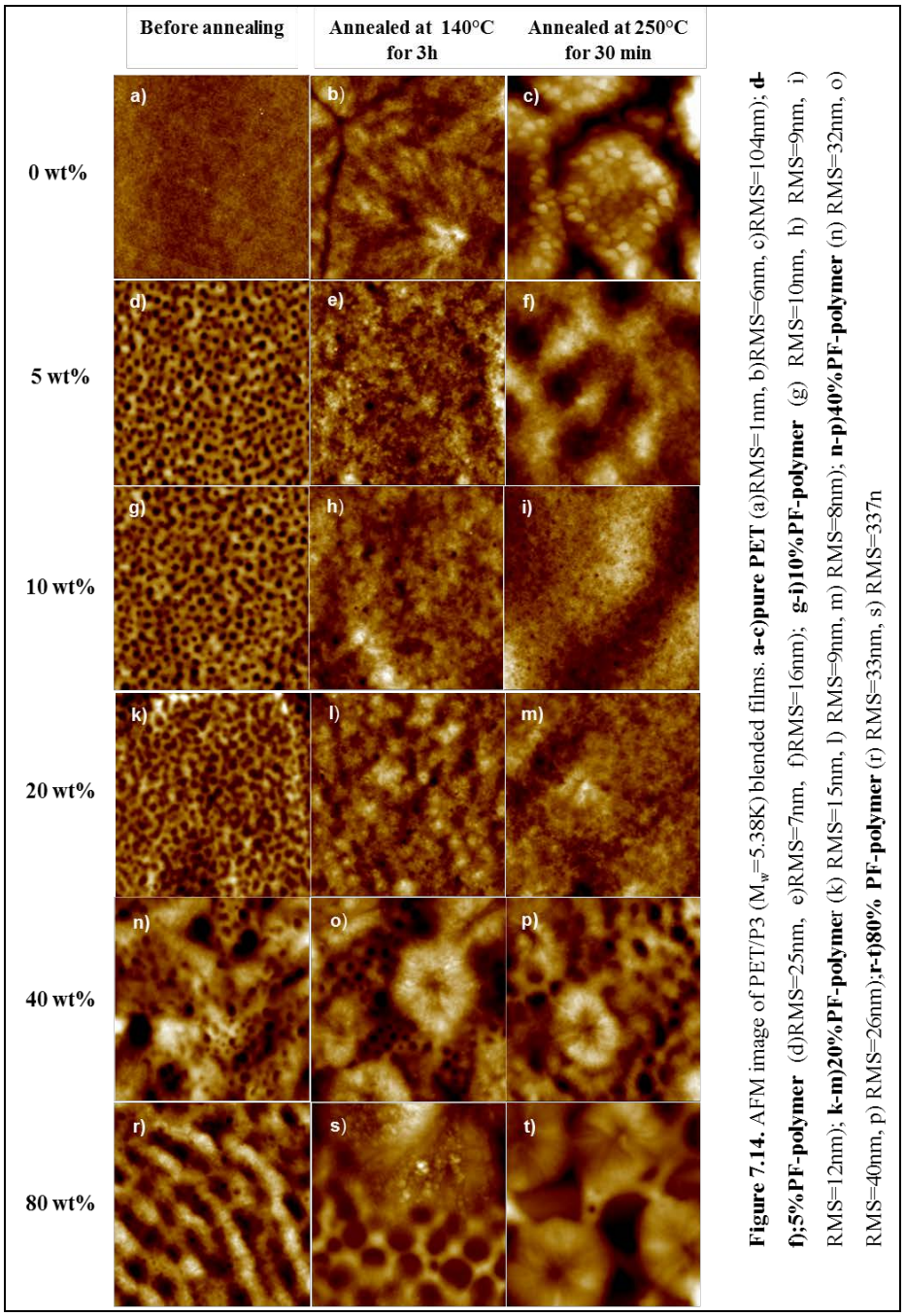

Figure 7.14. AFM image of PET/P3 (M_w=5.38K) blended films. **a-c)pure PET** (a)RMS=1nm, b)RMS=6nm, c)RMS=104nm); **d-f);5%PF-polymer** (d)RMS=25nm, e)RMS=7nm, f)RMS=16nm); **g-i)10%PF-polymer** (g) RMS=10nm, h) RMS=9nm, i) RMS=12nm); **k-m)20%PF-polymer** (k) RMS=15nm, l) RMS=9nm, m) RMS=8nm); **n-p)40%PF-polymer** (n) RMS=32nm, o) RMS=40nm, p) RMS=26nm);**r-t)80% PF-polymer** (r) RMS=33nm, s) RMS=337n

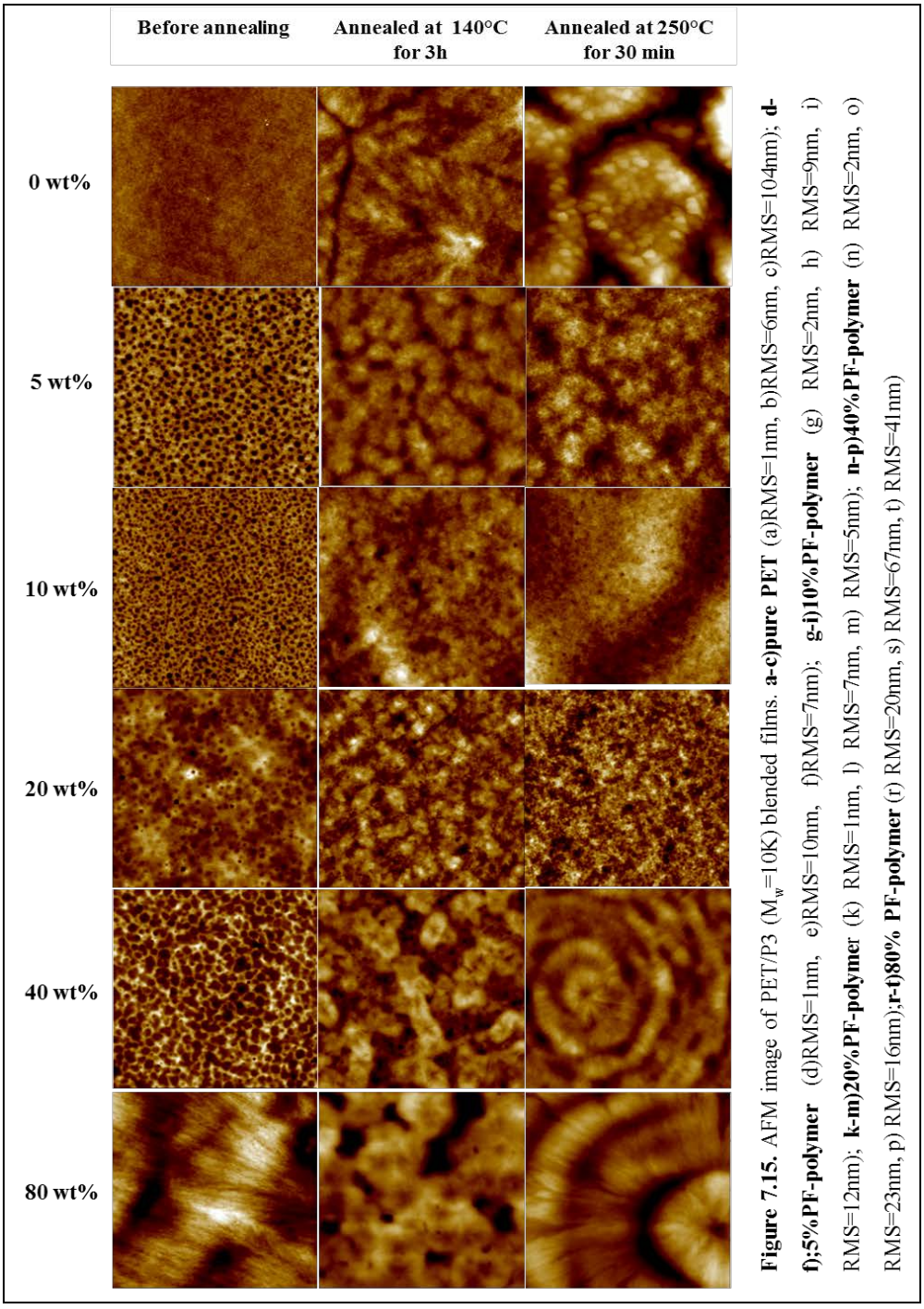

Figure 7.15. AFM image of PET/P3 (M_w=10K) blended films. **a-c)pure PET** (a)RMS=1nm, b)RMS=6nm, c)RMS=104nm); **d-f);5%PF-polymer** (d)RMS=1nm, e)RMS=10nm, f)RMS=7nm); **g-i)10%PF-polymer** (g) RMS=2nm, h) RMS=9nm, i) RMS=12nm); **k-m)20%PF-polymer** (k) RMS=1nm, l) RMS=7nm, m) RMS=5nm); **n-p)40%PF-polymer** (n) RMS=2nm, o) RMS=23nm, p) RMS=16nm);**r-t)80% PF-polymer** (r) RMS=20nm, s) RMS=67nm, t) RMS=41nm)

When the films were annealed, the CA of water on PET/P3 films (80%) increased from 85°–90°C up to 105°C. Annealing temperature plays a role on water/oil repellency.

Essentially, the CA of water increased with increasing the annealing temperature for both PET/P3-5 and PET/P3-10 films.

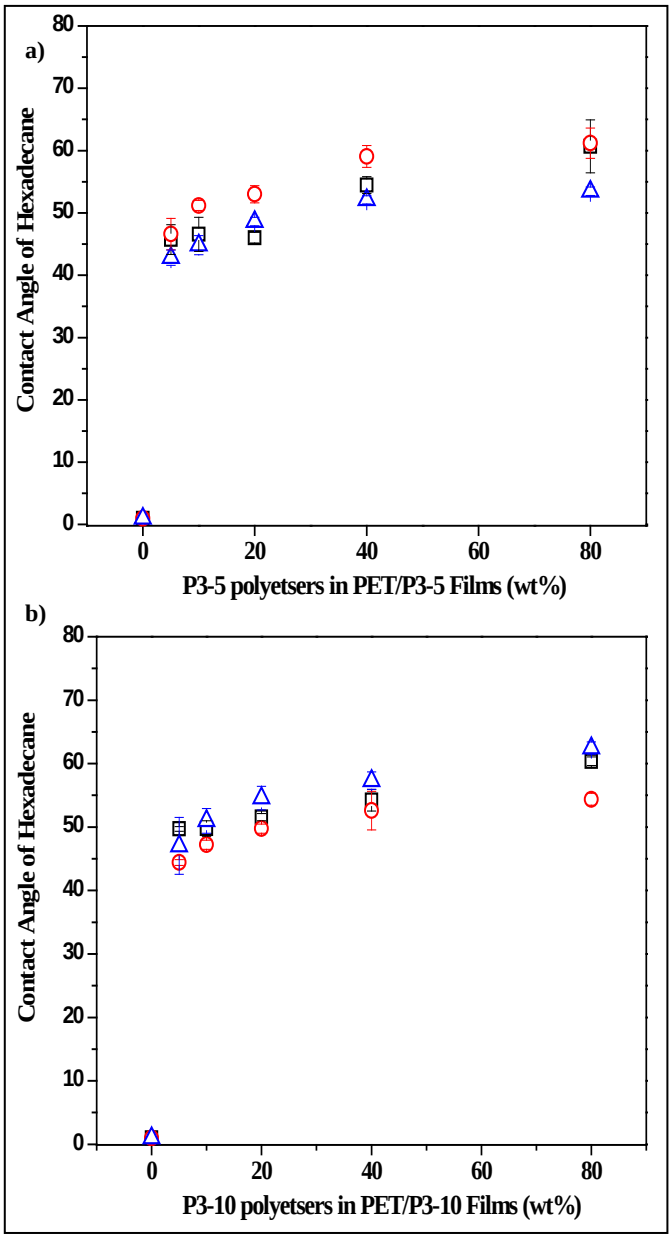

Figure 7.16. Contact angle of hexadecane on PET/P3 polyesters a)PET/P3-5 (5.38K) and b) PET/P3-10 (10K) . □)before annealing; ○)annealed at 140°C for 3h; Δ) annealed at 250°C for 30min.

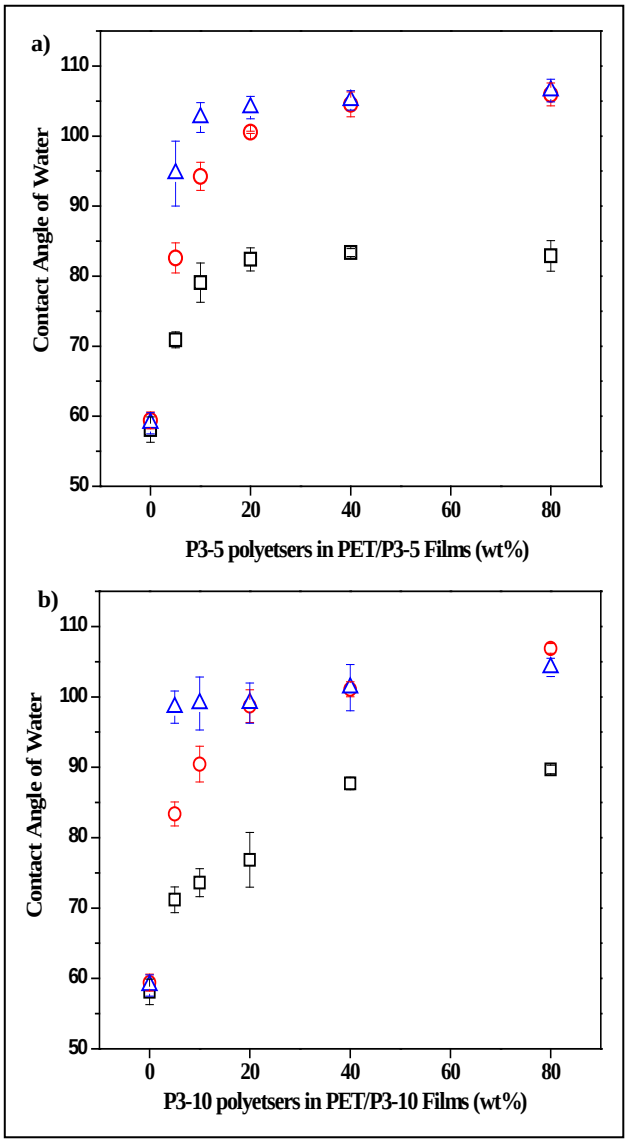

Figure 7.17. Contact angle of water on PET/P3 polyesters a)PET/P3-5 (5.38K) and b) PET/P3-10 (10K) . □)before annealing; ○)annealed at 140°C for 3h; Δ) annealed at 250°C for 30min.

Compared to the wettability of PET/P3-5 and PET/P3-10 films after annealing, it was found that when the concentration of P3 polyester in PET was up to 40%, PET/P3-5 possessed and exhibited higher water repellency than PET/P3-10. If it is more than 40%,

the latter possessed high repellency after annealing at 140°C. Again, the reason behind the observed behavior is the effect of conformational entropy. During annealing, the mobile high M_w polymer chains in blends experiences a large entropy penalty for migration to the surface. Lower M_w chains will enrich on the surface to lower surface free energy, resulting in greater concentration of polymer chain ends at surfaces. At high concentration, surfaces became enriched with P3-10 polymers, leading to high water repellency.

The surface energy of films before and after annealing at 140°C for 3h and 250°C for 30min was calculated using the Owens-Wendt method (**Equation 5.1** in **Chapter 5**) to evaluate the wettability of surfaces [4]. As seen in **Figure 7.18** and **Figure 7.19**, surface energy was reduced as P3 polyesters were added into the PET blends.

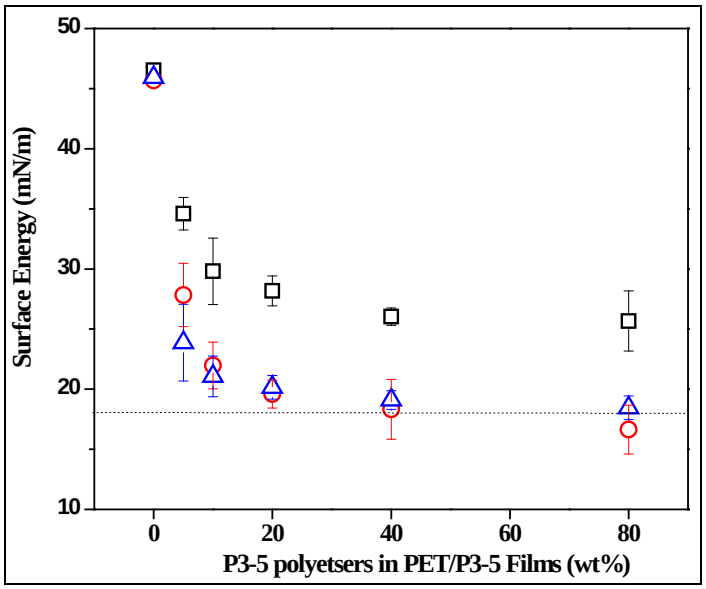

Figure 7.18. Surface energy of PET/P3-5 films (5.38 K). □) before annealing; ○) annealed at 140°C for 3h; Δ) annealed at 250°C for 30min and (---) PTFE.

In addition, the total content of the fluorocarbon groups on the surface was altered with heat treatment. It is clearly seen that the surface energy was reduced due to the enrichment of fluorinated chains on the surface after annealing. The results also show that the high concentration of P3-blended films exhibited lower surface energy than polytetrafluoroethylene (PTFE) shown as blue line in **Figure 7.18** and **Figure 7.19**.

As compared to the surface energy of PET/P3-5 and PET/P3-10 films, it was found that generally, PET/P3-5 films possessed lower surface energy than higher ones at low concentrations. Specifically, after annealing at 140°C, PET/P3-5 had low surface energy for all compositions, as compared to the high M_w of P3. It was expected since the high molecular weight of the polymer already has lack of entropy compared to the lower one. At the increase of the temperature of the system, the latter migrates to the surface easily.

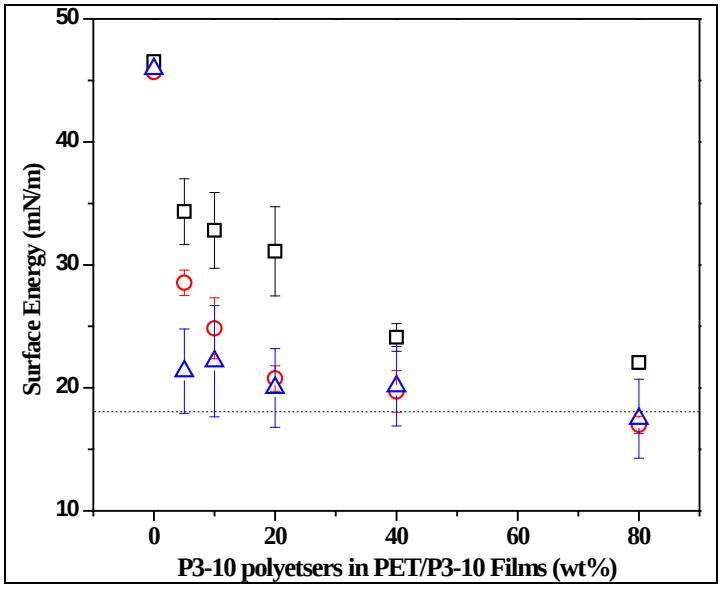

Figure 7.19. Surface Energy of PET/P3-10 films (10K). □) before annealing; ○) annealed at 140°C for 3h; Δ) annealed at 250°C for 30min and (---) PTFE.

7.4. Conclusions

Perfluoro diester isophthaloyl polymers, such as P3-5 (5.38K) and P3-10 (10K) were blended with PET to obtain oleophobic polyester films. It was found that the wettability of the surface depends on not only *the* M_w of P3 polyesters, but also on *annealing*. During the annealing, fluorinated species became more mobile and they migrated to the surface, resulting in a higher concentration of fluorine on the surface, and consequently, lower surface energy. It was found that the P3-5 polyester migrated to the surface more than the P3-10 when they were annealed at 140°C. However, PET/P3-10 films with high P3-10 concentrations exhibited lower surface energy when they were annealed at 250°C.

7.5. References

1. Boker, A.; Herweg, T.; Reihs, K., Selective Alteration of Polymer Surfaces by Thermal Cleavage of Fluorinated Side Chains. *Macromolecules* **2002,** *35* (13), 4929-4937.
2. Hutchings, L. R., stimuli responsive surface segregation of well-defined end-functionalized polymers. *Polymer Reprints* **2009,** *50* (1).
3. Lau, W. W. Y.; Burns, C. M., Effect of temperature and molecular weight on the rate of spreading of polystyrene melts on plane soda lime glass surfaces. *Journal of Polymer Science: Polymer Physics Edition* **1974,** *12* (2), 431-439.
4. Owen, M. J., Low Surface Energy Inorganic Polymers. *Comments on Inorganic Chemistry* **1988,** *7* (4), 195-213.

CHAPTER EIGHT

SUMMARY AND FUTURE WORK

8.1. Summary

Understanding the wettability of the surfaces provides fundamental information to develop oil repellent surfaces. According to literature, the general idea behind the ability of repelling a liquid from solid surface is that the surface of the film should be significantly lower than the surface tension of liquid. Although hydrocarbon based coatings are efficient for repelling water, fluorocarbon based coatings are used to repel oils due to their lower surface energy than hydrocarbons. Thus, this work has presented the synthesis of fluorinated polyesters with different end groups detailed in **Chapter 4** and their blending with PET at different concentrations to develop oleophobic polyester films (**Chapter 5**). The contact angle measurements demonstrate that the end-groups of fluorinated polyesters influenced the wettability of PET/fluorinated polyester film surfaces. Among the fluorinated polyesters, polymer (P3) terminated with $–CF_3$ groups in both sides exhibited the highest repellency because $–CF_3$ groups possess lowest surface energy.

The surface properties of solid surfaces are different than their bulks. Thus, the wettability of the surface depends on the chemical composition of the surface which is altered by the changing of concentration of polyesters. In addition, it is possible to improve oil repellency of the PET films by altering the molecular weight of fluorinated polyesters. For this purpose, **Chapter 6** reported the synthesis of the fluorinated polyester terminated with $–CF_3$ groups with two different molecular weights (P3-5: 5.38K and P3-

10: 10K). Then, the polyesters were blended with PET at different concentrations. It has been shown that at low concentration, the surface coverage by P3-5 polyester was higher than the P3-10 . Thus, it leads to more water and oil repellency. On the other hand, at high concentrations, the latter polyester reduced the wettability of the surface more than the former one. This could happen because the P3-10 polyester possessed more -CF_2 and –CF_3 groups as compared to their lower counterparts. Surfaces were enriched with P3-10 polyesters more than P3-5 at high concentrations.

In **Chapter 7**, the effects of annealing on the wettability of PET were also discussed. The PET/P3-5 and PET/P3-10 films at different concentrations were annealed at 140°C and 250°C. It was known that fluorocarbon chains became more mobile during annealing. They migrated to the surface, resulting in a higher concentration of fluorine on the surface, and consequently, lower surface energy. The contact angle measurements revealed that the P3-5 polyester migrated to the surface more than the P3-10 when they were annealed at 140°C. This could have happened due to the conformational entropy differences between the two polyesters. The former possessed higher entropy compared to the latter. However, PET/P3-10 films with high P3-10 concentrations exhibited lower surface energy when they were annealed at 250°C.

8.2. Future Work

We find that the annealing treatment of films enhances the repellency. Annealing temperature also influences the wettability of films. For future work, the PET/P3 films will be annealed at different temperatures (130°C, 150°C, 180°C and 210°C) between the T_c (129°C) and T_f (235°C) of PET materials in order to determine the most efficient

temperature, resulting in the maximum oil and water repellency. Recommendations for future work also include creating oleophobic PET films using block copolymers. The block copolymers will be synthesized using the PET and fluorinated polyesters with varying block ratios. The blending of copolymers with pure PET may improve the compatability of the films, enhancing the repellency.

It is well known that PET materials are received attention in numerous application such as textile, packaging. Thus, I would recommend that the blending of fluorinated polyesters and their copolymers with PET are also used as textile materials (fibers) to protect against water/oil-based stains.

Appendix A

The DSC results for PET/P3-5 and PET/P3-10 blended films

The DSC results for PET/P3-5 and PET/P3-10 blended films, which were annealed at 140°C for 3h, are shown in **Figure A-1** and **Figure A-2**, respectively.

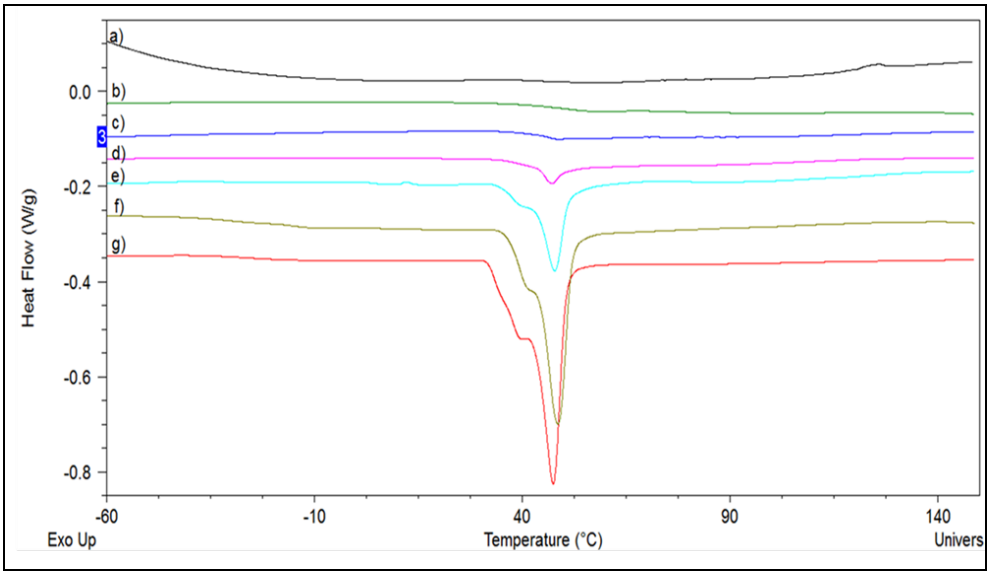

Figure A-1. DSC results of PET/P3-5 films after annealing at 140°C for 3h. a) PET; b)5%P3-5; c)10% P3-5; d) 20% P3-5; e)40% P3-5; f)80% P3-5 and g) 100%P3-5.

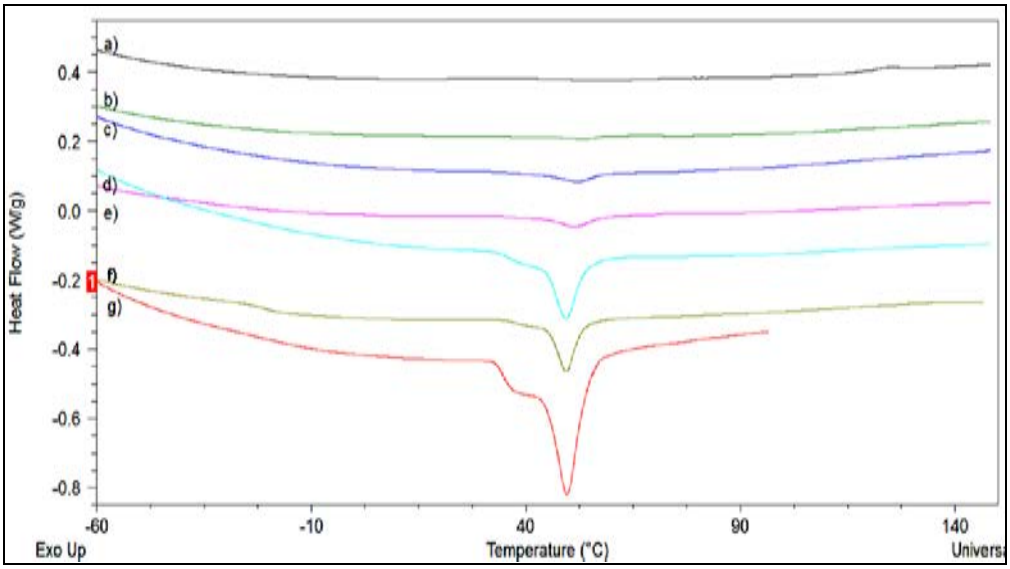

Figure A-2. DSC results of PET/P3-10 films after annealing at 140°C for 3h. a) PET; b)5%P3-10; c)10% P3-10; d) 20% P3-10; e)40% P3-10; f)80% P3-10 and g) 100%P3-10

The DSC results for PET/P3-5 and PET/P3-10 blended films, which were annealed at 250°C for 30min, are shown in **Figure A-3** and **Figure A-4**, respectively.

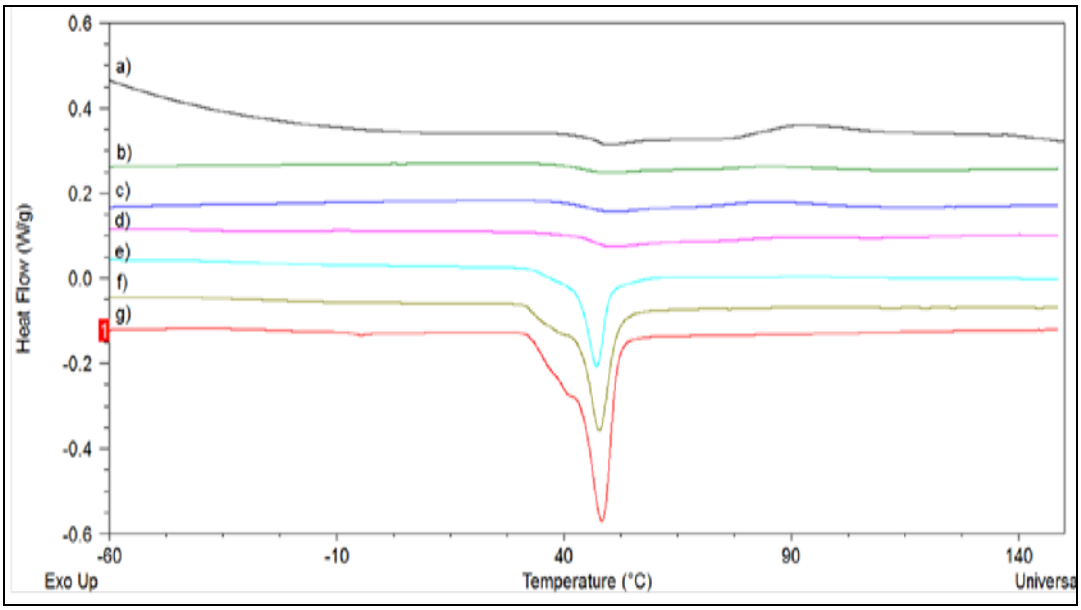

Figure A-3. DSC results of PET/P3-5 films after annealing at 250°C for 30min. a) PET; b)5%P3-5; c)10% P3-5; d) 20% P3-5; e)40% P3-5; f)80% P3-5 and g) 100%P3-5.

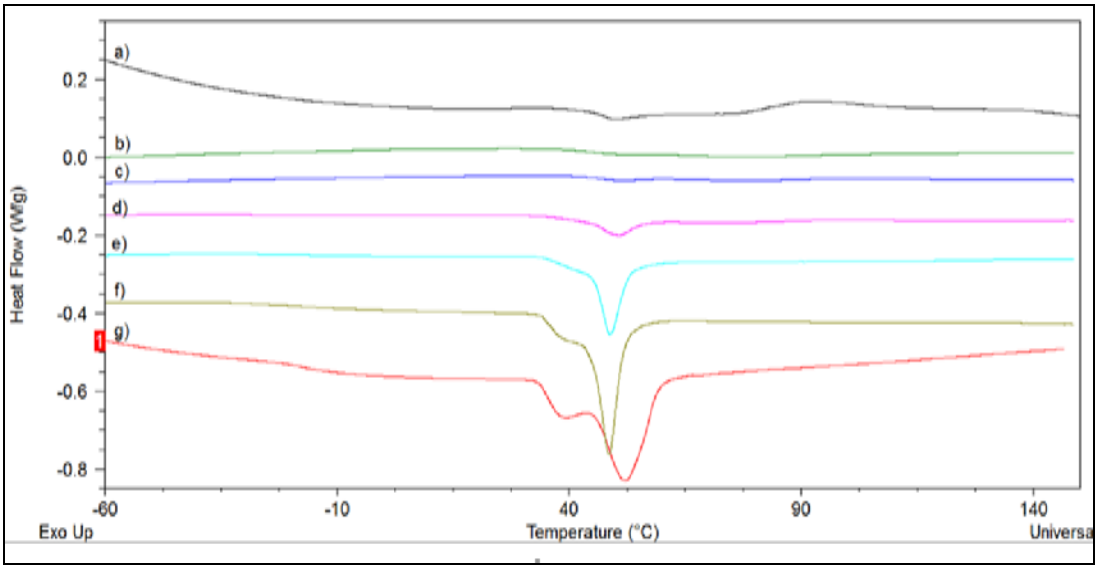

Figure A-4. DSC results of PET/P3-10 films after annealing at 250°C for 30min. a) PET; b)5%P3-10; c)10% P3-10; d) 20% P3-10; e)40% P3-10; f)80% P3-10 and g) 100%P3-10